2010

CHEMICAL MODIFICATION AND CHARACTERIZATION OF CARBON NANOTUBES

Kelby Brandan Cassity
University of Kentucky, kelby_cassity@yahoo.com

ABSTRACT OF DISSERTATION

Kelby Brandan Cassity

The Graduate School

University of Kentucky

2010

CHEMICAL MODIFICATION AND CHARACTERIZATION OF CARBON NANOTUBES

ABSTRACT OF DISSERTATION

This dissertation submitted in partial fulfillment of the
requirements for the degree of Doctor of Philosophy in the
College of Arts and Sciences,
University of Kentucky

By

Kelby Brandan Cassity

Lexington, Kentucky

Director: Dr. Mark S. Meier, Professor of Chemistry

Lexington, Kentucky

2010

ABSTRACT OF DISSERTATION

CHEMICAL MODIFICATION AND CHARACTERIZATION OF CARBON NANOTUBES

Carbon nanotubes (CNTs) are a relatively new allotrope of carbon that possess very unique and exciting physical characteristics. However, much is still unknown regarding their physical structure and chemical reactivity. The focus of this dissertation is to utilize the chemical modification of these filamentous carbon structures as a probe to investigate the structure and reactivity of carbon nanotubes. Also discussed is the ability of CNTs, once chemically modified, to interact with specific polymer matrices and how the addition of modified and unmodified CNTs affects the physical properties of these matrices.

Keywords: Carbon Nanotube, Nitrogen Doped Carbon Nanotube, Epoxy Resin, Composite, Longitudinal Cutting

Kelby B. Cassity

Student's Signature

8/31/2010

Date

CHEMICAL MODIFICATION AND CHARACTERIZATION OF CARBON NANOTUBES

By

Kelby Brandan Cassity

.Mark S. Meier, PhD
Director of Dissertation

John E. Anthony, PhD
Director of Graduate Studies

8/31/2010
Date

RULES FOR THE USE OF DISSERTATIONS

Unpublished dissertations submitted for the Doctor's degree and deposited in the University of Kentucky Libraries are as a rule open for inspection, but are to be used only with due regard to the rights of the authors. Bibliographical references may be noted, but quotations or summaries of part may be published only with the permission of the author, and with the usual scholarly acknowledgements.

Extensive copying or publication of the dissertation in whole or in part also requires the consent of the Dean of Graduate School of the University of Kentucky.

A library that borrows this dissertation for use by its patrons is expected to secure the signature of each user.

Name Date

_____

_____

_____

_____

_____

_____

_____

_____

_____

_____

_____

_____

DISSERTATION

Kelby Brandan Cassity

The Graduate School

University of Kentucky

2010

CHEMICAL MODIFICATION AND CHARACTERIZATION OF CARBON NANOTUBES

DISSERTATION

A dissertation submitted in partial fulfillment of the
requirements for the degree of Doctor of Philosophy in the
College of Arts and Sciences,
University of Kentucky

By

Kelby Brandan Cassity

Lexington, Kentucky

Director: Dr Mark S. Meier, Professor of Chemistry

Lexington, Kentucky

2010

TABLE OF CONTENTS

LIST OF TABLES ..... **iv**

LIST OF FIGURES ..... **v**

Chapter 1: Introduction **1**

Chapter 2: Functionalized MWCNTs for use in Epoxy composites **6**

Heat Flow of functionalized MWCNTs in EPON 826 22

Preparation of epoxy-nanotube composites 26

DMA Analysis 28

Summary 28

Storage Modulus 28

Loss Modulus 40

Tan Delta 43

Conclusions 46

Chapter 3: Longitudinal Cutting of NMWCNTs via reductive alkylation **49**

Longitudinal cutting of NMWCNTs 58

Porosity of channeled NMWCNTs 67

Comparison of Alkylating Agents 78

Investigation of the effect of the dissolving metal 83

Study of Li: C stoichiometry 84

Channeling on CH3CN-derived tubes 87

Chapter 4: Conclusions **92**

Chapter 5 Experimental Procedures **97**

References **116**

Vita **123**

LIST OF TABLES

Table 2-1: 3 Roll Mill sequence....27

Table 3-1 Comparison of porosity of as-produced NMWCNTs and channeled NMWCNTs (average of 3 runs)....71

Table3-2: Porosity data comparison of NMWCNTs, Pressed NMWCNTs, Channeled NMWCNTs and Pressed Channeled NMWCNTs (average of 3 runs)....75

Table 3-3: Comparison of porosity of channeled NMWCNTs and channeled-then-graphitized NMWCNTs (average of 3 runs)....77

Table 3-4 Comparison of porosity of GF- NMWCNTs and GF- NMWCNTs that have been channeled (average of 3 runs)....78

Table 3-5: Porosity data of NMWCNTs reduced with lithium and quenched with varying alkylating agents (average of 3 runs)....79

Table3-6: Std Reduction potentials, atomic radii, and surface area data of NMWCNTs channeled with different metals....84

Table 3-7: Surface area data of NMWCNTs reacted with increasing lithium concentration (average of 3 runs)....86

Table 3- 8: Comparison of surface area data of CH3CN NMWCNTs and channeled CH3CN NMWCNTs....89

Table 5-1: 3 Roll Milling Sequence....98

LIST OF FIGURES

Figure 1-1: SEM images of MWCNTs 2

Figure 1-2: Schematic of CVD MWCNT synthesis furnace 3

Figure 1-3: Schematic of root growth and tip growth of MWCNTs 4

Image from Reference 4

Figure 2-1: TGA of Raw vs Hydrogenated MWCNTs 11

Figure 2-2: TGA of TETA functionalized MWCNTs 16

Figure 2-3: DSC of TETA functionalized MWCNTs mixed with EPON 826 resin 17

Figure 2-4: Subunits and oligomers contained within EPON 826 19

Figure 2-5: Proposed mechanism for imidazole catalyzed crosslinking of epoxy resin with anhydride hardener 20

Figure 2-6**:** Schematic of crosslinked bisphenol-A diglycidyl ether monomers with NMA 22

Figure 2-7: DSC of 1,3,5,10 vol% Acid Chloride MWCNTs in EPON826 23

Figure 2-8**:** Plot of total heat flow versus wt% acid chloride MWCNTs in EPON 826 25

Figure 2-9: Proposed mechanism for the crosslinking of EPON 826 oligomers with acid chloride functionalize MWCNTs 26

Figure 2-10: DMA overlay of Raw Epoxy, 5, and 10vol% As-Produced MWCNTs 31

Figure 2-11: DMA overlay of Raw Epoxy, 5, and 10vol% Acid MWNTs 32

Figure 2-12: DMA overlay of Raw Epoxy, 5, and 10vol% Acid Chloride MWNTs 32

Figure 2-13: DMA overlay of Raw Epoxy, 5vol% As-Produced MWNTs, 5vol% Acid MWNTs, and 5vol% Acid Chloride MWNTs 33

Figure 2-14: DMA overlay of Raw Epoxy, 10vol% As-Produced MWNTs, 10vol% Acid MWNTs, and 10vol% Acid Chloride MWNTs 33

Figure 2-15: Comparison of Storage modulus of MWCNT-epoxy composites 34

Figure 2-16: Comparison of Storage Modulus Onset and Deset Temperature for Neat Epoxy, 5 vol%, and 10 vol% Raw MWCNTs 35

Figure 2-17: Comparison of Storage Modulus Onset and Deset Temperature for Neat Epoxy, 5 vol%, and 10 vol% Acid MWCNTs 36

Figure 2-18: Comparison of Storage Modulus Onset and Deset Temperature for Neat Epoxy, 5 vol%, and 10 vol% Acid Chloride MWCNTs 36

Figure 2-19: Loss modulus peak temperature of acid chloride functionalized MWCNT/Epoxy composites and raw MWCNT + benzoyl chloride/Epoxy composites 39

Figure 2-20: Loss Modulus Onset Temperature of Raw, Acid, and Acid Chloride MWCNT-epoxy composites 41

Figure 2-21: Loss Modulus Peak Temperatures of Raw, Acid and Acid Chloride MWCNT-epoxy Composites 42

Figure2-22: Loss Modulus deset temperature of raw, acid, and acid chloride MWCNT-epoxy composites 43

Figure2-23: Stress-Strain curves of a) a pure elastic material and b) a viscoelastic materal. The hysteresis loop shows the amount of energy lost in a loading-unloading cycle 44

Figure 2-24: Tan Delta onset temperature of Raw, Acid and Acid Chloride MWCNT composites 45

Figure 2-25: Tan Delta peak temperature of Raw, Acid and Acid Chloride MWCNT composites 45

Figure3-1: TEM image with graphical description of a stacked cup shaped carbon nanotube 49

Figure 3-2: Low magnification SEM image of a) NMWCNTs and b) cylindrical MWCNTs 50

Figure 3-3: TEM images of a) NMWCNT and b) regular cylindrical MWCNT 51

Figure 3-4: HRTEM of a NMWCNT with graphical description of tube axis compared to graphene axes 51

Figure 3-5: HRTEM image of GF-NMCNT 53

Figure 3-6: TEM images of NMWCNTs containing conical catalysts 55

Figure 3-7: TGA thermogram of NMWCNTs and GF-NMWCNTs in air 56

Figure 3-8: First derivative plot of TGA thermogram of NMWCNTs and GF-NMWCNTs in air 57

Figure 3-9: Second derivative plot of TGA thermogram of NMWCNTs and GF-NMWCNTs 57

Figure 3-10: Schematic of proposed shell separation mechanism 60

Figure 3-11: TEM images of Birch reduced NMWCNTs 61

Figure3-12: High Resolution TEM image of channeled NMWNT with graphical insert of as-produced NMWNT structure 62

Figure3-13: HRTEM image of channeled NMWCNT with arrows pointing to channel edges 63

Figure3-14: TGA thermograms of NMWCNTs (red) and Channeled NMWCNTs (green) 64

Figure 3-15: TGA thermograms of NMWCNTs (red), GF-NMWCNTs (green), Channeled NMWCNTs (black), and NMWCNTs that have been channeled and then subjected to graphitization conditions (blue) 66

Figure 3-16: a,b) TEM images of channeled-then-annealed NMWCNTs and c,d) SEM images of same sample....67

Figure 3-17: Examples of the six typical isotherms....70

Figure 3-18 a) TEM image of as-produced NMWCNT b) TEM image of channeled NMWCNT....71

Figure 3-19: BET isotherm of as-produced NMWCNTs....73

Figure 3-20: BET isotherm of channeled NMWCNTs....74

Figure 3-21 a) TEM image of channeled NMWCNT b) TEM image of channeled NMWCNT that has been graphitized....77

Figure 22 a) TEM image of GF-NMWCNT b) TEM image of GF-NMWCNT that has been channeled....78

Figure 3-24: structure of alkylating agents examined....79

Figure 3-25: TGA of as-produced NMWCNTs, and NMWCNTs Birch-alkylated with NH_4Cl, CH_3I, and $CH_3(CH_2)_{14}Br$....82

Figure 3-26: TGA of as-produced NMWCNTs, and NMWCNTs Birch-alkylated with t-Butyl Bromide, TMSCl, and Bromomethylcyclohexane....82

Figure 3-26: Representative TEM images of NMWCNTs reacted with increasing lithium concentration....87

Figure 3-27: TEM images of acetonitrile derived NMWCNTs....88

Figure 3-28: TEM images of channeled acetonitrile derived MWCNTs....88

Figure 4-1: SEM images of helical cut NMWCNTs....95

Chapter 1: Introduction

Carbon nanotubes (CNTs) have been known for many years[1-6] and over the past few decades much attention has been given to the study of their structure, properties, and potential applications. Despite being a relatively new material compared to other synthetic materials, a large number of academic papers and commercial patents have been produced in this quickly expanding field.[7]

The most basic nanotube, a single wall carbon nanotube (SWCNT) can be conceptualized as a single layer of graphene[8-11] which is rolled into a cylinder. Lengths can average around a few dozen microns and diameters range from a few angstroms up to 70 or 80nm depending upon the conditions of synthesis[12-13] When SWCNTs are arranged as concentric cylinders in a nesting configuration, a multi walled carbon nanotube (MWCNT) is described.

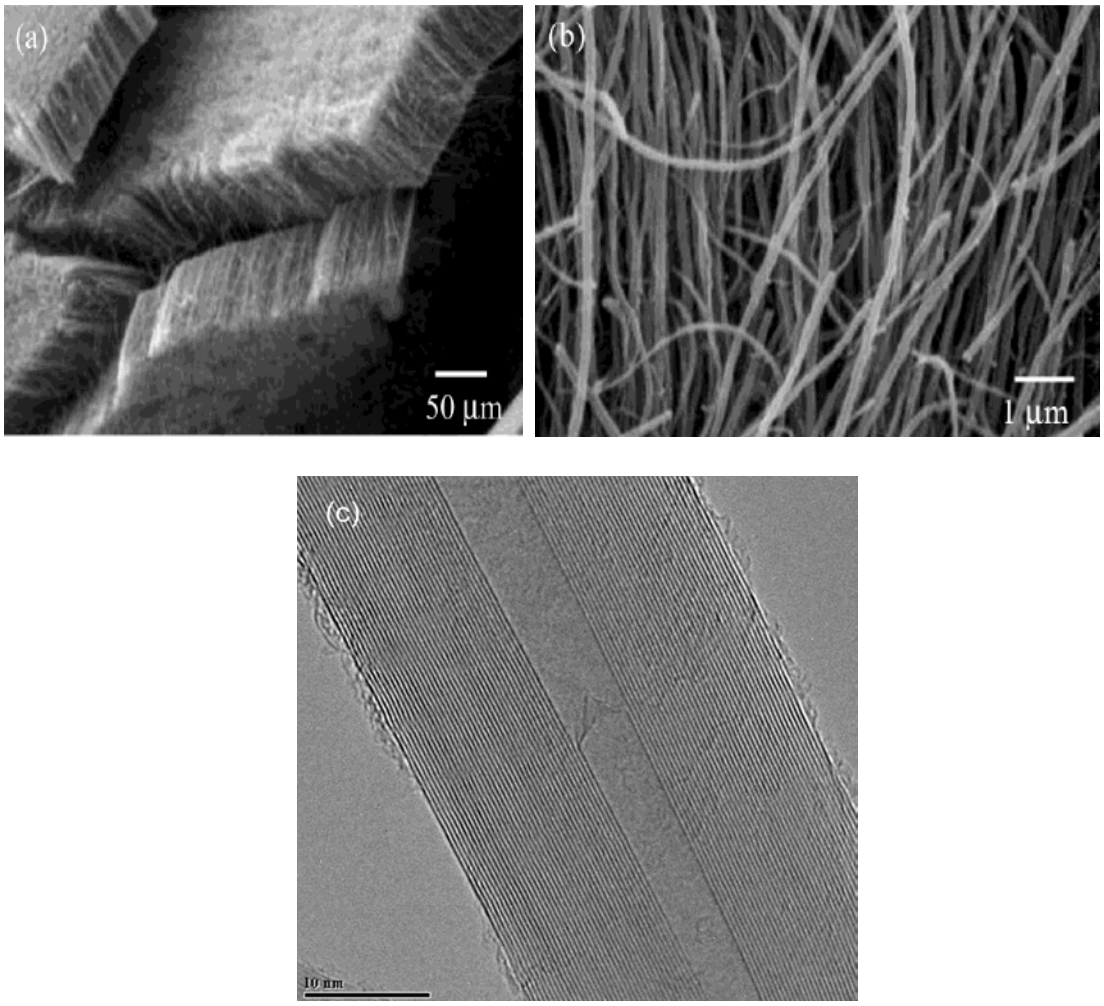

Figure 1-1: SEM images of MWCNTs
a) SEM image of aligned arrays of MWCNTs, b) SEM image of individual MWCNT[14]s, c) TEM image of a purified individual MWCNT

The unique physical properties of CNTs are the basis for the explosion of interest in the materials. Owing to its sp^2 hybridized carbon structure, an individual nanotube can have a tensile strength well over 50 GPa and a Young's modulus of more than 1TPa.[15] These values represent increases of up to 10-100 times over the same properties of other more common reinforcing materials such as stainless steel and Kevlar. While steel has a density of 7.85 g/cm^3, an individual carbon nanotube has a density around 1.3 g/cm^3,

giving it an extremely high strength-to-weight ratio, which is what makes CNTs ideal fillers for composites.[16]

Because of their extraordinary mechanical and electrical properties, carbon nanotubes are considered to be promising materials for a variety of applications, such as fillers for polymer matrices, [17-19] sensors, [20] field effect transistors, [21-22] and many others.

MWCNTs produced at the University of Kentucky Center for Applied Energy Research (CAER) are made by a catalytic vapor deposition (CVD) method as developed by Andrews, et al.[14] A prescribed mixture of xylene and ferrocene is injected into a multi-zone furnace, vaporized, and carried by an inert gas (He, Ar, or N_2). Once in the furnace, ferrocene decomposes and deposits iron nanoparticles on a quartz substrate. Once deposited, these nanocatalysts facilitate nanotube growth.

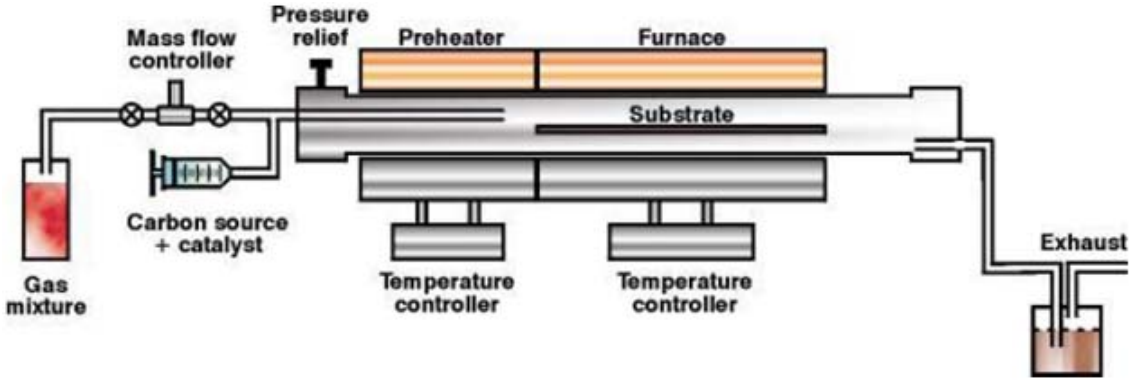

Figure 1-2: Schematic of CVD MWCNT synthesis furnace
Image from Reference[14]

Once the iron catalyst particles are deposited, MWCNTs can either be grown up from the catalysts in a root growth mechanism, or grown down from the catalysts in a tip growth mechanism as illustrated in figure 1-3 below. The growth mechanism is

dependent upon the structure of the catalyst particles and reaction conditions. MWCNTs grown at CAER are predominately of the tip-growth variety.

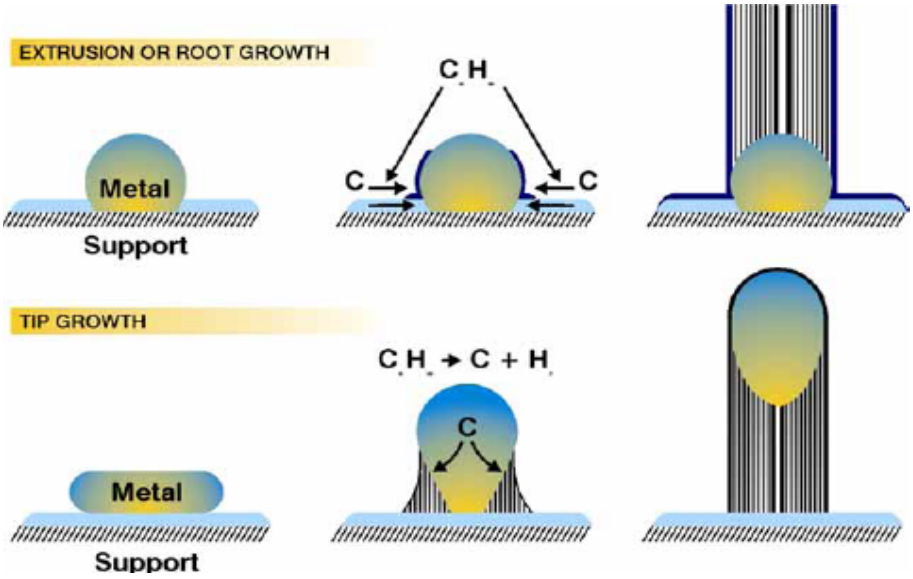

Figure 1-3: Schematic of root growth and tip growth of MWCNTs
Image from Reference[23]

While carbon nanotubes have been viewed as 'materials,' they are simply large aromatic compounds, and the chemistry of a variety of different types of aromatic compounds has been studied for many years. The reactions of more traditional aromatic compounds are very well known. Most small, planar aromatic compounds will react at their edges via electrophilic substitution reactions, retaining their aromaticity. However, due to their unique properties, some aromatic systems, such as fullerenes and graphite, undergo reactions of a different nature.[24] Having no edges on which to perform aromatic substitution reactions, and with highly distorted sp^2 C-C bonds, fullerenes readily undergo addition reactions in which the driving force for the reaction is the relief of angle strain.[25] In contrast, graphite is flat, with few edges. Therefore, electrophilic substitution reactions can take place at these edges, but only a small

percentage of a graphitic sheet is edges. Also, being flat, graphite does not readily undergo addition reactions due to the lack of a driving force (i.e. relief of angle strain) for such reactions to proceed.

As a class of aromatic compounds, carbon nanotubes can be considered to fall somewhere in between that of fullerenes and graphite. Smaller diameter tubes, like most SWCNTs, are more highly curved and might contain "fullerene-like" end caps.[26] In a larger diameter tube, like most MWCNTs, the surfaces become more graphitic and less curved, and thus should have reactivity more similar to that of graphite. In an ideal case, a CNT would have no edges, except at one open end of the tube due to the catalyst particle. However, in practice, the nanotubes produced today are far from ideal structures and have many defect sites all over their sidewalls, and thus many of the reactions that are not likely to take place on fullerenes and graphite should be possible, to an extent, on nanotubes.

While many different types, sizes, and structures of carbon nanotubes exist, it is in multiwalled carbon nanotubes that our interests lay, and as such we hope to investigate the main question "What is the chemistry of a MWCNT?" In doing so, we seek to answer a few more pointed questions regarding the chemistry of MWCNTs, specifically: What chemical transformations can be performed? Where do the reactions occur? What analytical methods can be used to characterize these reactions?

Chapter 2: Functionalized MWCNTs for use in Epoxy composites

Study of the chemistry of multiwalled carbon nanotubes is complicated by the fact that many traditional characterization methods used by organic chemists are not viable for characterizing chemical reactions on heterogeneous, insoluble material. Because they are insoluble, highly conductive, strongly adsorb light across a broad region of the electromagnetic spectrum, and are poorly dispersible in most solvents and polymer matrices, the common analytical methods used with small molecules (NMR, IR, and MS) are difficult or impossible to use for characterizing the chemistry of carbon nanotubes.

In the literature, the most widely used methods for the characterization of nanotube chemistry include Raman spectroscopy, [27] reflectance IR spectroscopy,[28] and thermal gravimetric analysis (TGA). [29] The use of Raman spectroscopy has been almost entirely confined to the study of single-walled nanotubes (SWNTs), as the spectra are fundamentally simpler in that system. Reflectance IR techniques have also been used to characterize chemically functionalized MWNTs, but this method has proven problematic in our hands. Solid state NMR has only rarely been used in the study of carbon nanotubes. [30-31] However, this method has a great deal of promise and is of future interest of this project, but to date has proven difficult in our hands.

In the absence of the traditional characterization methods, we have turned to using thermal techniques to evaluate the chemical changes we accomplish with these compounds. TGA (thermal gravimetric analysis), DSC (differential scanning calorimetry), and DMA (dynamic mechanical analysis) are a few of the techniques that are more common in the fields of polymer chemistry and materials science that we have decided

to utilize to help us determine if and in what way we have modified the surfaces of the MWCNTs. In order to utilize such thermal techniques, we have set out to investigate the chemistry of MWCNTs by reactions that introduce functionality which can be detected by thermal methods. The general plan of attack is shown below. A reaction that is intended to attack a particular site (or class of sites) on the nanotube is used to introduce a reactive group **R**. In the small-molecule context, the presence of this group would normally be detected by NMR or IR methods. In the CNT context we will detect reactive group **R** (and therefore determine the 'success' of the probe reaction) by observing the heat of reaction of **R** with a reactive partner **P**, chosen for well-precedented reactivity with **R**.

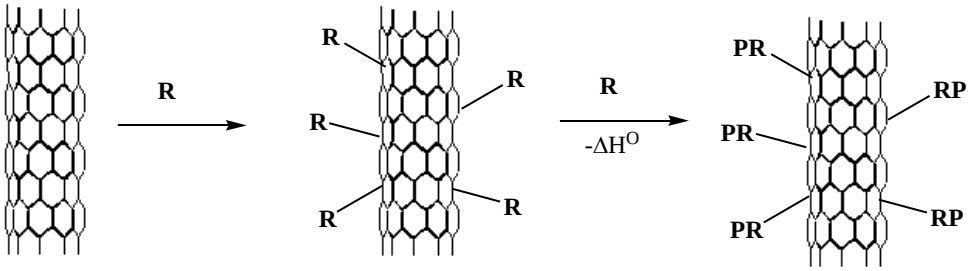

Scheme 2-1

Nucleophilic species such as alcohols and amines, as well as highly electrophilic species such as acyl chlorides, are a few of the functionalities that we have investigated through calorimetry. Amines and alcohols will react with epoxides and with isocyanates, both of which are readily available in suitable forms for DSC experiments. Acid chlorides will react with hydroxyls, again available in a host of different forms suitable for DSC experiments.

When attempting to chemically modify carbon nanotubes and to achieve the covalent attachment of new structures to the nanotube, it is intuitive to attempt the types of reactions that have been known to functionalize smaller, more pedestrian aromatic systems. Indeed, there have been reports of the reactions of MWCNTs under the conditions of electrophilic aromatic substitution, [32] oxidations, [33] and reductions [34]. Whereas oxidations and aromatic substitution reactions are likely to occur almost exclusively only at defect sites and at end caps of carbon nanotubes, the reduction of the nanotubes followed by subsequent alkylation or hydrogenation can presumably modify the tubes not only at defect sites and end caps, but also on the more graphitic surfaces.

While vigorous oxidations of CNTs are known to produce a significant number of carboxylate groups, they are also known to shorten the tubes. [35] These vicious reactions offer limited insight into the reactivity of the nanotube and have limited versatility in subsequent transformations. It is our objective then, to identify reactions that can introduce many reactive sites onto the surface of multiwalled carbon nanotubes, while still maintaining the overall integrity of the nanotube structure.

To do this, we have performed a multi-electron reduction of MWCNTs using a modification of the Birch reduction. [36] This *n*-fold reduction creates what we assume to be a highly delocalized nanotube carbon polyanion of charge n^-. From this point, a variety of alkylating agents, typically alkyl halides or alternatively a proton source, were

used to form a bond between the outer surface of the tube and the electrophilic element of the alkylating agent (or proton source). [34,37]

Noticeable differences could be observed between the thermal analyses of as-produced MWCNTs and MWCNTs that had been subjected to Birch reduction with NH_4Cl as the proton source. As the sample was heated from low temperature to high temperature in an air atmosphere, the first change in mass is a loss of mass that occurs near 300^{o}C (Figure 2-1). We believe that this loss of mass is likely due to the oxidation and loss of covalently bound atoms (in this case, hydrogen atoms) from the graphitic surface. It is possible that the loss of mass could be due to the expulsion of tightly adsorbed, non-covalently bonded small molecules. At such high temperatures, however, it is very difficult to imagine that any such adsorbed molecule would persist. In this particular system, the likely candidates for adsorbed impurities are lithium, ammonia, and hydrochloric acid; none of which are likely to be desorbed at this temperature.

The second observable change in the TGA thermogram is the drop in the onset temperature of combustion from 540^{o}C for as-produced MWCNTs to 525^{o}C for the hydrogenated MWCNTs. This is consistent with the covalent modification and subsequent disruption of the graphitic surface of the MWCNTs. We believe that the less ordered the nanotube surface becomes, the more vulnerable it is to oxidation. Therefore, it follows that a nanotube surface which has been modified to contain many sites of sp^3-hybridized carbons is likely to combust at a lower temperature than its more graphitic counterpart.

The third change that is visible in the TGA is the slight reduction in the amount of material that remains at high temperatures following oxidation. The iron catalyst particles that are used in the synthesis of the MWCNTs are oxidized in air during the TGA run, and persist to the 1000 ^{o}C limit of the TGA experiment. A slight drop (1-2%) in the amount of residue can be attributed to mechanical exfoliation of a small percentage of the nano-catalysts by stirring during the reaction, and the free particles are then removed during the washing procedure.

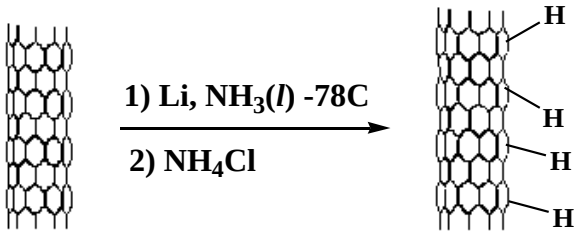

Scheme 2-2
Birch reduction of as-produced MWCNTs using ammonium chloride as a proton source

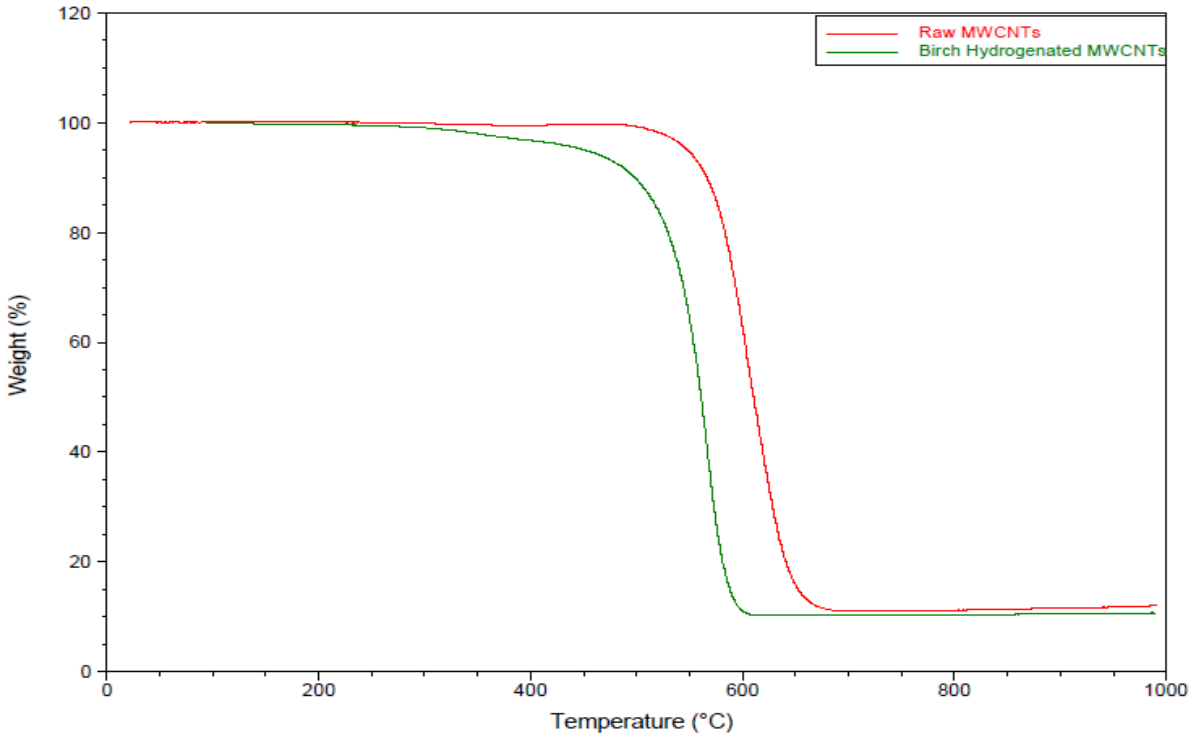

Figure 2-1: TGA of Raw vs Hydrogenated MWCNTs
TGA in air of as-produced MWCNTs and Birch-hydrogenated MWCNTs

While the Birch hydrogenation provides an initial proof-of-concept of the idea that the reductive alkylation approach is both reproducible and efficient in our hands, it does not provide a means for crosslinking into any polymer matrix.

We felt that by modifying MWCNTs with the appropriate functional groups that can react with the epoxy resin, we should be able to observe in the DSC the heat flow from an exothermic reaction corresponding to the cross-linking reaction. Many epoxy systems cure by reaction of an epoxy resin with a polyamine hardener which reacts by nucleophilic addition to the epoxide. Thus, our initial goal was to functionalize MWCNTs

with a derivative of TETA (triethylene tetramine) or DETA (diethylene triamine), both of which are traditional amine hardeners for epoxy systems. This would result in functionalized MWCNTs-based curing agents. Evidence that this system had been created and that it cross-links with epoxy resin would be demonstrated observation of an exothermic heat flow by differential scanning calorimetry (DSC).

We chose the approaches shown below to functionalize MWNTs. In both cases, Birch reduction was used to generate nanotube anions, which were alkylated with ethyl bromoacetate. These esters were then converted to the desired amides by standard means.

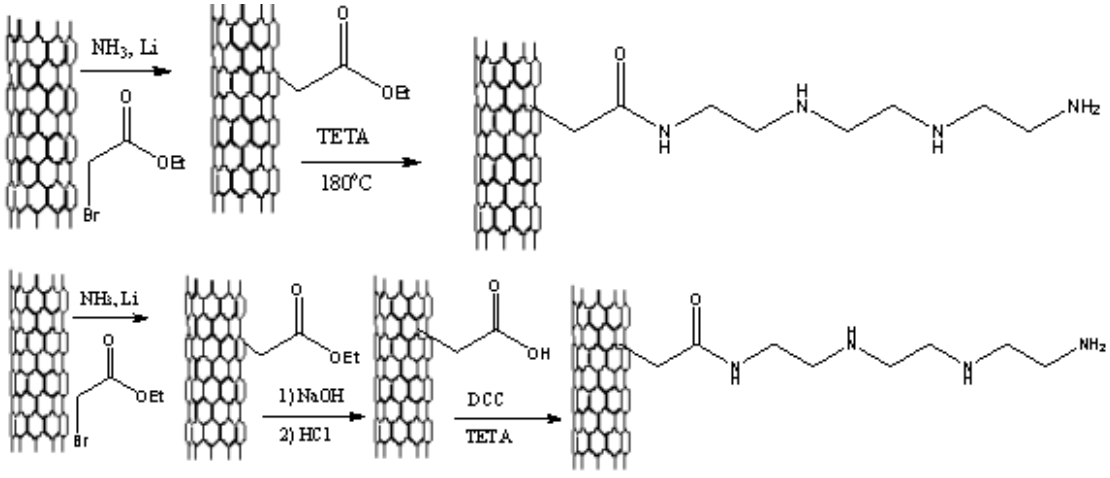

Scheme 2-3

Attempted reaction schemes to produce TETA-functionalized MWCNTs by
a) ester-amide exchange and b) peptide coupling

Samples for DSC were prepared by mixing MWCNTs with an appropriate amount of EPON 826 resin, transferred to a DSC pan and *topped but not sealed* with a DSC lid. The sample was then heated from room temperature to about 200^{o}C at a rate of 20^{o}C/min.

Neither of these routes produced material that showed consistent results in DSC experiments when mixed into the epoxy resin. On occasion, a small exotherm was observed but more often than not, no heat flow could be observed. It was our feeling that by performing the multiple functional group manipulation steps to get to the desired amide functionality, we were going from a very small percentage of ester functional sites (relative to the size of the nanotube) in the initial Birch functionalization step, to an even smaller number of amide functional sites in the final step. Therefore, in an effort to perform as few manipulations on the MWCNTs as possible, we synthesized a "complete" precursor that could be directly attached to the MWCNTs via the Birch reduction/alkylation reaction. To do so, it would be necessary to synthesize a molecule that contained both the amine functionality necessary for a cross-linking reaction with an epoxide, and an alkyl halide necessary to alkylate the MWCNTs as per the Birch procedure. Accordingly, we set out to prepare TETA amides of bromoacetic and bromovaleric acid. Specific examples of the attempted syntheses are shown below.

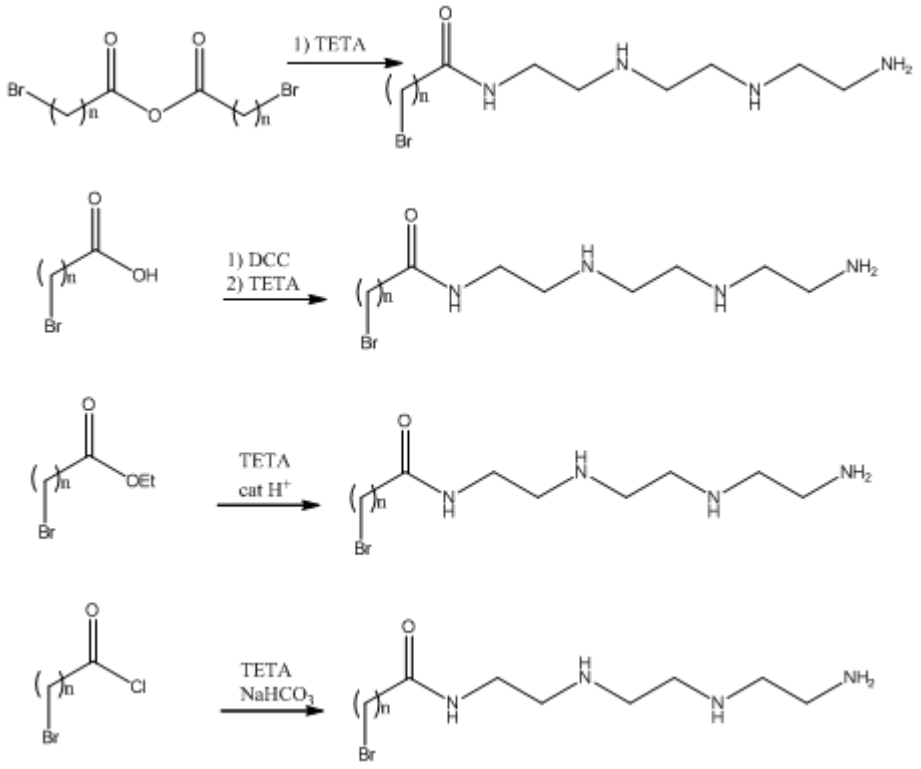

Scheme 2-4
Attempted reaction schemes to synthesize a TETA bromo amide precursor

As may be predicted, there exist a few fundamental difficulties in synthesizing the desired products. First, all of these bromoamide end products contain both a nucleophilic and an electrophilic moiety. It is possible that one of the free amines could cyclize by attacking the electrophilic carbon adjacent to the halide, or the material could simply polymerize. Such reactions would destroy the functionality needed to attach the molecule to the MWCNTs in the Birch step. The cyclization problem can potentially be minimized by manipulating the length of the carbon chain of the alkyl halide such that any intramolecular cyclization would result in a kinetically disfavored ring closing reaction[38]. A second problem that is apparent with this synthetic strategy is that the halo-carbonyl starting material has two different electrophilic centers. In principle, the

amine could not only attack the carbonyl carbon as desired, but could also attack the carbon bearing the halide, thus again removing the necessary functionality for alkylation of the MWNTs in the next step. We attempted to mitigate this problem by keeping the concentration of TETA low relative to the concentration of the halo-carbonyl compounds.

Ultimately, however, a solubility problem defeated this synthetic route. The ammonium salt by-product formed from most of these reactions was found to be only soluble in water. When we dissolved the reaction material in water and attempted to extract the desired product into an organic solvent, very little if any of the desired bromoamide could be removed from the aqueous phase, presumably due to its high solubility in water. In one instance, however, we were able to get what appeared to be some product into the organic phase. NMR spectroscopy indicated that we had a very impure product, but even so we decided to proceed with this material as the alkylating agent in the Birch step and got some initially promising results. The reaction scheme for this specific reaction is shown below.

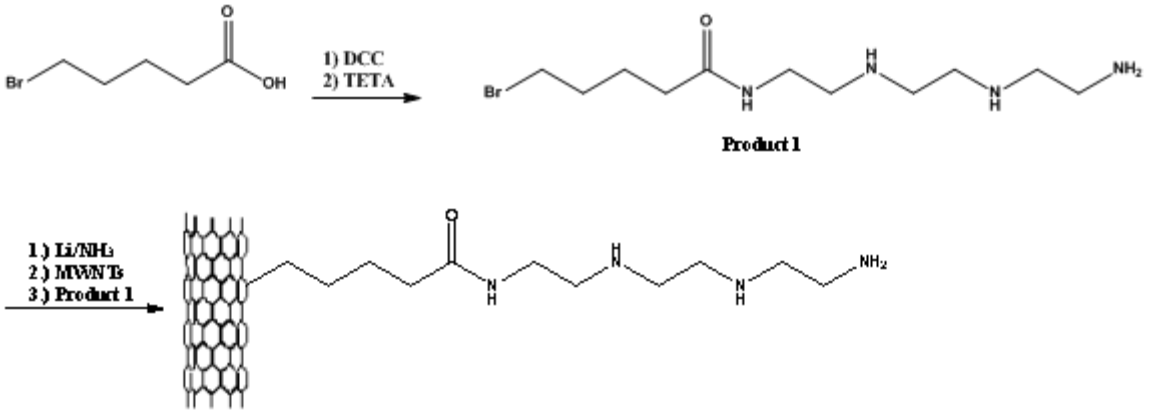

Scheme 2-5
DCC coupling of bromovaleric acid with TETA followed by Birch alkylation

The TGA thermogram of the functionalized MWCNTs shows a significant (~10-15%) mass loss around 200°C which, for a precursor molecule of this size, is consistent with the previously reported TGA data for smaller alkylating agents.

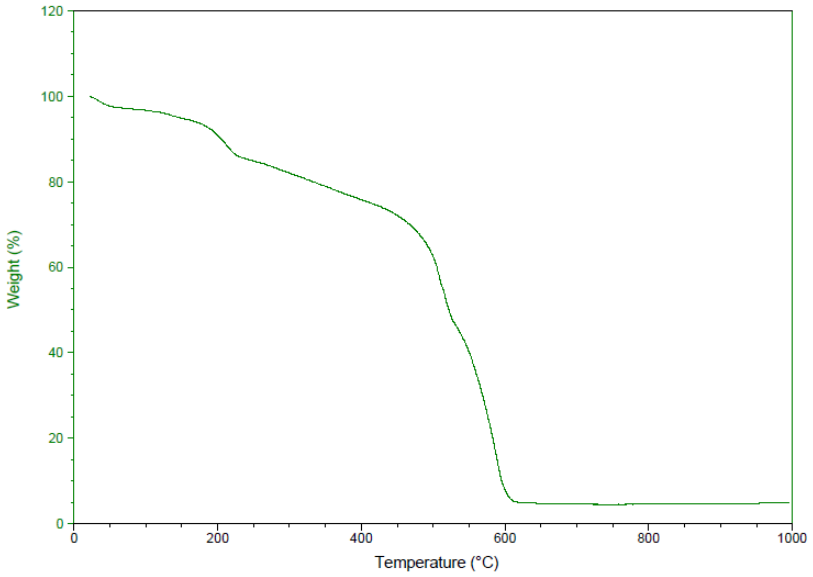

Figure 2-2: TGA of TETA functionalized MWCNTs

When this sample was mixed into the EPON826 resin, an exothermic reaction could clearly be observed by DSC in the temperature range expected.

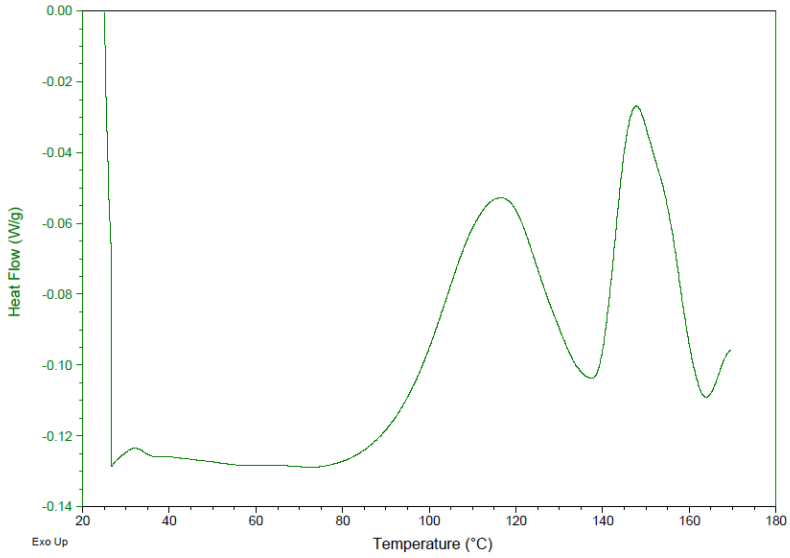

Figure 2-3: DSC of TETA functionalized MWCNTs mixed with EPON 826 resin

Control experiments that were conducted with unfunctionalized MWCNTs did not exhibit this exotherm. The two step exothermic process observed can be attributed to two different phases of TETA reacting with the EPON 826 resin. The first exotherm is over the temperature range in which TETA reacts with the resin when no nanotubes are present, and the second exotherm is likely a surface effect of bound (either covalently or tightly adsorbed) TETA reacting with the EPON resin. If the observed exotherm is due to reactions involving the nanotubes, the total heat liberated should be proportional to the amount of nanotube present in the sample (the MWNT loading). However, due the inefficient extraction of the bromoamide from the aqueous phase, only a very small quantity of functionalized MWNTs was available, thus a loading study of increasing nanotube concentration could not be performed. The attempts to synthesize more

starting material were not effective for the reasons stated above. This result was significant because it was our first indication that the reaction of epoxy resin with MWNTs functionalized by the reduction/alkylation method could be observed in the DSC experiment.

The next advance on this project came when we attempted to cross-link functionalized MWCNTs into a polyurethane matrix. We prepared acid chloride functionalized MWCNTs in hopes of reacting them with the polyol portion of polyurethane. The synthesis is shown below.

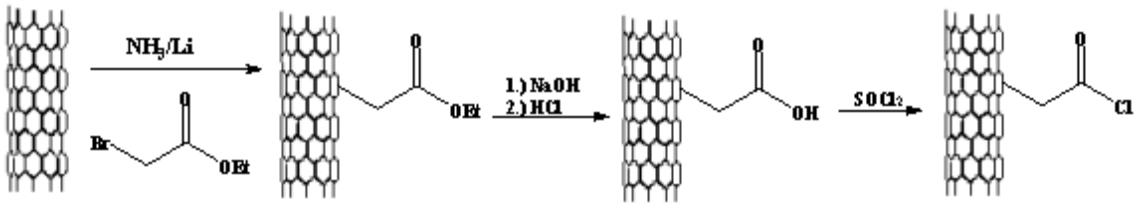

Scheme 2-7
Synthesis of acid chloride functionalized MWCNTs by an alkylation-saponification-chlorination route

Upon hand mixing of the acid chloride functionalized MWCNTs with the polyol, a reaction could be visibly observed as the mixture gave off fumes (presumably HCl). The reaction could not be observed in the DSC because it likely occurs before we can manually get the mixed sample into the DSC and drop the temperature. This is not unexpected as the reactions of acid chlorides and water (which is a major component in the polyol portion of the polyurethane mixture) are known[39] to take place rapidly at room temperature.

Having produced a functionalized nanotube sample that we believed to be capable of reacting with a polymer matrix, we decided to investigate how it would react with an epoxy. The epoxy system we used consisted of EPON 826 resin, a bisphenol-A (BPA) derivative, Nadic methyl anhydride (NMA) as a hardener, and a catalytic amount of EMI-24 (2-ethyl, 4-methyl imidazole). From the molecular weight of the resin provided by the manufacturer (178-186g/eq weight per epoxide, Hexion), we determined that the resin is likely a mixture of oligomers where n is approximately 2.5, and the most likely oligomeric linkage is between two epoxy groups giving rise to a glycerol moiety with a free hydroxyl at each linkage (figure 2-4).

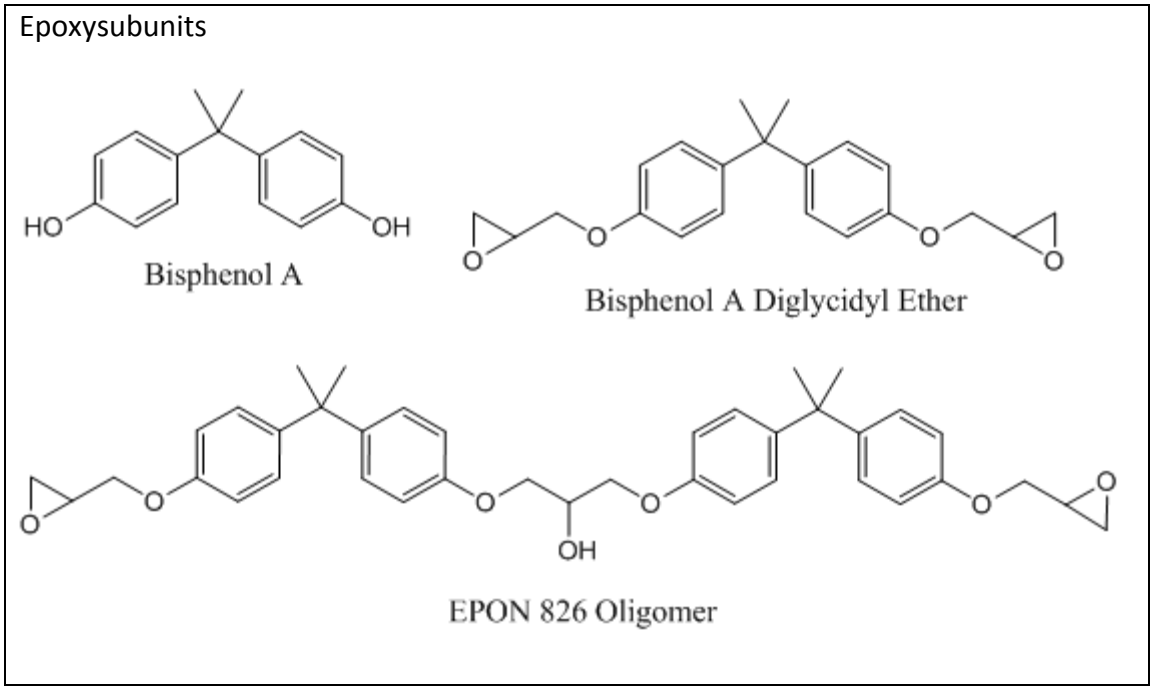

Figure 2-4: Subunits and oligomers contained within EPON 826

The proposed mechanism for epoxy crosslinking involves the activation of the anhydride functionality by nucleophilic attack of the imidazole catalyst creating a free carboxylate which can react via a Sn2-type mechanism with an epoxy group, giving the expected ester linkage (figure 2-5). This generates a free alkoxide group, which can then react with another equivalent of anhydride in an acyl addition/elimination reaction to generate another carboxylate, thus propagating the chain reaction. It is possible for the carboxylate to react with another equivalent of anhydride, but this will simply generate an acyclic anhydride that will be cleaved by an alkoxide.

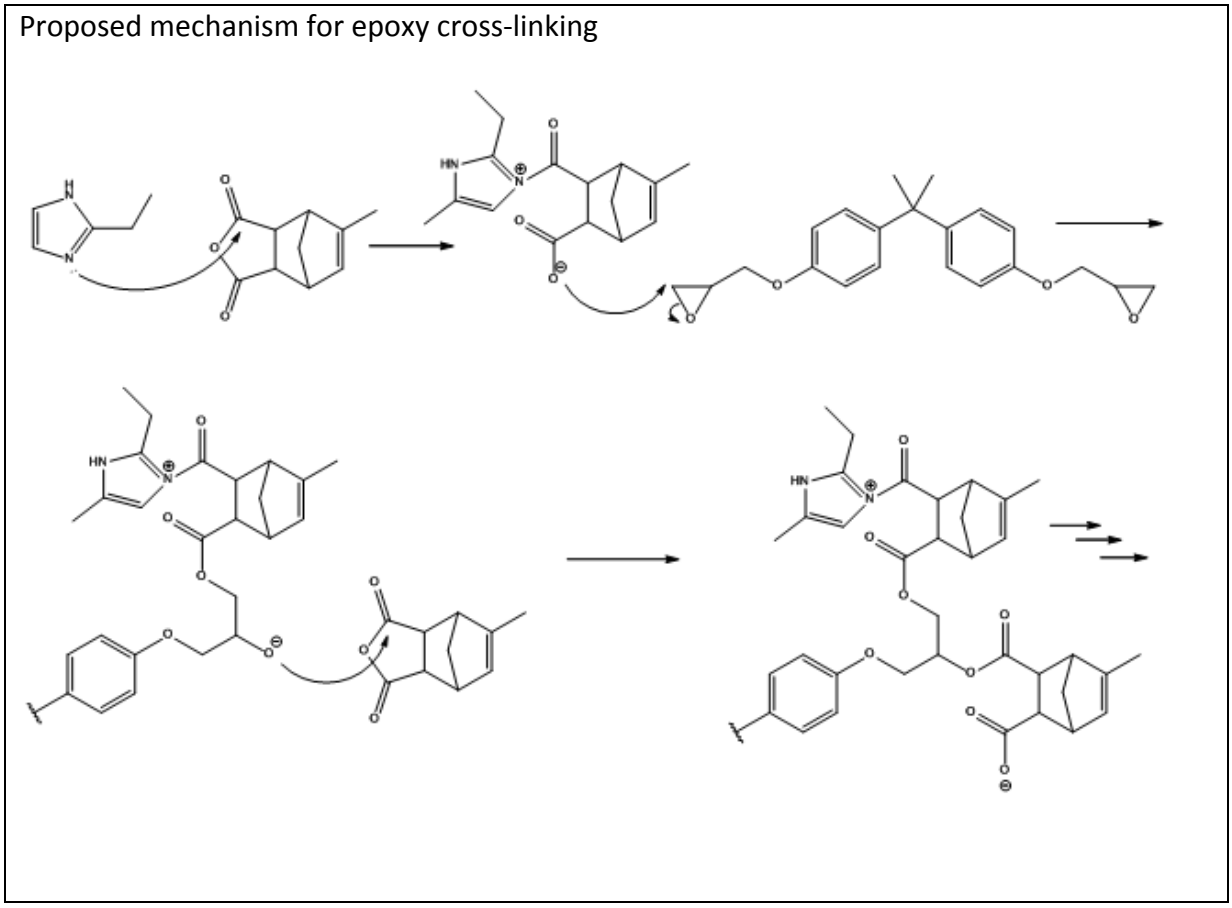

Figure 2-5: Proposed mechanism for imidazole catalyzed crosslinking of epoxy resin with anhydride hardener

The catalyst is regenerated by attack of an alkoxide or carboxylate ion with the N-acyl imidazolium ion, giving rise to either an ester or anhydride linkage.

Once the polymerization reaction is initiated, a series of ester linkages are formed in one of two ways. Either an alkoxide anion reacts with an anhydride in an acylation reaction thus generating a new carboxylate, or a carboxylate anion reacts with an epoxide carbon (likely the least substituted) in an Sn2-type displacement, thus generating a new alkoxide (Figure 2-5).

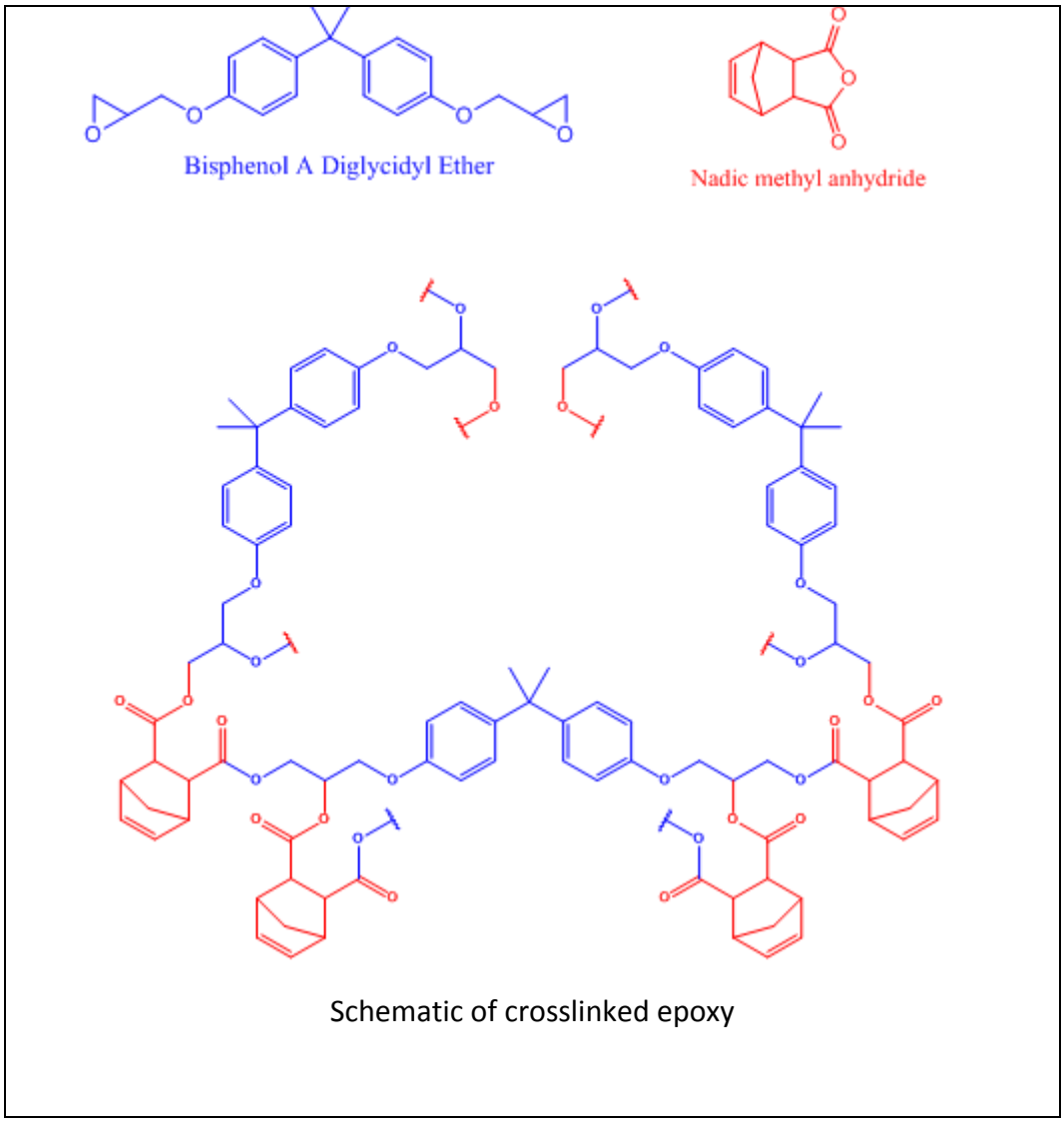

Figure 2-6: Schematic of crosslinked bisphenol-A diglycidyl ether monomers with NMA

Heat Flow of functionalized MWCNTs in EPON 826

When the acid chloride functionalized MWCNTs were mixed with the EPON 826 resin, we were able to witness an exothermic reaction in the DSC. Thus, it follows that if the concentration of functionalized MWCNTs in epoxy resin were increased, we should be able to observe a linear increase in the total heat that is produced by the crosslinking reaction. When we mix raw as-produced MWCNTs with EPON 826 resin, no exothermic

reaction is observed by DSC; even at loadings up to 25 wt%, demonstrating that raw MWCNTs are not reactive with epoxy resin. Using an average of 3 runs at a loading of 1 wt%, the integrated heat flow measured by DSC was calculated to be 0.67 J/g. When the loading was increased to 3 wt%, an integrated heat flow of 1.49 J/g was calculated. At loadings of 5 wt% and 10 wt% MWCNTs, integrated heat flows were calculated to be 3.52 J/g and 5.51 J/g, respectively (figure 2-8).

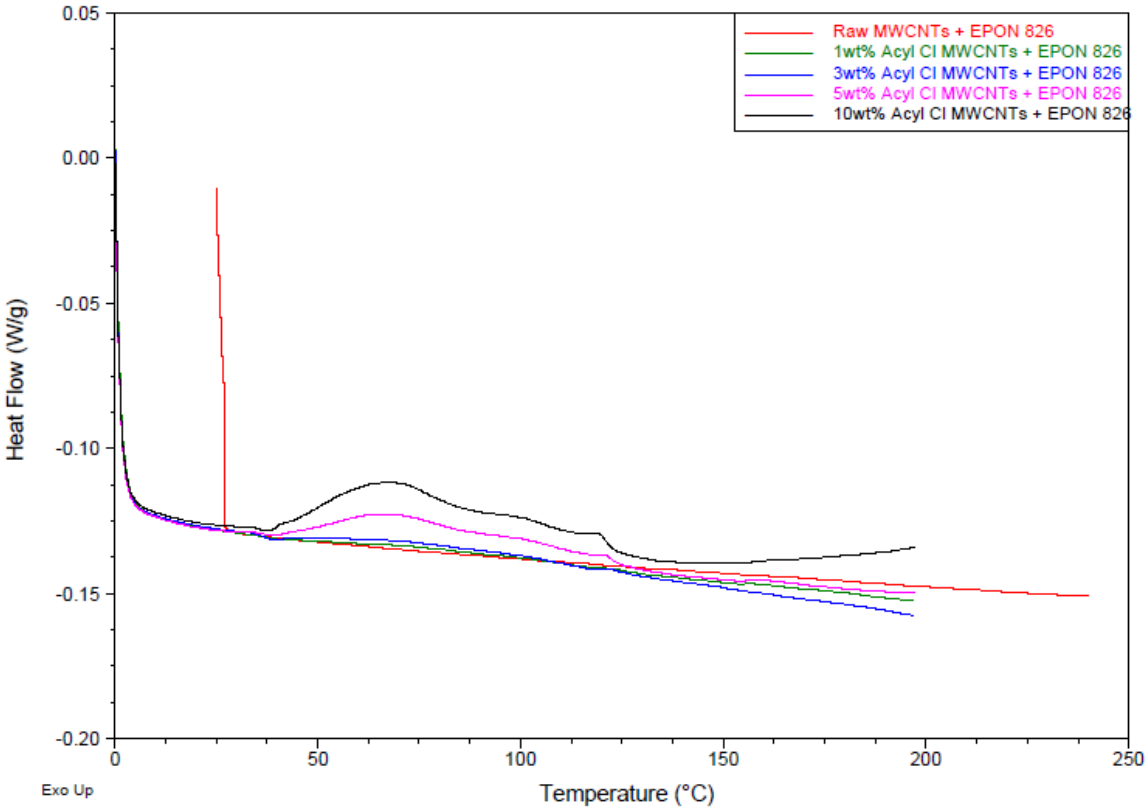

Figure 2-7: DSC of 1,3,5,10 vol% Acid Chloride MWCNTs in EPON826
DSC thermogram of stepwise increasing loadings of acid chloride functionalized MWCNTs with EPON 826 resin

When these data are plotted in a graph of heat flow versus the percent loadings of acid chloride functionalized MWCNTs (figure 2-7), the linear nature of increase in heat flow is

clear. At the highest loading we attempted (10 wt%), the heat flow value falls slightly below the linear relationship that was observed at lower concentrations. This can easily be rationalized by the inability to thoroughly mix the samples at such a high loading. At 10 wt%, the samples are extremely dry and difficult to mix, and with a system as reactive at the acid chloride MWCNTs, milling (which will be discussed) is not a practical mixing method for the DSC experiment. In order to achieve the maximum exotherm, every functionalized nanotube must be thoroughly wetted by the epoxy resin. At increased loadings, however, it becomes increasingly more difficult to wet out every individual MWCNT, or even to wet out the entirety of each MWCNT. Thus, some of the acid chloride functionality are unavailable to crosslink with epoxy resin. It should follow, then, that if it were possible to effectively mix higher and higher loadings of functionalized MWNCTs into EPON 826 resin, then the amount of heat flow observed would asymptotically approach a value such that further increased loadings of MWCNTs would have no impact on the observed heat flow. As molecular motion becomes more restricted, fewer and fewer epoxy molecules would be capable of interacting with the nanotube crosslinkers. Due to the impracticality of mixing such high loadings, however, this experiment was not performed.

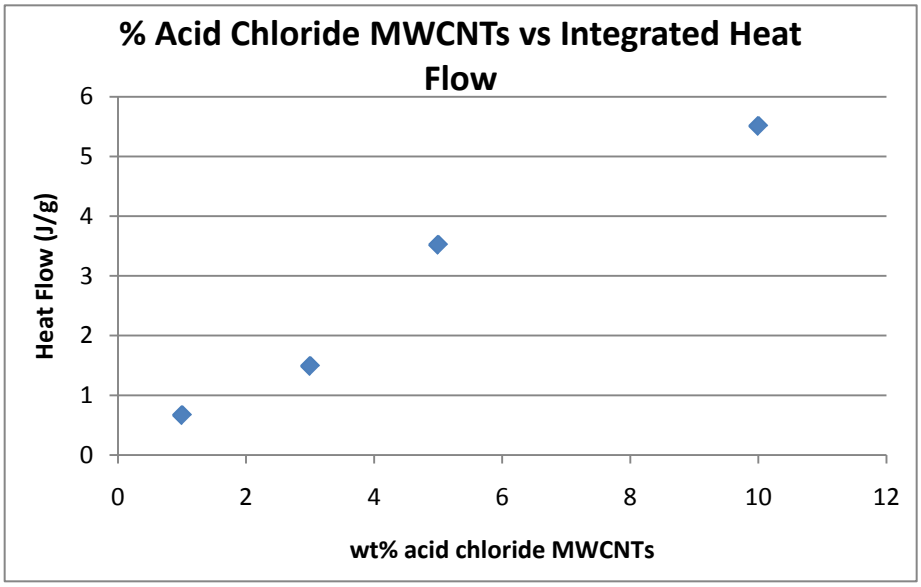

Figure 2-8: Plot of total heat flow versus wt% acid chloride MWCNTs in EPON 826

If the epoxy resin consisted solely of bisphenol-A diglycidyl ether monomer, it would be difficult to understand how the acid chloride functionalized MWNCTs could effectively crosslink with the matrix. However, since we know that the EPON 826 resin is mixture of oligomers, it is intuitive that the secondary hydroxyls created by epoxy-epoxy linkages are likely the nucleophilic component in the functionalized nanotube-epoxy crosslinking reaction (figure 2-9).

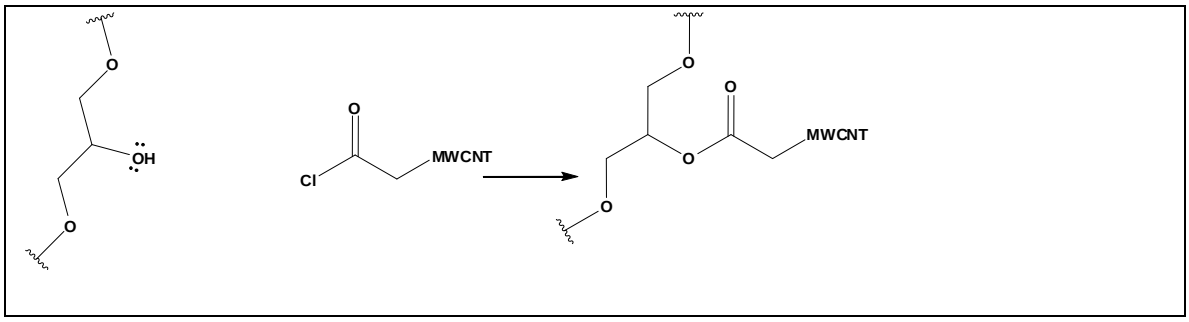

Figure 2-9: Proposed mechanism for the crosslinking of EPON 826 oligomers with acid chloride functionalize MWCNTs

In the preparation of MWCNT-epoxy composites, thorough mixing and dispersion of the nanotube filler is important for consistency between samples and for full realization of the potential of the filler. In order to achieve good dispersions, two main mixing techniques were used. First a Thinky® planetary mixer was used, in which the sample is placed in a cup shaped container, then rotated in a planetary manner, causing centripetal force to constantly push the sample out to the wall of the container, while continuously pushing the sample down in a spiraling direction along the container wall. Second, a 3-roll mill was used to mix by passing the samples between two stainless steel rollers, turning at different speeds, at a fixed distance. The sample then passes up through the middle roller and a third roller moving at an even higher speed (again at a fixed distance) and is finally deposited on a collection tray.

Preparation of epoxy-nanotube composites

An epoxy system consisting of EPON 826 (resin), nadic methyl anhydride (NMA, curing agent) and 2, 4-ethyl methyl imidazole (EMI-24, catalyst), in a ratio of 100:85:1 respectively, was used in preparing epoxy- carbon nanotube composites containing 0, 1,

2, 5 and 10 vol% nanotube filler in the following manner: The appropriate amounts of EPON 826, NMA, and CNTs were mixed in a Thinky® planetary mixer for 3 minutes at 2000 rpm, and then defoamed for 2 min at 2200rpm. This served to mix the nanotube powder into the liquid epoxy resin, so it could be further mixed. This mixture was then placed on an EXAKT 80E 3-roll mill and mixed 5 times using the following protocol:

Pass	Gap 1 (μm)	Gap 2 (μm)	Speed (rpm)
1	50	40	200
2	25	20	200
3	10	5	200
4	5	5	250
5	5	5	250

Table 2-1: 3 Roll Mill sequence

Once milling was complete, the EMI-24 catalyst was added and the planetary mixing procedure was repeated in order to disperse the catalyst throughout the sample. The epoxy-nanotube mixture was then poured into 80mm x 10mm x 2mm PTFE molds and placed under vacuum at 60 ^{o}C for 30 minutes. The samples were then removed from the vacuum, placed in a programmable furnace, and cured with the following protocol: heated at 50 ^{o}C for 6 hours, warmed to 150°C at 0.5 ^{o}C/min, and held at 150°C for 3 hours. Cured samples were cut into 30mm x 10mm x 2mm rectangular specimens. These samples were smoothed and polished to 600 grit, and measured prior to DMA testing. Samples were subjected to single cantilever bending measurements. Sample deflection was 5 microns at a fixed frequency of 1 Hz, carried out over a temperature range of 100 ˚C to 200 ˚C at an applied heating ramp of 2 °C/min.

DMA Analysis.

Summary

The overriding generality of the DMA results was as follows; 1-2 vol% of raw or acid functionalized MWCNTs was insufficient to cause significant changes in the visco-elastic response of the composite when investigated by single frequency DMA (1Hz) under a small applied strain over a range of temperatures that included the glass transition temperature (Tg) event. However, composites containing 5 and 10 vol% MWCNTs, of any variety, were sufficient to increase the glassy storage modulus by up to 43% over the modulus of neat epoxy. 10 vol% acid MWNTs yielded the best reinforcement by 6% over 10% raw MWNTs at 25 °C (up to 3.23 GPa), while 5 vol% acid chloride MWNTs yielded the best reinforcement by 23% over 5% raw MWCNTs. With respect to changes in Tg, 10 vol% acid chloride MWCNT-epoxy clearly shifted it to lower temperature by approximately 14 °C. In contrast, 1 to 2 vol% acid chloride MWNT-epoxy was slightly effective for shifting the T_g event to higher temperatures.

Storage Modulus

The storage modulus, E', is the constant of proportionality between the applied strain (from the 5 micron deflection) and the resulting stress (the force required to produce the strain) that is in phase with the applied strain. It only applies to the portion of the applied strain energy which is stored in the sample as elastic strain, and is completely reversed upon release of the applied deflection (at fixed temperature and deflection frequency). In the most basic sense, it is a gauge of the stiffness of the material, and quantifies the elastic character of a visco-elastic material. Here, composite specimens

of differently functionalized MWCNTs in an epoxy matrix were evaluated. Across all observed DMA data, no secondary peaks or transitions emerged from the neat epoxy background; which is to say that the MWCNTs, apart from any functionalization, did not promote the formation a second, discrete visco-elastic phase, but were found to only shift the magnitude or temperatures of the neat epoxy-background transitions. Very little contrast in peak shape was observed between neat and MWCNT composite epoxy. Changes in peak shape would indicate the emergence of separate, discrete visco-elastic phases, or indicate that the MWCNTs were preferentially associating with only a given population of the epoxy matrix, leaving the remaining population unchanged.

As expected, the composite storage modulus increased with MWCNT content in the glassy region with respect to both MWCNT concentration and functionalization type. This is shown in Figure 2-11. At 100^{o}C, a 5% increase in E' over neat epoxy was observed in 5 vol% raw MWCNTs, while a 42% increase was observed in 10 vol% raw MWNTs (Figure 2-10). At identical conditions, acid-functionalized MWCNTs performed slightly better showing an 11% increase in E' at 5 vol% and a 48% increase at 10 vol% (Figures 2-13, 2-14). Acid-chloride functionalized MWCNTs performed a bit better than the others, in terms of increasing E'. 5 vol% increased E' by 28%, and 10 vol% increased E' by 46% (from 2.04 to 2.98 GPa at 100 ºC) (Figure 2-12). Overall, 5 vol% acid chloride MWCNTs most efficiently increased the glassy-region storage modulus of the epoxy matrix, +28% (Figure 2-13), while 10 vol% acid MWCNTs had the largest effect at +48% (Figure 2-14).

Generally, with respect to the glassy E', samples prepared with the acid chloride functionalization performed slightly better than the others.

A few interesting observations can be made from this set of data. First, the acid functionalized MWCNT composites performed better than as-produced MWCNT samples in all cases, and as well as the acid chloride MWNCT samples at 10 vol%. This is intriguing because previous DSC studies did produce an observable heat flow that would have indicated an exothermic reaction when acid MWCNTs were mixed with EPON 826 resin, even at high loadings, suggesting that a crosslinking reaction is not likely to be occurring in those cases. As such, one would not expect the acid functionalized MWCNTs to significantly improve the storage modulus over the modulus observed in composites containing as-produced MWCNTs. This phenomenon can be explained, however, as an issue of processability. In *all* cases, functionalized MWCNTs lowered the viscosity of the MWCNT-epoxy composites relative to composites made at the same loading but using raw MWNTs, thus significantly improving their processability. Because of this, MWCNT dispersions were increased, and thus a decrease in the concentration of defects in the composite samples. At 10 vol% loadings of both functionalized MWCNT samples and as-produced MWCNT samples, however, the observed E' were very similar (although slightly greater for functionalized samples). At such high loadings, the viscosity of all samples was very high and the processability of all samples could be classified as "poor." Due to the high loadings, poor processability, and, consequently,

the increase in defect concentration, the effects of any crosslinking from the MWCNTs to the matrix are essentially nullified.

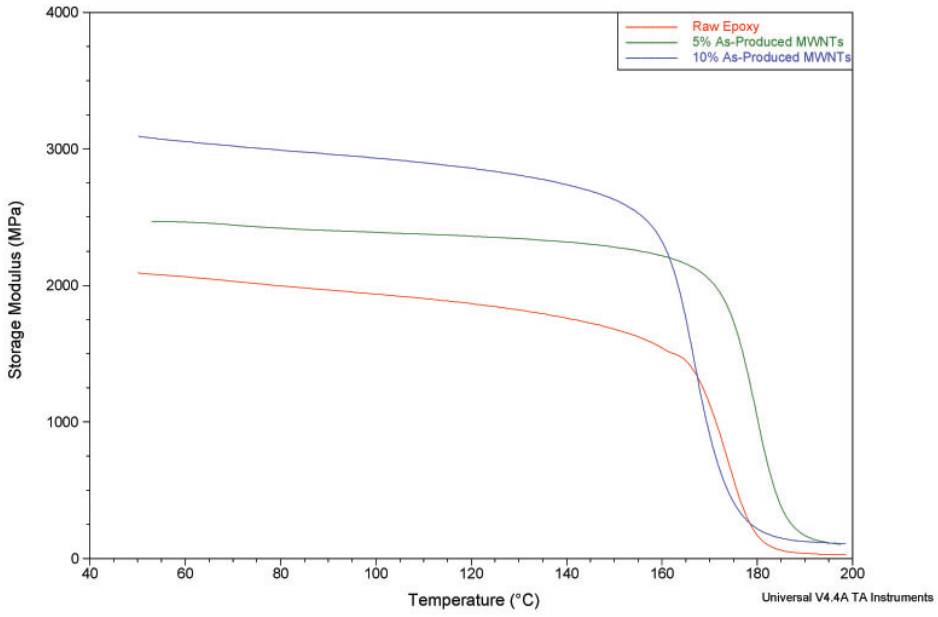

Figure 2-10: DMA overlay of Raw Epoxy, 5, and 10vol% As-Produced MWCNTs

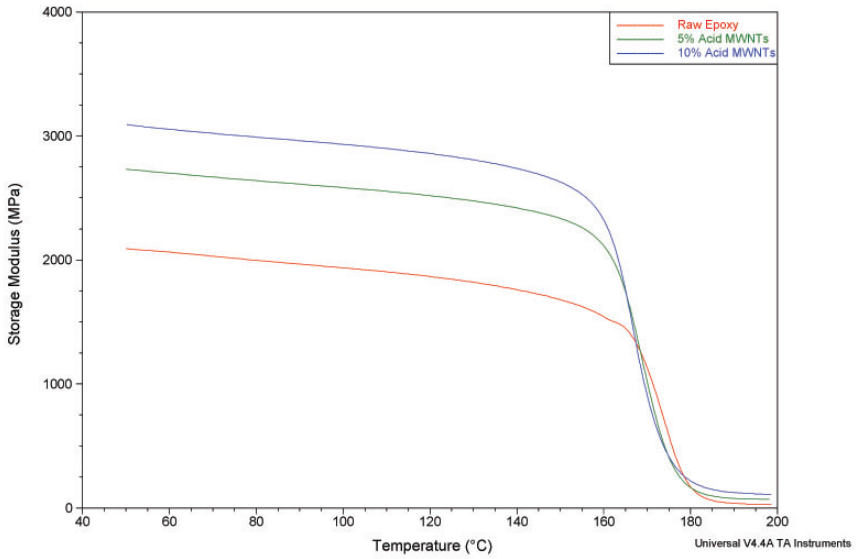

Figure 2-11: DMA overlay of Raw Epoxy, 5, and 10vol% Acid MWNTs

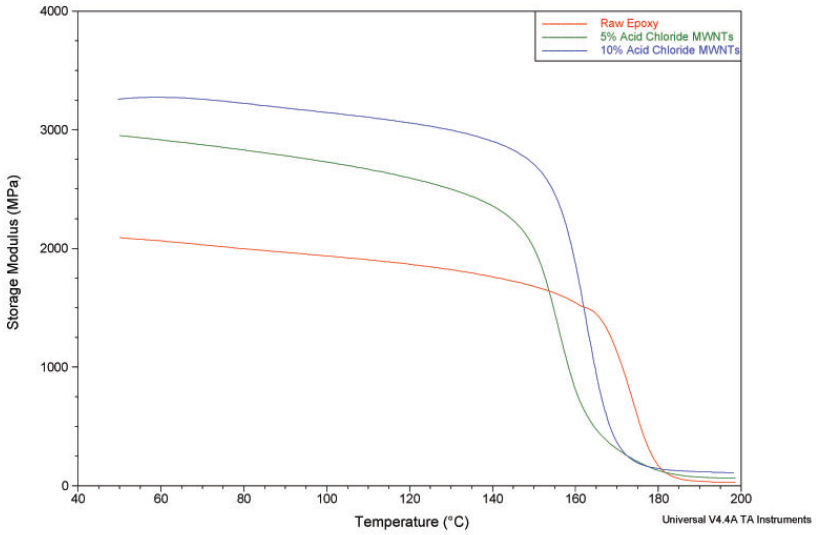

Figure 2-12: DMA overlay of Raw Epoxy, 5, and 10vol% Acid Chloride MWNTs

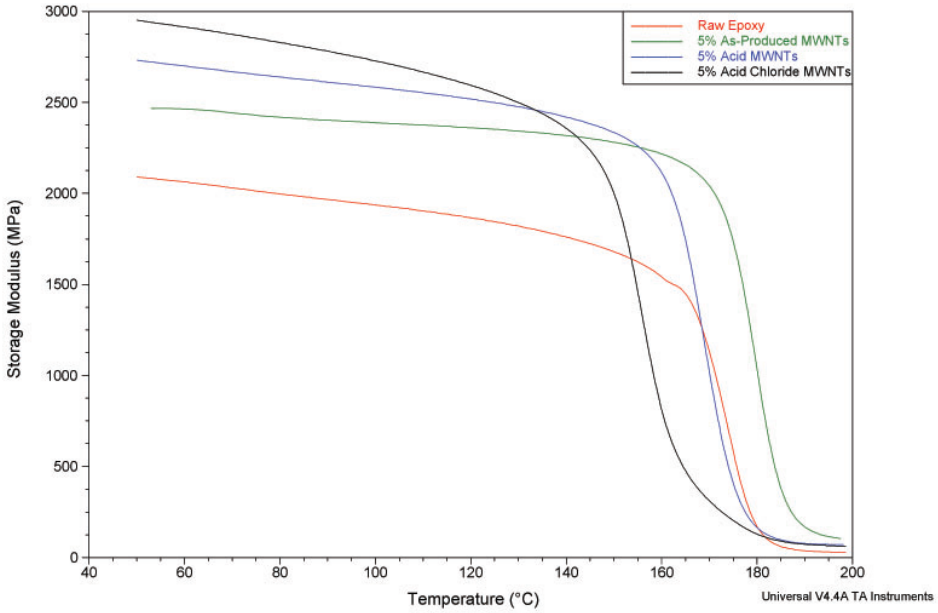

Figure 2-13: DMA overlay of Raw Epoxy, 5vol% As-Produced MWNTs, 5vol% Acid MWNTs, and 5vol% Acid Chloride MWNTs

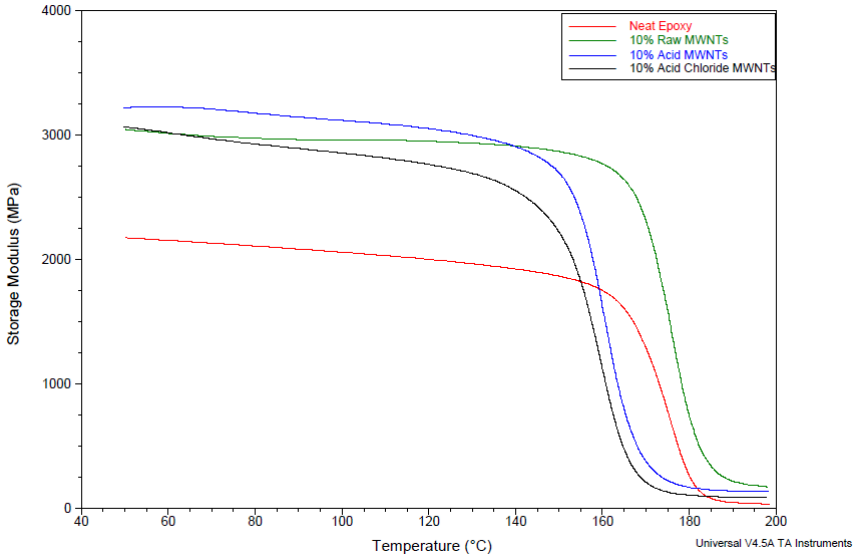

Figure 2-14: DMA overlay of Raw Epoxy, 10vol% As-Produced MWNTs, 10vol% Acid MWNTs, and 10vol% Acid Chloride MWNTs

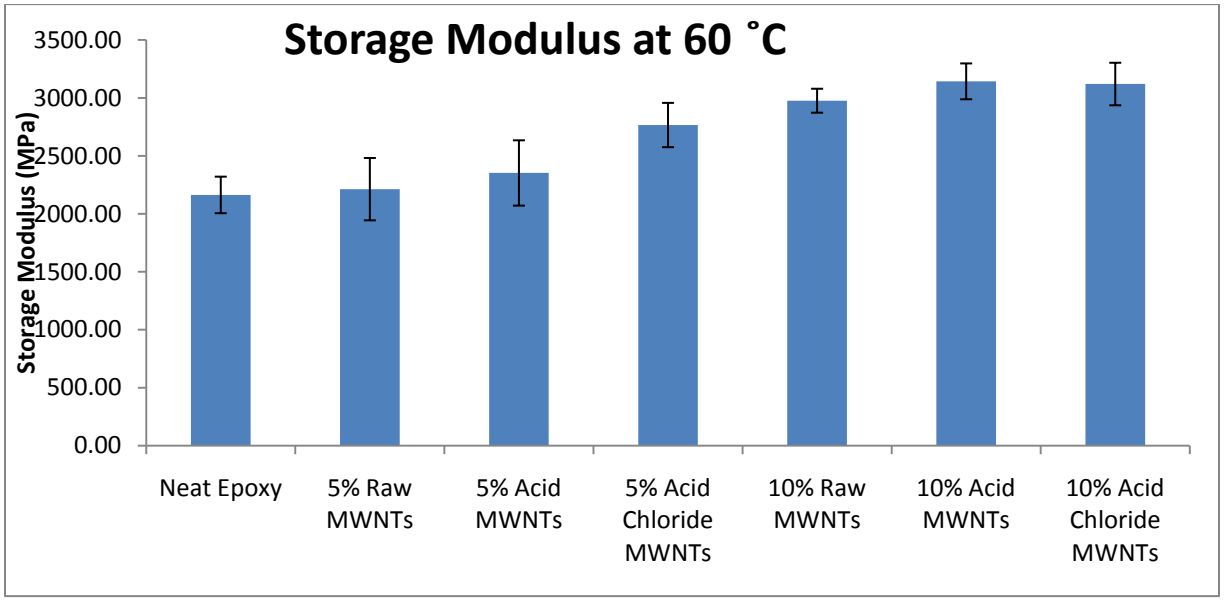

Figure 2-15: Comparison of Storage modulus of MWCNT-epoxy composites

In the region of the glass-rubber *transition* (T_g) the storage modulus (E') results were examined in terms of event temperatures; onset and deset of the step-wise drop in E' with increasing temperature (the temperature corresponding to the maximum rate of change in E' will be later evaluated using the peak of the loss modulus E"). We will use the term "deset" to describe the end of the glass-to-rubber transition event where the material comes out of the transition and is converted to its rubbery state. Both onset and deset temperatures were studied to gain insight into the effects the MWCNTs had on the elastic character of the epoxy matrix throughout the entire T_g event transition, not just at a single, arbitrary T_g temperature (ie. inflection of E', peak of E", or peak of tan δ), as shown in Figure 2-16. It should be noted that event temperatures are considerably more reproducible than are magnitudes of the mechanical properties, due

to the fact that Tg is not a function of sample dimensions while mechanical properties can be strongly affected by defects and other sample-specific characteristics.

Apart from increasing the magnitude of E', it was expected that the addition of MWCNTs that form strong bonds to the epoxy matrix would cause the T_g event to shift to higher temperature as the MWNTs would function collectively to pin large-scale molecular motion between adjacent regions of cross-linked epoxy. However, this increase in Tg was not always observed. With respect to the T_g event onset, the only positive shifts observed, relative to neat epoxy (172^{o}C) occurred with 5 and 10 vol% raw MWCNTs (+5^{o}C and +1.5^{o}C, respectively). Similarly for the T_g event deset, shifts in the same materials relative to neat epoxy (180^{o}C) were noted for 5 and 10vol% Raw MWCNT (+5.5^{o}C and +3^{o}C, respectively).

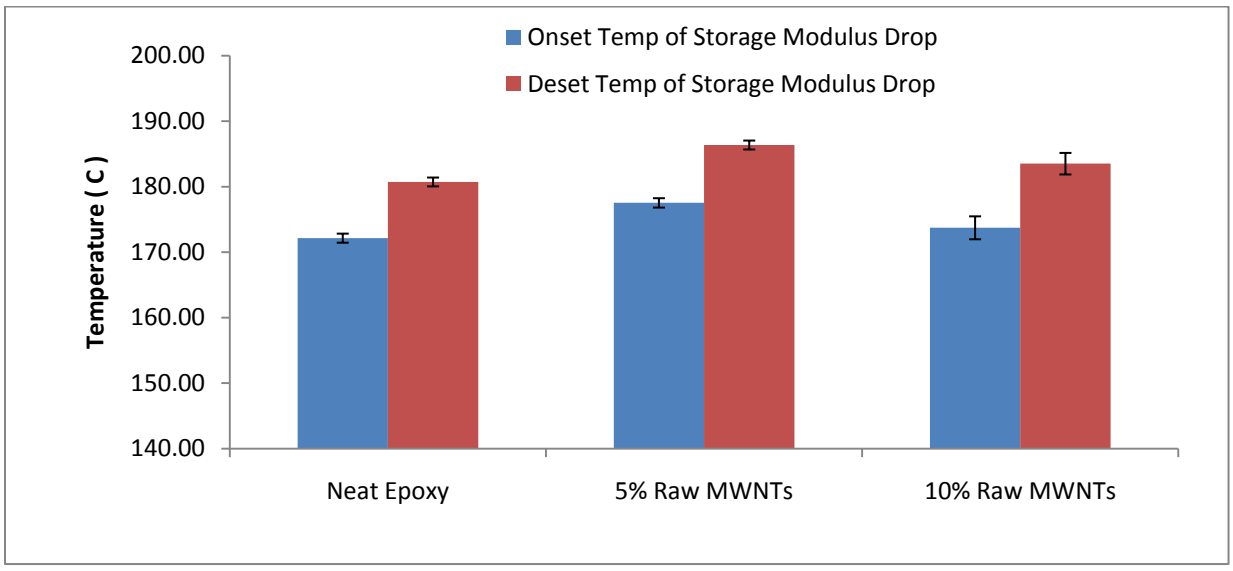

Figure 2-16: Comparison of Storage Modulus Onset and Deset Temperature for Neat Epoxy, 5 vol%, and 10 vol% Raw MWCNTs

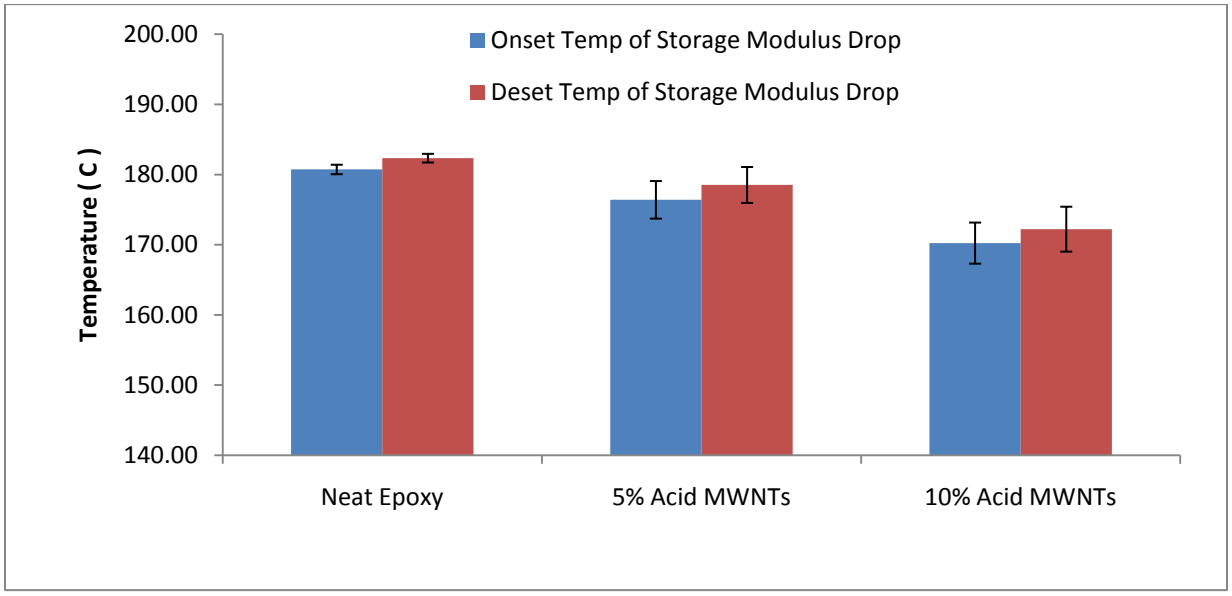

Figure 2-17: Comparison of Storage Modulus Onset and Deset Temperature for Neat Epoxy, 5 vol%, and 10 vol% Acid MWCNTs

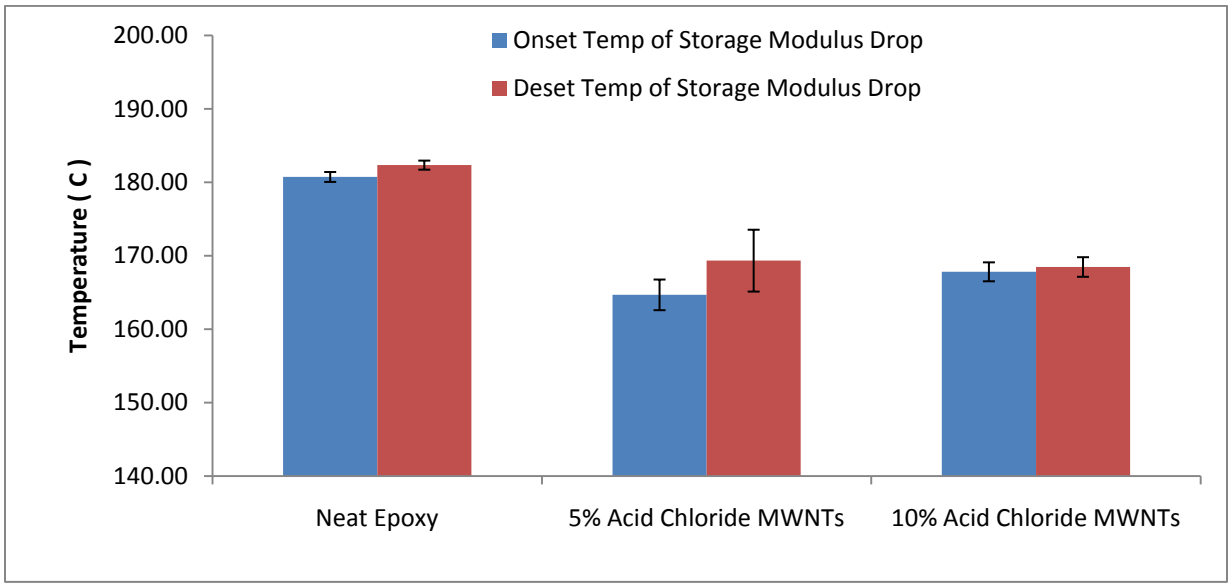

Figure 2-18: Comparison of Storage Modulus Onset and Deset Temperature for Neat Epoxy, 5 vol%, and 10 vol% Acid Chloride MWCNTs

With composites prepared with functionalized MWCNTs, both the acid and acid chloride functionalized nanotubes resulted in a decrease in both onset and deset temperature relative to neat epoxy. In samples containing 5 and 10 vol% acid functionalized MWCNTs, the onset temperature shifts to lower temperatures by $6^{o}C$ and $13^{o}C$, respectively, while concurrent shifts in the storage modulus deset temperature of $4^{o}C$ and $10^{o}C$ to lower temperatures, respectively, were also observed. Likewise, samples prepared using acid chloride functionalized MWCNTs also showed a negative shift in both storage modulus onset and deset temperatures, but to a greater extent. In terms of onset temperature, 5 and 10 vol% acid chloride MWCNTs caused a negative shift by $19^{o}C$ and $15^{o}C$, respectively. The deset temperature of 5 and 10 vol% MWCNTs also showed a negative shift by $16^{o}C$ and $13^{o}C$, respectively.

These results stand in contrast to the increase in E' observed in composites containing the functionalized MWCNT samples. One would reason, based on molecular motion as mentioned above, that increases in E' and shifts to higher temperature in T_g should occur together. Therefore, although acid functionalized MWCNTs had a minor effect on moving the Tg to lower temperatures, 5 and 10 vol% acid chloride MWCNT-epoxy stands apart from all other materials. One potential explanation for this may be the relative reactivity of the acid chloride functionality towards epoxy resin in comparison to the reactivity of acid functional groups or of the unfunctionalized surface of raw MWCNTs. Our previous DSC studies have successfully measured exothermic heat flow

associated with curing reactions in the epoxy resin when a minimum of 1 vol% acid chloride MWCNTs was mixed with the resin (figure 2-7). No such exothermic heat flow was observed with in mixtures of raw or acid functionalized MWCNTs in epoxy. These two observations point towards an explanation for the wildly different DMA behavior of the 5 vol% acid chloride MWCNT-epoxy composites. First, the acid chloride MWCNTs contain the most reactive functionality. And second, acid chloride groups are present in enough abundance to sufficiently change the crosslink character of the neat epoxy matrix causing a clear change in response of the material to temperature and strain. That is, the acid chloride functionalities may have reacted in such a way as to effectively transform the otherwise anhydride-cured matrix into a "new" polymer. This new matrix, being partially acid chloride cured, likely has a much lower molecular weight due to the "mono-functionality" of the acid chloride functionalized MWCNTs, and may simply transition from a rubber to a glass at a lower temperature. It can be argued that even when a crosslinking epoxy terminates at a functionalized nanotube, more functional sites are present, and are thus able to continue the chain reaction. However, in this instance, the acid chloride functionality participates strictly in an electrophilic nature and can only serve to terminate the reaction at the nanotube surface, as no new nucleophilic site is produced upon reaction of the epoxy resin with the acid chloride group. However, at lower concentration, the acid chloride functionalities serve to improve MWCNT-epoxy adhesion without significantly affecting the crosslink character of the epoxy matrix.

In order to probe this result further, a DMA study was performed on samples that contained the standard epoxy mixture, as-produced MWCNTs, and an arbitrary amount (5 wt%/MWCNT) of benzoyl chloride. This serves to introduce a known amount of mono-functional acid chloride functionality, which is non-covalently linked, into the matrix. As expected, the trend observed for acid chloride MWCNT-epoxy composites was the same as in the new non-covalently bound acid chloride-containing MWCNT-epoxy composites. At 5% CNTs, the benzoyl chloride sample had a loss modulus peak temperature of 155 ^{o}C, while the 10% sample was at 163 ^{o}C. This result helps to support the conclusion that insertion of reactive functionality into the epoxy matrix inhibits the propagation of chain grown at each new reactive site, thus lowering the average molecular weight of the epoxy that is not covalently bound the nanotubes.

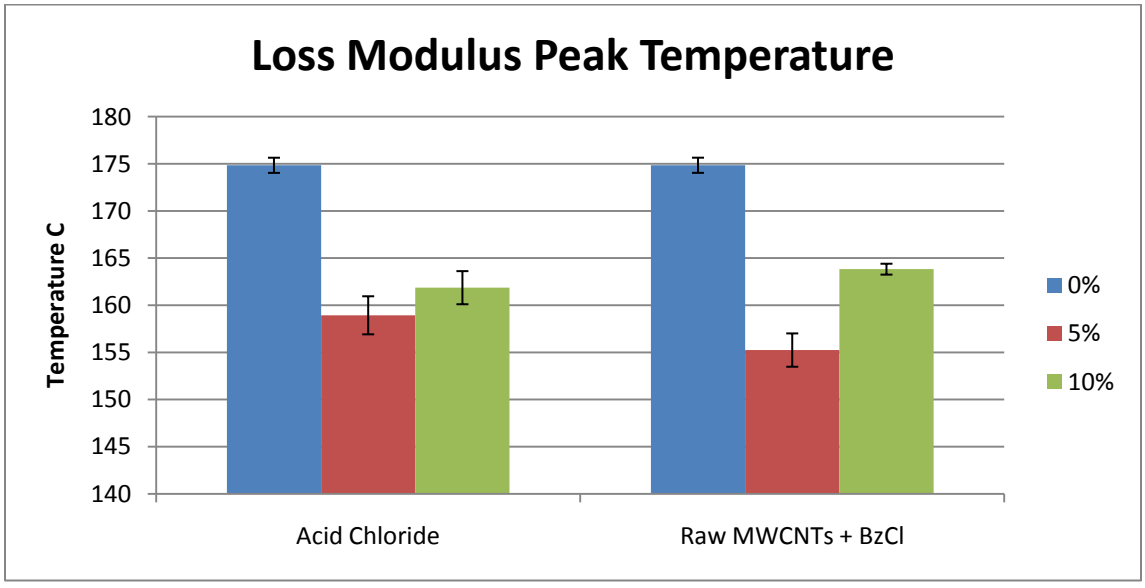

Figure 2-19: Loss modulus peak temperature of acid chloride functionalized MWCNT/Epoxy composites and raw MWCNT + benzoyl chloride/Epoxy composites

Loss Modulus

Much as the storage modulus, E', is derived from the portion of the applied strain energy which is stored in the sample as elastic stress in phase with the applied strain, the loss modulus, E", is derived from the remainder of the applied strain energy, resulting in an out-of-phase stress which is "lost" in the sample and transformed to frictional heat and plastic deformation if deformed too far (at fixed temperature and deflection frequency). In the most basic sense, it is a gauge of the damping of the material, and quantifies the viscous character of a visco-elastic material. In DMA, much interest is focused on the temperature where the loss modulus reaches a maximum, which occurs when the storage modulus is decreasing at the fastest rate with respect to temperature. In other words, when one examines the glass transition event, the loss modulus begins to increase coincident with the T_g onset, and reaches a peak corresponding to the temperature at which the applied strain energy is most efficiently being converted ("lost") to intermolecular frictional heat, and plastic deformation. It is this molecular motion that is associated with the glass-rubber transition, T_g, event. Then, as the rubbery state is reached, the loss modulus (and storage modulus) stabilizes at a lower value, completing the peak and reflecting the arrival to the rubber state. The peak of the loss modulus is therefore quite useful for probing the T_g event.

Because E' and E" are related, a similar story of the T_g event is told by the E" peak in the epoxy composites we studied. Referring back to the onset and deset temperatures of the E' through the T_g event, many similar trends were observed. Composites containing

5 and 10 vol% of raw MWCNTs began to shift the E" peak onset 6-9 °C to higher temperatures relative to the neat epoxy (figure 2-20). The functionalized samples, however, shifted the peak onset to lower temperatures. Once again, the acid chloride MWCNTs resulted in the largest shift at any concentration. At 5 and 10 vol% acid chloride MWCNTs, the onset in the E" peak shifted down 12-13 °C each. The acid MWCNTs shifted the E" onset peak down 7 °C for the 10 vol% sample, but remained virtually the same for the 5 vol% sample. Even at lower concentrations, we have shown that the acid chloride MWCNTs crosslink into the epoxy matrix, and by doing so, they inhibit the epoxy from fully crosslinking with itself, thus lowering the molecular weight of the crosslinked polymer and shifting the onset to a lower temperature.

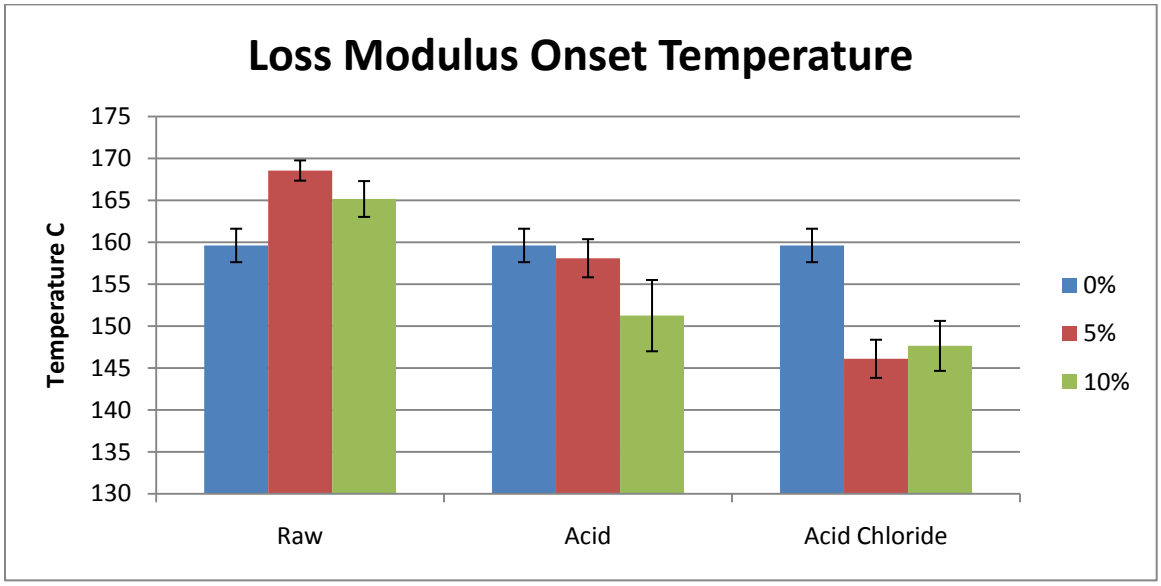

Figure 2-20: Loss Modulus Onset Temperature of Raw, Acid, and Acid Chloride MWCNT-epoxy composites

Similar trends were observed in the shifts in the E" peak (Figure2-21). In composites made using raw MWCNTs, the E" peak temperature in the 5 vol% sample increased by 7°C, while in the 10 vol% sample the peak moved about 4°C to higher temperatures. Use of the acid chloride MWCNTs, however, shifted the peak to lower temperatures by 17 °C and 14 °C for the 5 and 10 vol% samples, respectively. The acid MWNTs also decreased the E" peak temperature, but to a lesser extent than the acid chloride MWNTs, moving the peak temperature down 4 °C and 10 °C for the 5 and 10 vol% samples, respectively.

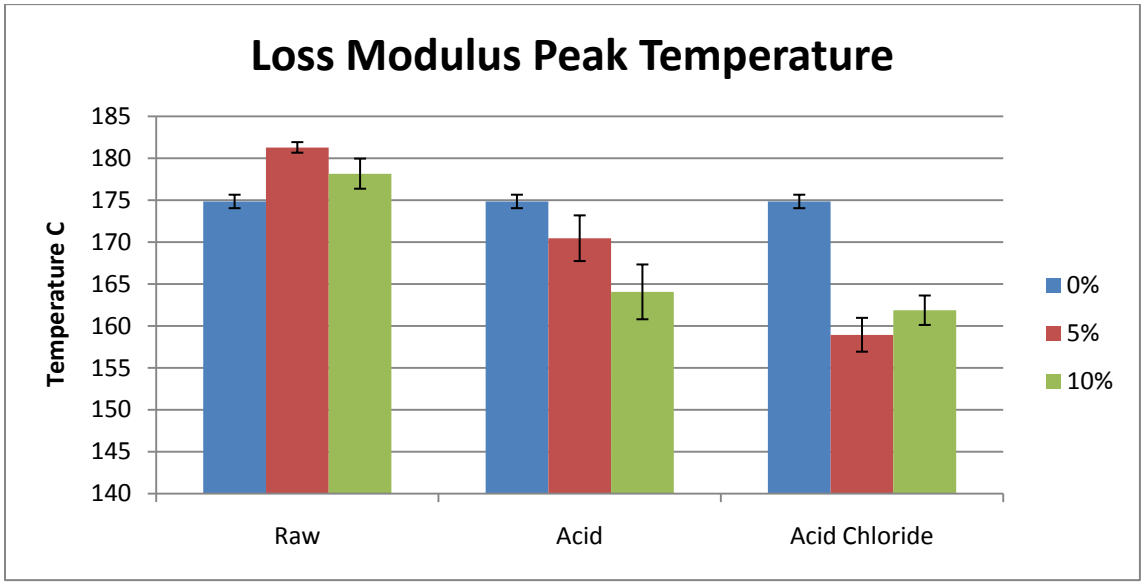

Figure 2-21: Loss Modulus Peak Temperatures of Raw, Acid and Acid Chloride MWCNT-epoxy Composites

The same trends can be observed when investigating the loss modulus deset temperature. Addition of 5 and 10 vol% raw MWNTs to epoxy moves the E" deset temperature 5-6 °C to higher temperature, while addition of the acid chloride MWNTs

moves the deset temperature down 10-11^{o}C for both the 5 and 10 vol% samples. Likewise, the acid MWNTs move the deset temperature down 3 ^{o}C and 7 ^{o}C, respectively, for the 5 and 10 vol% samples.

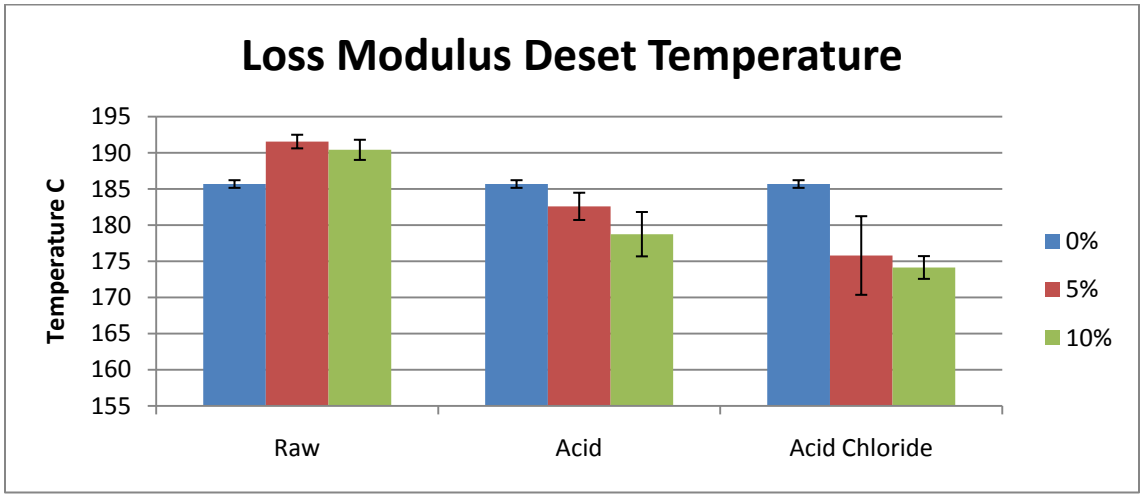

Figure2-22: Loss Modulus deset temperature of raw, acid, and acid chloride MWCNT-epoxy composites

Tan Delta

At a given frequency of oscillatory deformation, the stress response of a perfectly elastic material is exactly in-phase with the deformation frequency; the stress response of a perfectly viscous material lags the applied strain by 90°. For visco-elastic materials, which have both elastic and viscous character, a stress response that is intermediate between the two is observed, and the degree of phase-lag between 0 and 90° is the phase-lag angle delta (δ).

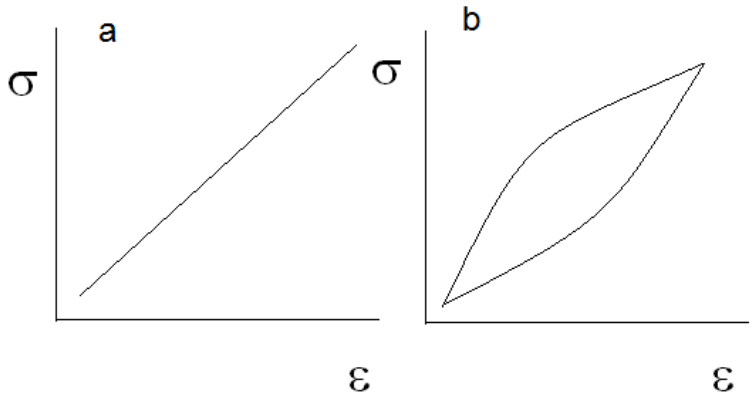

Figure2-23: Stress-Strain curves of a) a pure elastic material and b) a viscoelastic materal. The hysteresis loop shows the amount of energy lost in a loading-unloading cycle

From geometrical considerations, the ratio of the loss modulus to the storage modulus, E"/E', is equal to the tangent of delta. Therefore, as the material approaches the glass-rubber transition, E' begins to decrease while E" begins to increase, resulting in the onset of a peak. One can think of the tan□ as the strain energy lost to heat, normalized to the strain energy stored in the deformed specimen. The tan δ is then often considered the best way to characterize the glass transition event. The peak is completed as the material completely passes through the glass-rubber transition.

When observing the onset and peak temperatures, the tan δ data showed similar trends as the loss modulus data of the corresponding samples. The 5 and 10 vol% raw MWCNT composites showed an increase in the tan δ onset temperature of 7°C and 3°C, respectively. Similarly, composites prepared with functionalized showed a marked decrease in onset temperature with a respective change of 3°C and 11°C for 5 and 10 vol% acid MWCNTs and 15°C and 13°C for acid chloride MWCNT composites (Figure 2-

24). Regarding the tan δ peak temperatures, composites containing 5 and 10 vol% raw MWCNTs increased the peak temperature by 5 °C and 2 °C, respectively. Again, both functionalized samples moved this value to a lower temperature with 5 and 10 vol% acid MWCNT composites shifting down 4°C and 10°C each, and acid chloride MWCNT composites shifting down 13-14°C (Figure 2-25).

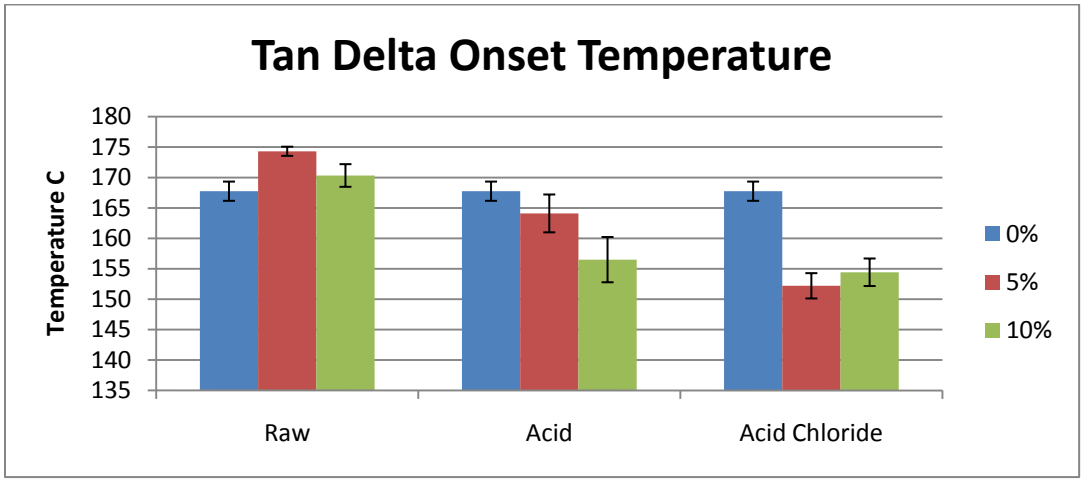

Figure 2-24: Tan Delta onset temperature of Raw, Acid and Acid Chloride MWCNT composites

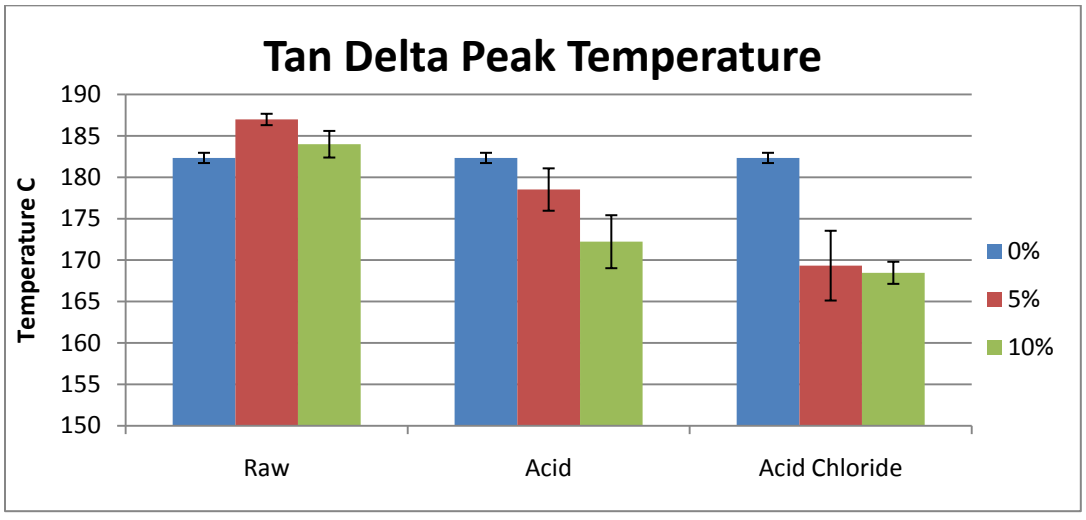

Figure 2-25: Tan Delta peak temperature of Raw, Acid and Acid Chloride MWCNT composites

Conclusions

MWCNTs were chemically modified with an acid and acid chloride functionality, using Birch reduction – alkylation chemistry. Bulk uncured MWCNT-epoxy composite dispersions were produced at 0, 1, 2, 5 and 10 vol% of raw, acid and acid chloride MWCNT, by a combination of planetary mixing and 3 roll milling, but uninterpretable changes at lower concentrations necessitated the use of only 0, 5 and 10 vol% samples. Bulk MWCNT-epoxy dispersions were cast, degassed, and cured, from which DMA specimens were machined. Single cantilever DMA measurements were taken of all specimens under constant amplitude of deflection (5 microns) at fixed frequency (1 Hz), carried out over a temperature range of 100 ˚C to 200 ˚C at an applied heating ramp of 2 °C/min. The resulting storage modulus, loss modulus, and tan δ curves were than analyzed to deduce the effect of the MWCNTs on the composite epoxy's visco-elastic properties, and to evaluate the relative effect of the MWCNT functionalization.

The overriding generality of the DMA results was as follows; 1-2 vol% of any variety MWCNTs was insufficient to cause unambiguous changes in the visco-elastic response of the epoxy when investigated by single frequency DMA (1Hz) under a small applied strain over a range of temperatures including the glass transition temperature event. However, 5 vol% MWNTs, of any variety, was sufficient to increase the glassy storage modulus by at least 5% over neat epoxy. 10 vol% acid MWCNTs yielded the best reinforcement by 48% over 10 vol% raw MWCNTs at 100 °C (up to 3.03 GPa, Figure 2-

14). With respect to changes in glass transition, 5 vol% acid chloride MWCNT-epoxy clearly shifted the Tg to lower temperature by approximately 14 °C.

The acid chloride functionalization of the MWCNTs had the greatest effect on the epoxy matrix. At all concentrations, increases in E' were observed, which suggested improvement in interfacial bonding over raw or acid MWCNTs. We believe that such enhancements to the elastic character of the epoxy shift the rubber-glass transition event to higher temperatures. The reasoning here was that highly adhered, high modulus, temperature resistant MWCNTs, would impart an overall barrier effect to large scale molecular motion in the epoxy matrix. However, any functionalization of MWCNTs resulted in a decrease in the Tg of the overall composite sample, but the acid chloride MWCNT-epoxy composites did so much more significantly.

One potential explanation for this may be found in the relative reactivity of the acid chloride functionality in comparison to acid or raw MWCNTs. DSC studies have successfully measured exothermic heat flow associated with curing reactions in the epoxy resin when a minimum of 1 vol% acid chloride MWCNTs was mixed with the resin. No such exothermic heat was observed with raw or acid functionalized MWNTs. These two observations point towards an explanation for the wildly different DMA behavior of the acid chloride MWNT-epoxy composites. First, it contains the most reactive functionality. And second, it is present in enough abundance to sufficiently change the crosslink character of the neat epoxy matrix causing a clear change in response to temperature and strain. That is, the acid chloride functionalities may have reacted in

such a way as to effectively transform the otherwise anhydride-cured matrix. This new matrix, being partially acid chloride cured, may simply transition from a rubber to a glass at a lower temperature.

While no single characterization technique used explicitly proves that we have formed a new carbon-carbon bond from to outer surface of the MWCNTs, we believe that the accumulation of data using many different methods has helped us to build a very strong argument in favor of this assertion. In short, TGA data suggests that upon reductive alkylation of MWCNTs, changes to the outer surface have occurred, as they appear to be more vulnerable to thermo-oxidative degradation. From the DSC experiment, we have shown that functionalized MWCNTS are capable of reacting with an epoxy resin and a linear increase in MWCNT loading results in a linear increase in the integrated heat flow of the reaction. By fabricating MWCNT-epoxy composites with both raw and functionalized MWCNTs, we have shown the addition of any MWCNTs serves to increase the storage modulus of the epoxy, while adding functionalized MWCNTs increases it even further over raw MWCNTs. Because of this, we believe that the presence of covalent bonds to the nanotubes allows for better load transfer from the epoxy matrix to the nanotubes themselves, and that the functionalized MWCNTs are more capable of allowing their individual mechanical properties to manifest themselves in the overall strength of the composite.

Chapter 3: Longitudinal Cutting of NMWCNTs via reductive alkylation

When a nitrogen-containing feedstock is used in place of a pure hydrocarbon source in the CVD synthesis of carbon nanotubes, very different tube morphologies can be produced.[40-46] Several different techniques have been used to synthesize stacked cup shaped carbon nanotubes (Figure 3-1), including chemical vapor deposition[47-49], plasma-enhanced chemical vapor deposition[50] (PECVD), electric arc discharge[51-52], pyrolysis[14-16], substrate growth[53-55], ball milling[56], and explosions.[57] Using a variety of nitrogen containing feedstocks such as benzylamine[47], pyridine[48], and melamine[58], many groups have utilized these techniques to create a variety of different nitrogen doped carbon nanotubes (NMWCNTs), which are produced whenever iron and nitrogen are present at temperatures above approximately 700 ^{o}C.

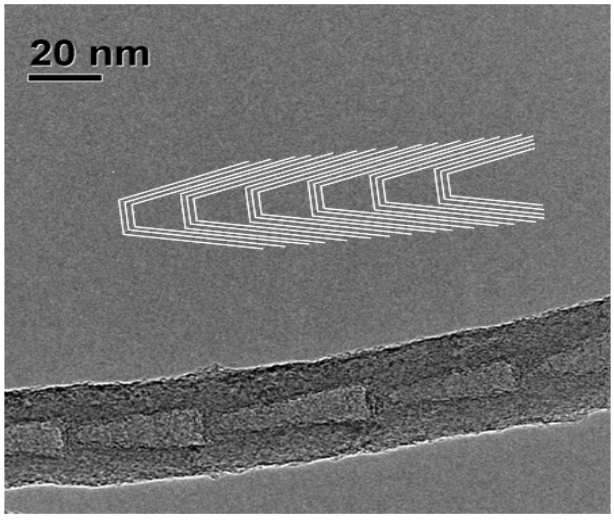

Figure3-1: TEM image with graphical description of a stacked cup shaped carbon nanotube

In our lab, we have produced carbon nanotubes using a pyridine/ferrocene mixture to create what can be described as stacked cup shaped nitrogen containing carbon nanotubes[48]. Using a large, continuous CVD reactor[59-60] operating at 800 ˚C in a nitrogen atmosphere, nicely ordered stacked cup-like N-MWNTs were produced from a pyridine-ferrocene feedstock.

From low magnification SEM, NMWCNTs can be seen to be very similar to “regular” or “cylindrical” MWCNTs in terms of their length, and aspect ratio.

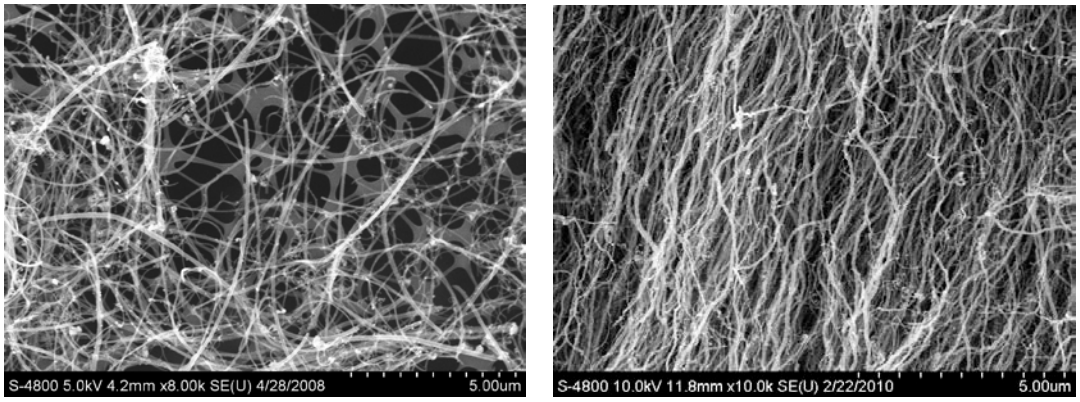

Figure 3-2: Low magnification SEM image of a) NMWCNTs and b) cylindrical MWCNTs

When observed under TEM, the differences in the two structures become very noticeable.

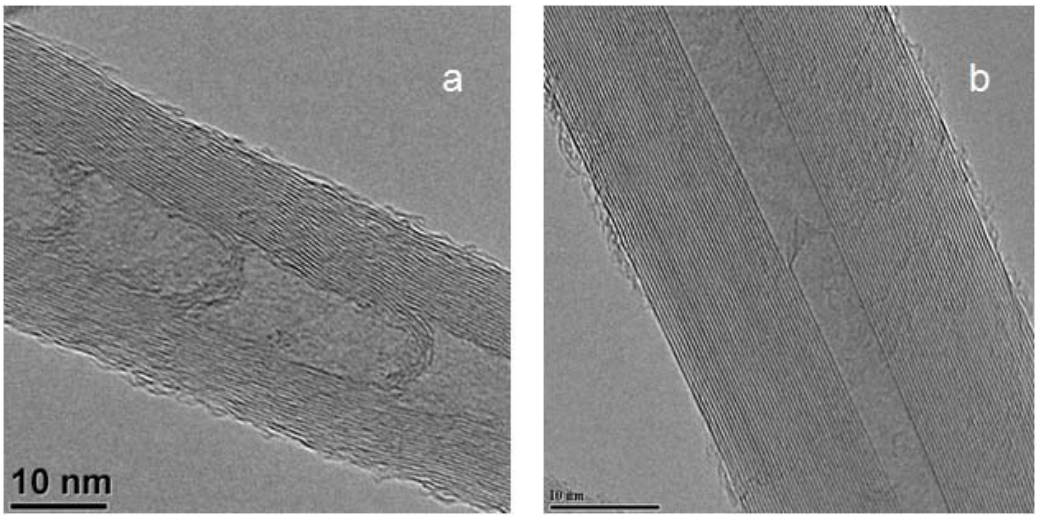

Figure 3-3: TEM images of a) NMWCNT and b) regular cylindrical MWCNT

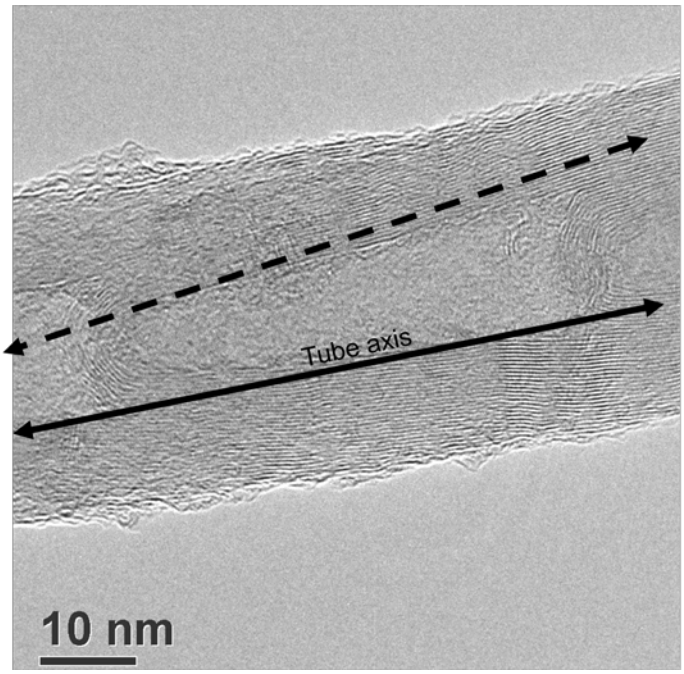

Figure 3-4: HRTEM of a NMWCNT with graphical description of tube axis compared to graphene axes

As is illustrated, one can clearly see that the individual layers of graphene are not parallel to the axis of the tube, but instead are orientated at approximately 5.3 degrees off-axis on average (as measured manually and average). This is very significant to our efforts because it implies that every shell must eventually terminate at some point on the sidewall of the nanotube. It is possible to calculate the frequency of cup edges terminating along a tube's axis by first calculating the distance between each cup edge (in an ideal system). Using the equation:

$$x = d / \sin\theta \qquad \text{Equation 1}$$

Where x = the distance between cup edges,

d = interlayer spacing of graphite (0.334nm)

θ = angle of graphene layers off the nanotube long axis (average of 5.3^{o})

It was found that, on average, the distance between cup edges along and NMWCNT's long axis is approximately 3.6nm, meaning for every 20nm of tube length, there are approximately 5.5 reactive edges on which to perform chemistry. Following our previous hypothesis, these are the sites that are likely to be the most reactive and therefore the most conducive to chemical modification. Another very interesting feature of these particular nanotubes is the septum that occurs at the base of each "cup." Although our NMWCNTs are actually grown via a root growth mechanism[48], meaning that each cup bottom is more accurately described as a cone top, once the nanotubes are removed from the substrate the two terms can be used interchangeably.

It should be noted that while these materials are not technically “tubes,” due to their overall cylindrical shape and high aspect ratio, they resemble tubes on a macroscopic level, and the current convention is to refer to them as such.

When annealed at 2750^{o}C, multiple changes occur, some of which allow them to be more easily imaged by TEM. First, most of the nitrogen is removed and, similarly to cylindrical MWCNTs, the iron catalyst is also removed. Likewise, the graphene edges transform from somewhat rough to a quite smooth surface.

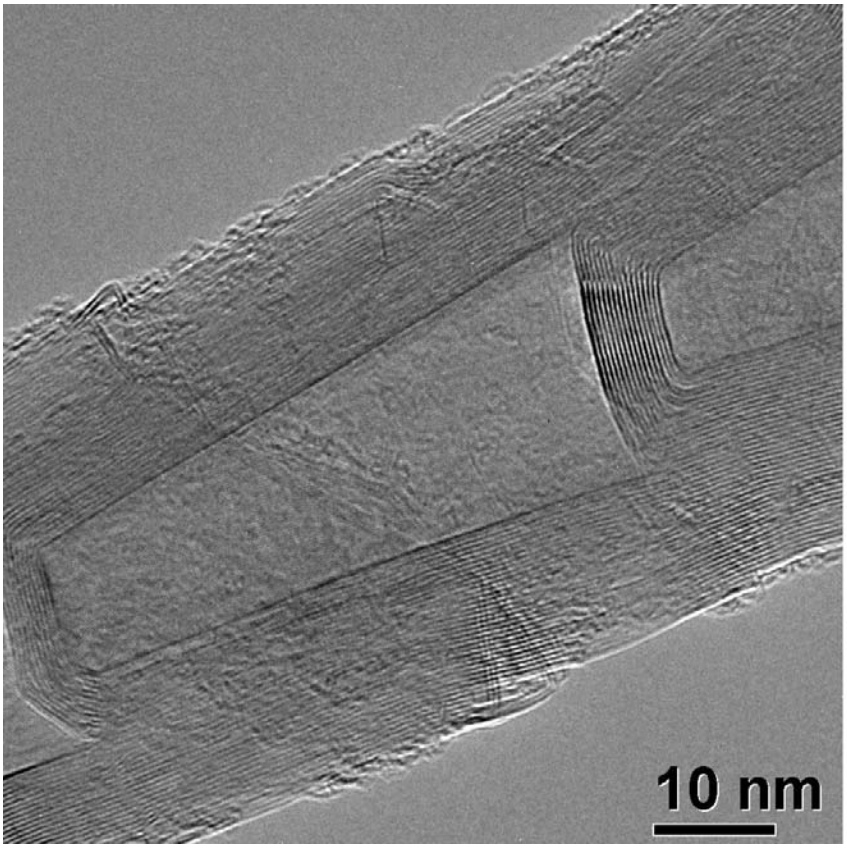

Figure 3-5: HRTEM image of GF-NMCNT

The graphitic nature of the above image allows one to very clearly observe the well-defined sidewalls and bottom septa of the NMWCNTs. At this magnification, it is also possible to observe a few layers of cup rims, running approximately perpendicular to the tube axis through the inner core of the tube above. These are very difficult to image in the as-produced NMWCNT samples, due to the more amorphous nature of the material. The morphology of these tubes is likely a function of the catalyst particles generated during the CVD process. Previous studies in our group have determined that the majority of nitrogen present in these tubes is concentrated in the features along the central core, which, due to the unique bonding pattern of pyridine and pyrole-like nitrogen, can partially explain the origin of curvature.[48]. Unlike with traditional cylindrical MWCNTs, the catalyst particles generated have a conical morphology, which makes it easier to understand how the resulting NMWCNTs get their shape. In the case of these specific NMWCNTs, the catalysts produced consist of an iron-carbon-nitrogen ternary phase[48], but further discussion of the catalyst composition or formation is beyond the scope of this document.

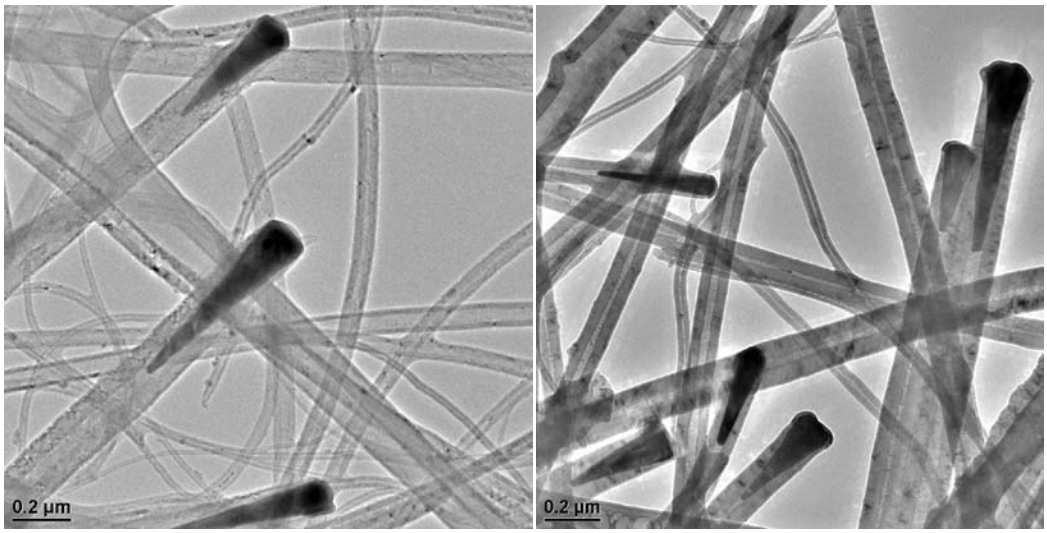

Figure 3-6: TEM images of NMWCNTs containing conical catalysts

When comparing the thermal decomposition of our pyridine-derived NMWCNTs and the subsequent graphitized samples, it appears that they behave very similarly to cylindrical MWCNTs. Neither sample shows any weight loss prior to the onset of oxidation. The temperature value for the onset of oxidation, however, is shifted approximately 215^{o}C higher in the graphitized sample, which is consistent with previous observations that the more graphitic the material, the more resistant it is to oxidation. Also, the residue at high temperature in the graphitic samples is almost zero, which indicates that, as expected, the majority of the iron catalyst is removed under annealing conditions (Figure 3-7). Also consistent with the properties of cylindrical MWCNTs are the comparative rates of decomposition of the two samples. At their max, the as-produced NMWCNT samples decompose at a rate of 1.2 wt%/^{o}C, whereas the graphitized samples decompose slightly quicker at a rate of 1.35 2 wt%/^{o}C, as observed by their first derivative plots (Figure 3-8). A quick look into their second derivative plots reveals an interesting difference between the two samples that is not apparent in either the

original plots or the first derivative plots. In the second derivative plot of the NMWCNTs, a broad, yet mostly symmetrical peak can be observed. Both the positive and negative peaks of the plot are of essentially the same area and shape (Figure 3-9). This is in contrast to the GF-NMWCNTs where a more narrow and unsymmetrical plot is produced. This indicates that GF-NMWCNTs are initially more recalcitrant toward oxidation, even upon the onset of oxidation. Once the oxidative process begins, however, they decompose over a more narrow temperature range, due to the less heterogeneous nature of the bulk sample.

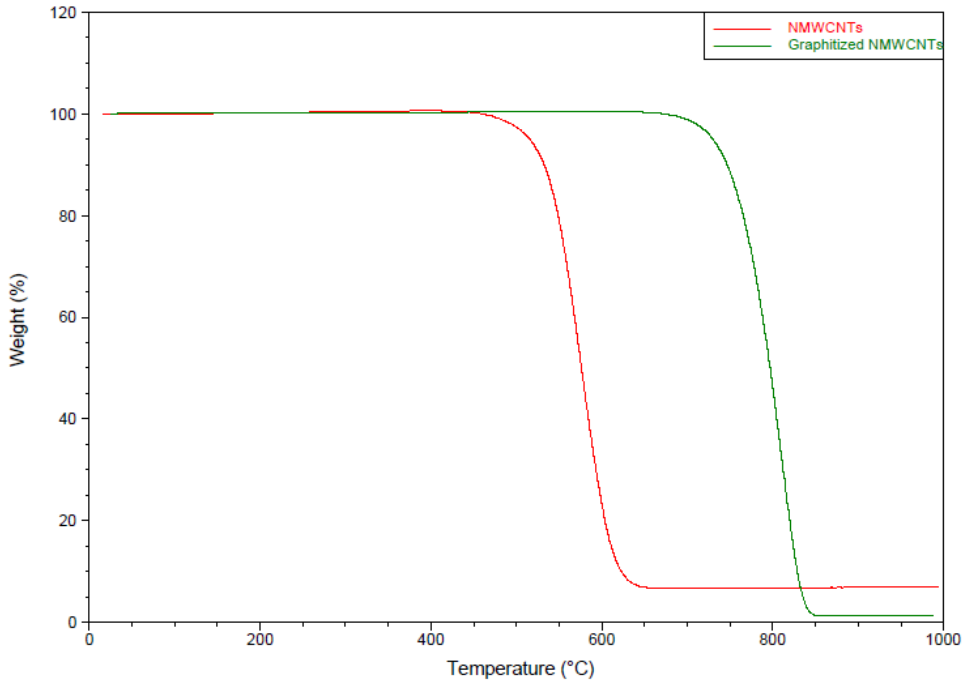

Figure 3-7: TGA thermogram of NMWCNTs and GF-NMWCNTs in air

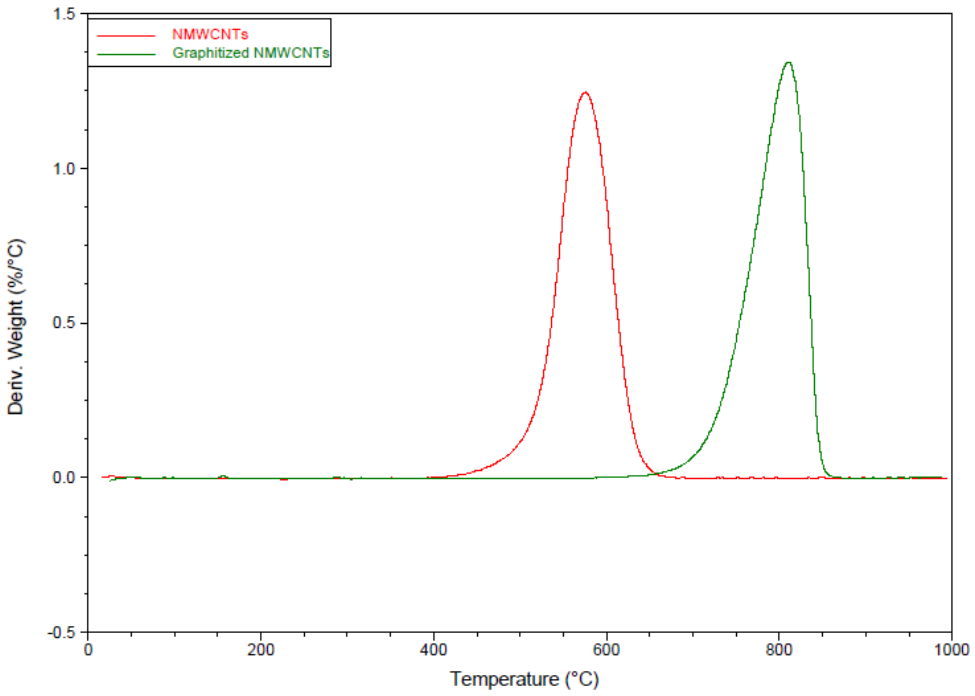

Figure 3-8: First derivative plot of TGA thermogram of NMWCNTs and GF-NMWCNTs in air

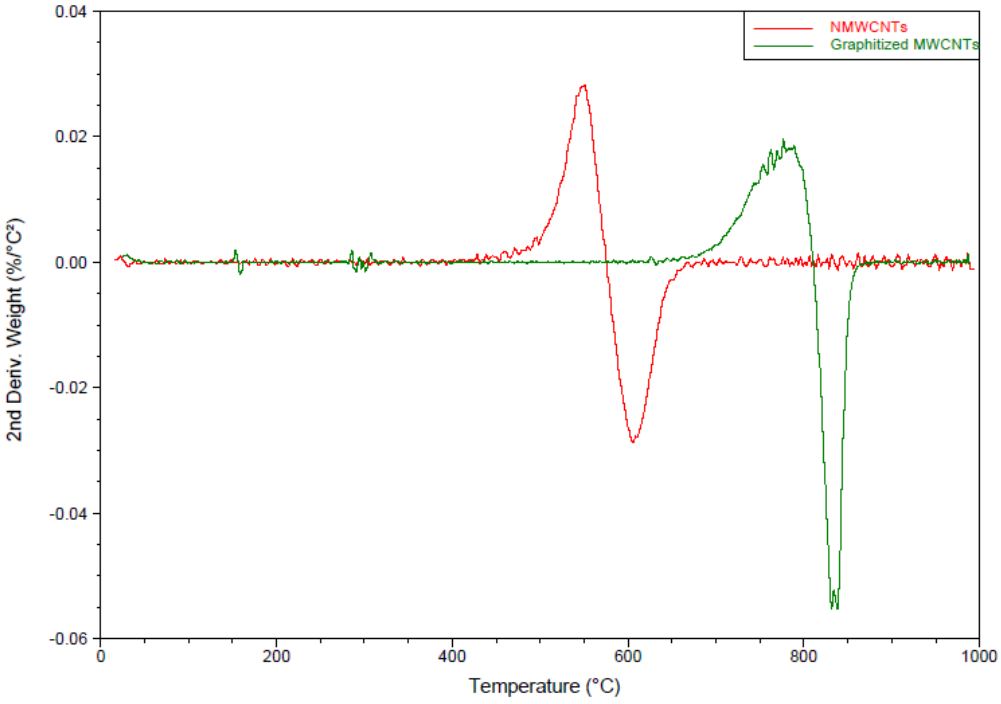

Figure 3-9: Second derivative plot of TGA thermogram of NMWCNTs and GF-NMWCNTs

Longitudinal cutting of NMWCNTs

We predicted that the exposure of NMWCNTs to Birch conditions could result in the exfoliation of cup layers, giving rise to individual, single layer graphene cups. It was thought that lithium intercalation into the graphitic layers would generate enough charge, and thus enough energy, to force the layers to simply slide apart forming individual layers of cups. Metal intercalation into graphitic carbons is very well studied in the literature[61-67], and a similar process should occur with this particular graphite morphology.

Cutting carbon nanotubes in the transverse direction, resulting in shorter sections of nanotubes, is a well-established process. Many different processes have been used to convert long tubes into short ones including, for example, simple mechanical methods,[68-69] electron beams,[70] ultrasonication,[71-72] and treatment with oleum,[73] or bromine.[74] Acid oxidation of SWCNTs produces shortened SWCNTs, partially from oxidation from the endcaps, but likely from oxidative cutting of nanotubes at kinks or other defect sites. [75]

Several recent articles have reported processes for cutting open carbon nanotubes in the lengthwise (longitudinal) direction. These are surprising and exciting results, as the specificity of the processes themselves is generally not obvious and the materials formed by longitudinal opening of nanotubes (graphene and thin sections of graphite) are potentially very useful. Graphene, single sheets of sp^2 hybridized carbon, is of great interest at this time as this material should be very high surface area, it should be electronically active, and it could be used in a variety of different applications.[76]

In 2009, Tour[77-78] reported that SWCNTs can be opened lengthwise along their axis by severe oxidation using a $H_2SO_4/KMnO_4$ mixture. The acidic conditions are thought to aid in the exfoliation process, and the resulting structures can best be described as graphene nanoribbons (GNR). Dai[79] and co-workers have developed a method in which MWCNTs are partially embedded in poly (methyl methacrylate) (PMMA) matrix, and subsequently etched using an Ar plasma, thus selectively removing the exposed material. Depending on the type of CNT, the remaining structures are single, bi, and multi-layer graphene. Terrones[80] has reported the cutting of CNTs by the use of Ni and Co nanoparticles. They describe the nanoparticles as acting as "nanoscalpels" to unzip the CNT structure. They also report the resulting structures to be GNRs. Concurrently, Vega-Cantu[81] and co-workers have used lithium in liquid ammonia followed by an acid workup to exfoliate MWCNTs. The resulting material consists of GNRs, partially opened MWCNTS, and graphene flakes.

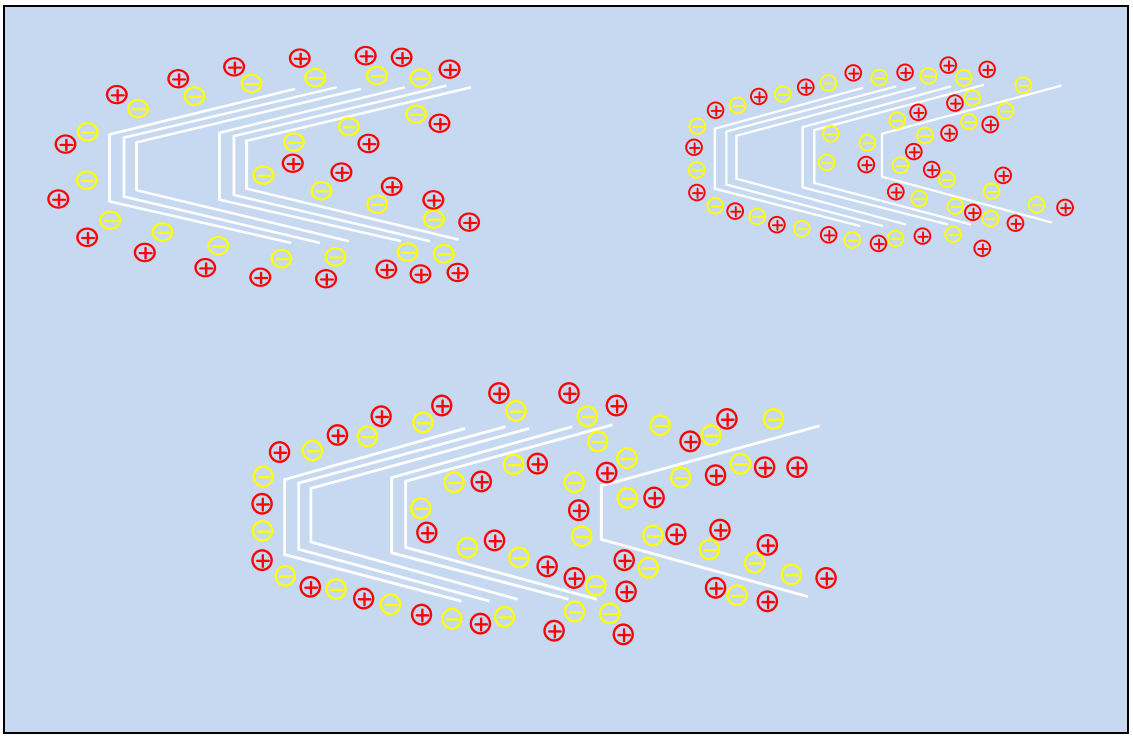

Figure 3-10: Schematic of proposed shell separation mechanism

However, upon treatment of of NMWCNTs with the Birch conditions, a very different result was observed. After reduction with lithium in ammonia, followed by quenching with methyl iodide, we obtain material that appears to be very similar to the starting material. However, TEM analysis reveals many features within individual tubes that appear to be "cuts" or "channels" running approximately along the long axis of the tubes. At relatively low magnification, it appears that almost every individual nanotube has been affected in a similar way.

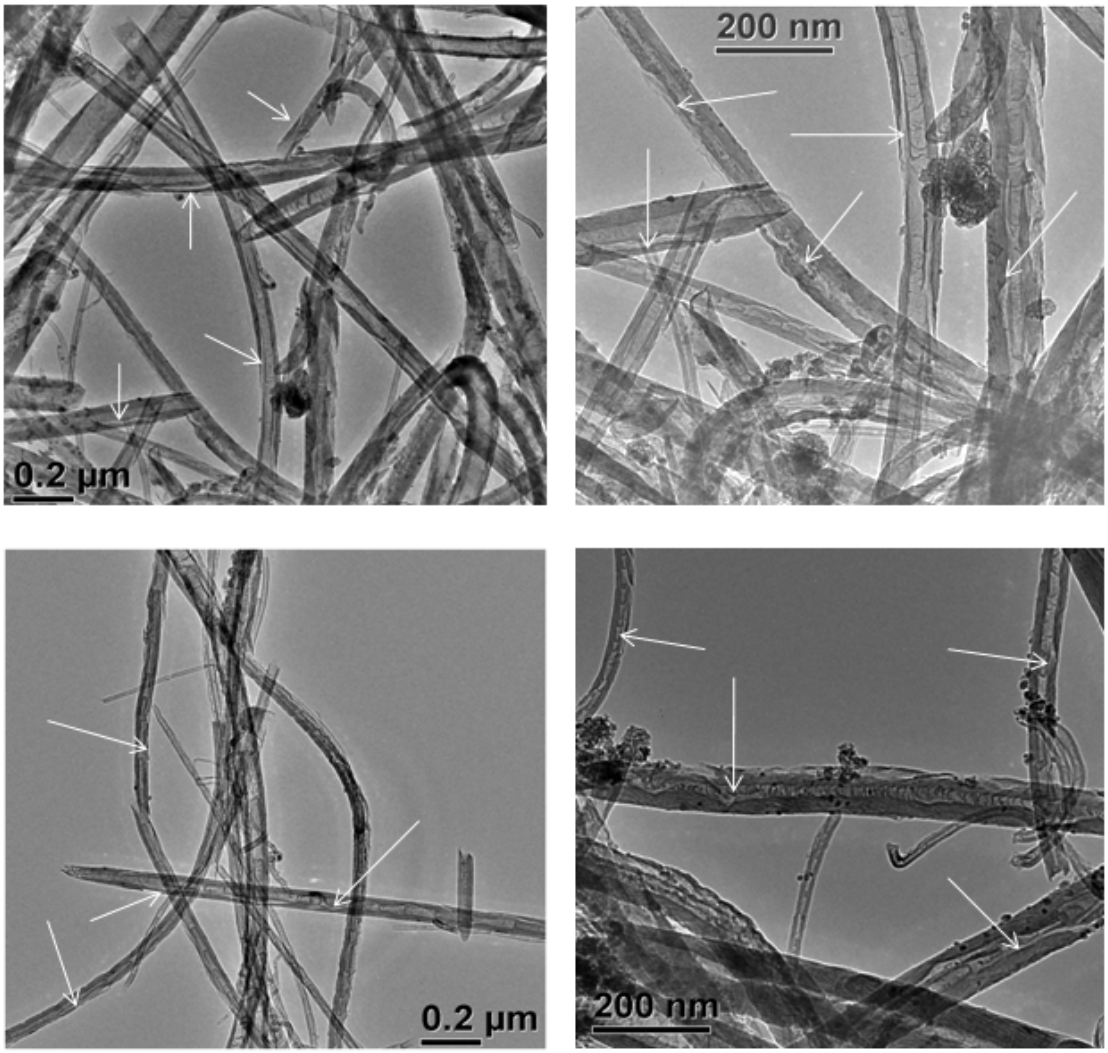

Figure 3-11: TEM images of Birch reduced NMWCNTs

When an individual nanotube is magnified, it becomes evident that new features are actually cuts that run *against* the graphitic planes of the CNT.

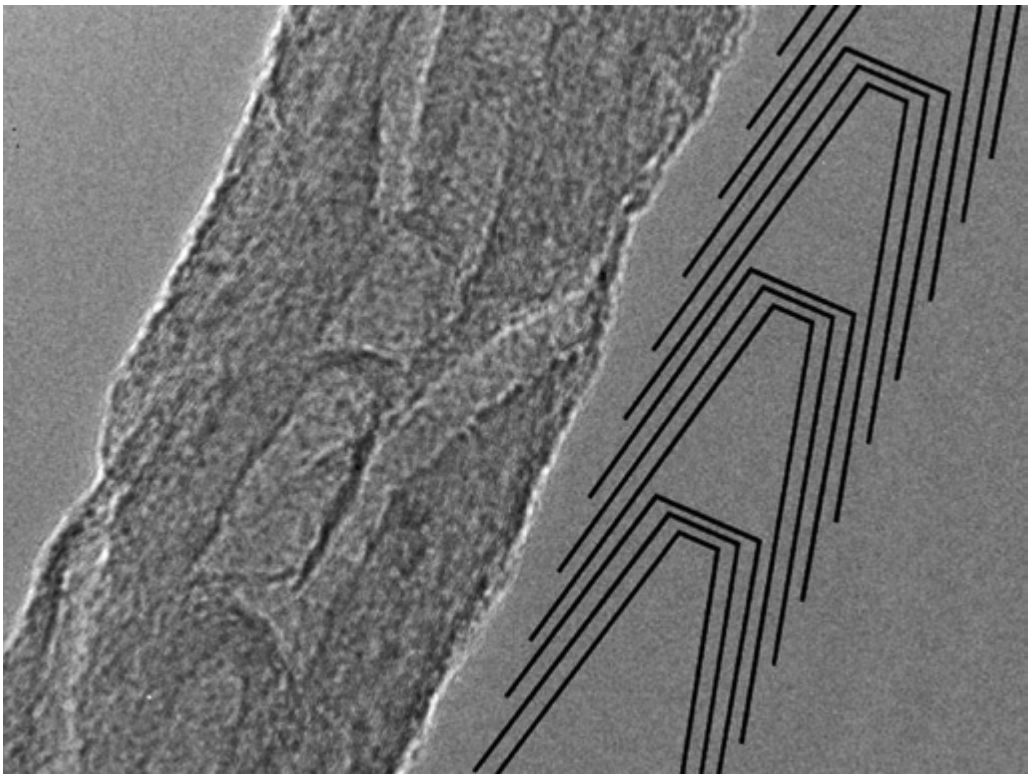

Figure3-12: High Resolution TEM image of channeled NMWNT with graphical insert of as-produced NMWNT structure

The cutting of channels across the graphitic planes is quite counterintuitive, as one would expect, if anything, the graphitic layers to "peel open" and leave voids that run parallel to the axis of the graphitic sidewalls. When magnified higher, a few interesting observations can be made. First, from the scale of the image, it appears that these particular channels are all on the order of 8-12nm across, which would classify them as mesoporous (a more detailed discussion of porosity will follow later). Secondly, the channels extend into the inner core of the CNT, cutting through every layer of graphene. Finally, it is very evident that many new edge sites have been formed along the channel face, as each layer of graphene now has a new edge where the channel cuts through.

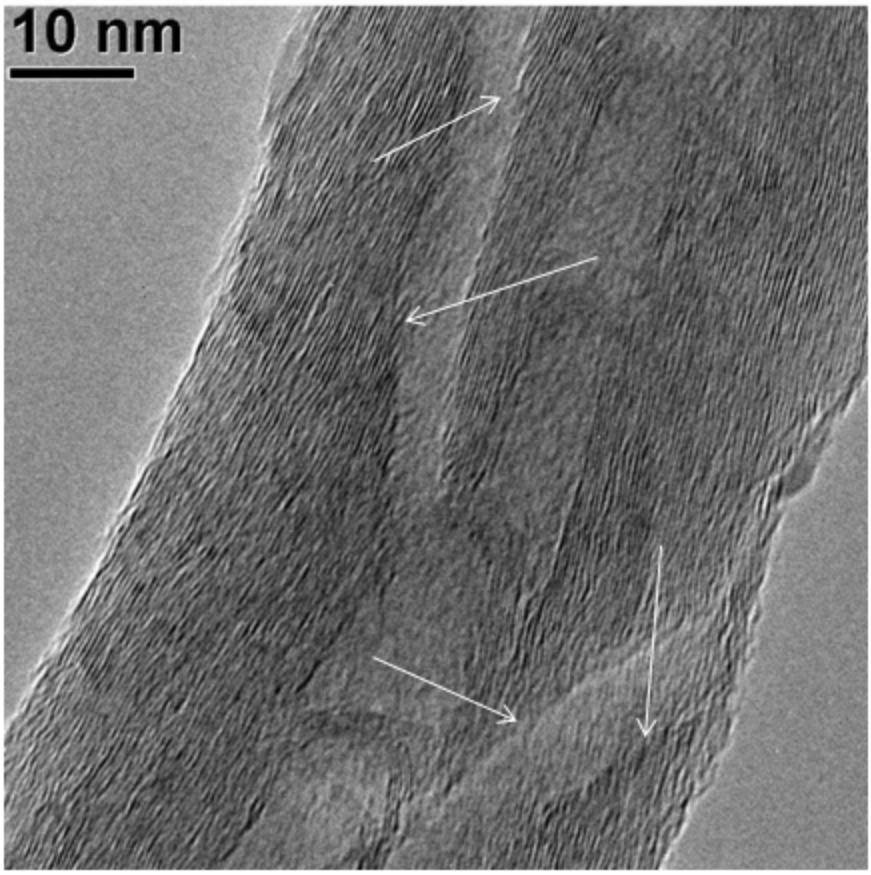

Figure3-13: HRTEM image of channeled NMWCNT with arrows pointing to channel edges

Looking at the TGA comparison of as-produced NMWCNTs versus the channeled sample (quenched with CH_3I), a few observations can be made. As with functionalized cylindrical MWCNTs, an initial weight loss that begins around 250^{o}C can be observed. This is likely due to oxidation of organic groups (in this case methyl groups) that are covalently attached to the surface of the CNT, which should be the first part of the sample to thermally decompose in air. Secondly, a decrease (about 35^{o}C) in the onset temperature of combustion (decomposition) can be observed in the channeled sample. This is consistent with the idea that when the sp^2 hybridized graphitic surface of the tubes are disrupted and converted to more sp^3 in nature, the material is more prone to thermal decomposition, and will begin the process at a lower temperature. Due to its

highly ordered backbone, graphite is highly crystalline in nature, and is much more resistant to thermal oxidation.

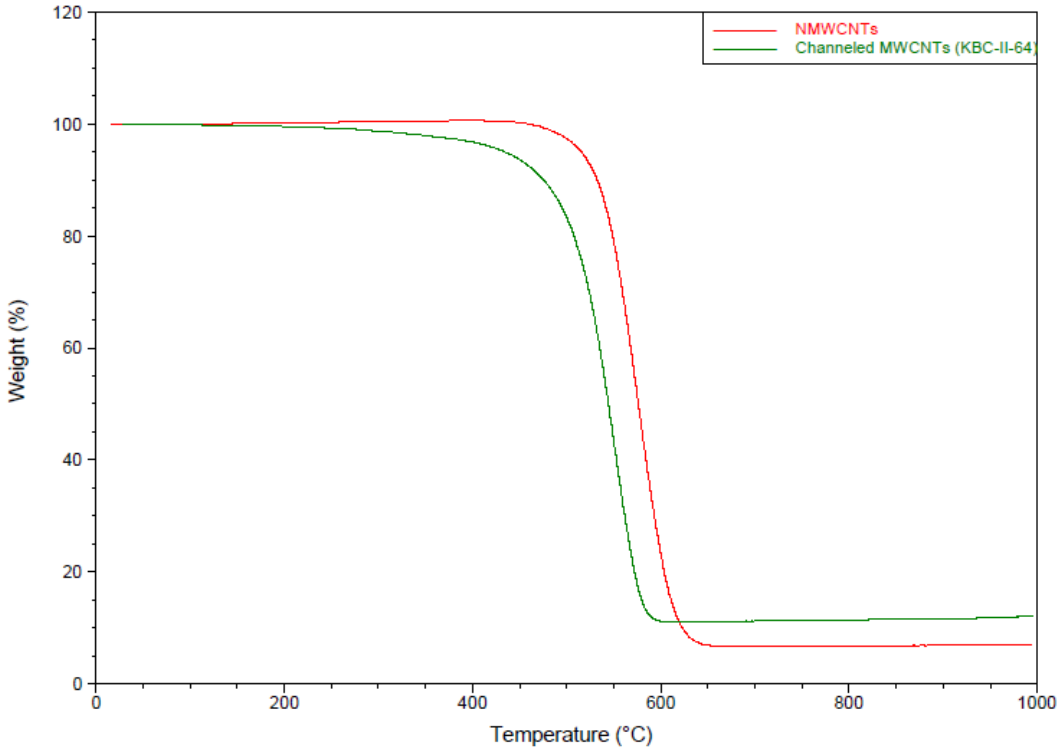

Figure3-14: TGA thermograms of NMWCNTs (red) and Channeled NMWCNTs (green)

It is important to characterize these channels, but also to answer some fundamental questions about their origin, structure, and properties. What is the thermal stability of the channels? Can they be "healed" by annealing? Are defect sites necessary for channeling to occur? Is the presence of nitrogen critical to channel formation? How does varying the reaction conditions affect the channel formation?

First, we investigated what happens to the channeled NMWCNTs when they are subjected to graphitization conditions (2700^{o}C). Samples of channeled MWCNTs were

heated to 2700˚C in a helium atmosphere, and held at that temperat ure for an hour before being cooled back to room temperature.

Thermal analysis of the graphitized samples reveals some important features. First, as seen in figure 3-14 and discussed above, the functionalization of NMWCNTs (channeling) results in materials that are less stable at high temperatures in air. In the TGA, this is evident as a lower onset temperature of oxidation. When the channeled samples are subsequently annealed at 2700^{o}C, the onset temperature increases significantly, as expected, to about 735^{o}C. This is consistent with graphitization of the remaining carbon. Also, the amount of post-oxidation residue drops to essentially 0%, which is consistent with observations made on other graphitized CNTs, as most of the iron catalyst is vaporized and removed during the graphitization process It is more appropriate, then, to compare the channeled-then-annealed sample to unfunctionalized GF-NMWCNTs.

When we compare the TGAs of channeled-then-graphitized NMWCNTs to the TGA of GF-NMWCNTs, we find that neither sample exhibits an initial mass lost at a temperature below the oxidation onset temperature (Figure3-15). This is consistent with previously discussed graphitic carbons, and indicates that in the channeled-then-graphitized sample, it is unlikely that any small molecule side chains (either chemisorbed or physisorbed) persisted during the annealing process. The second important feature that can be interpreted from the TGA data is that the onset of oxidation for the channeled-

then-graphitized is about 17 ^{o}C lower than the unmodified GF-NMWCNTs. This would indicate that even upon annealing, the channeled NMWCNTs do not return to a "completely" graphitized state, as per their unmodified counterparts.

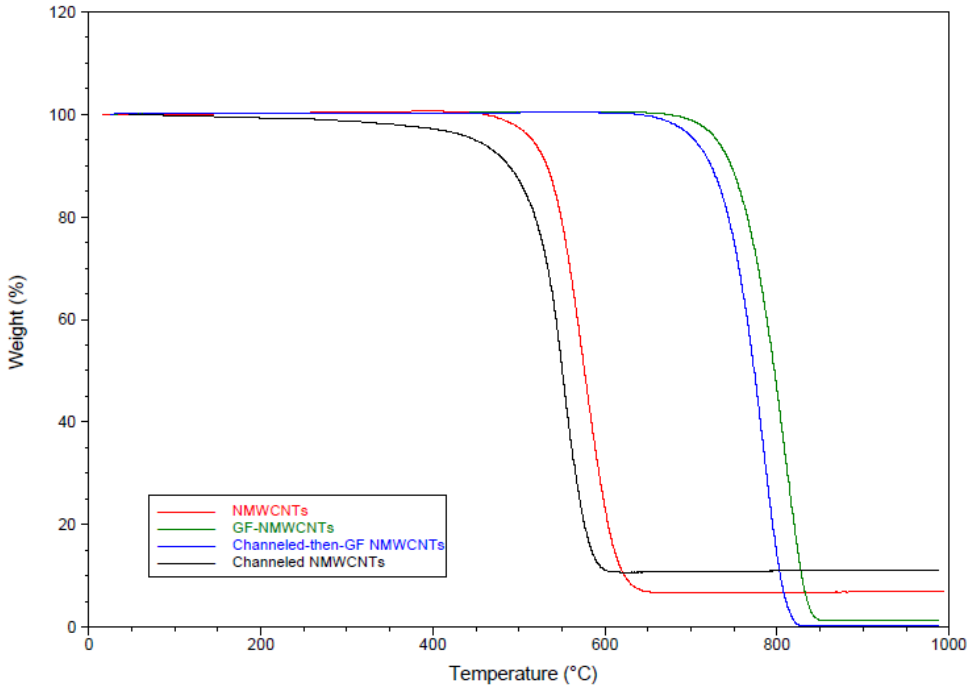

Figure 3-15: TGA thermograms of NMWCNTs (red), GF-NMWCNTs (green), Channeled NMWCNTs (black), and NMWCNTs that have been channeled and then subjected to graphitization conditions (blue)

When electron microscopy was performed on this sample, it becomes very clear that the images are consistent with the observations made by TGA. In a high resolution TEM image (figure 3-16a) of a sample that had been treated under Birch conditions to create channels, then graphitized at high temperature, channels with the same dimensionality of the pre-annealed channeled samples can be observed. When lower magnification TEM images are taken (figure 3-16b), one can see the presence of channels in virtually every tube, which is also unchanged from the situation in the pre-annealed samples.

Finally, when this sample was viewed in the SEM (figure 3-16c,d) the presence of channels are clearly observable in almost all tubes.

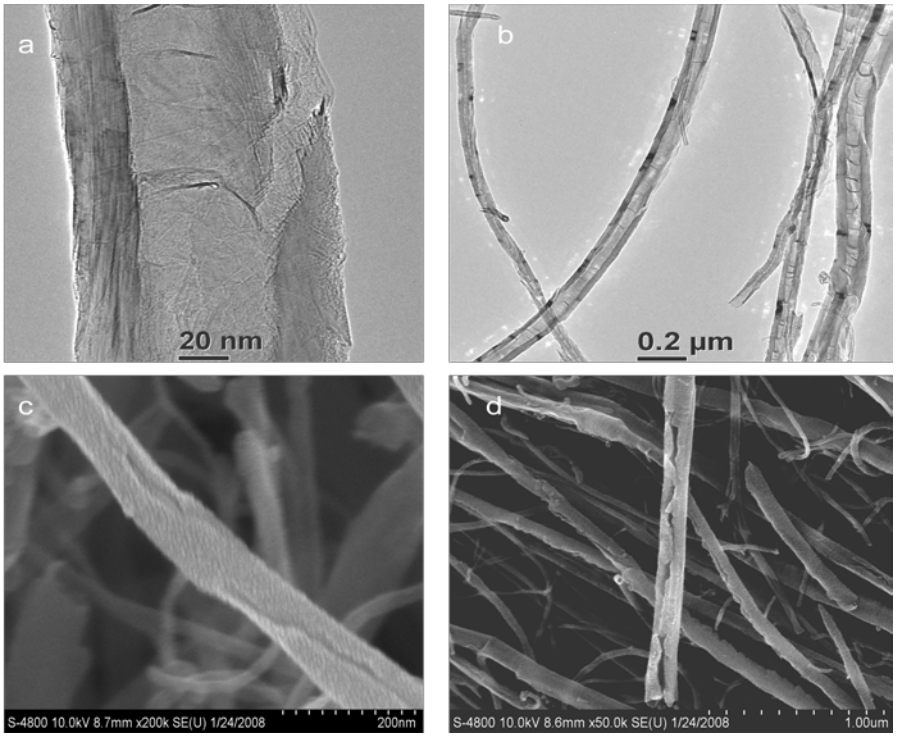

Figure 3-16: a,b) TEM images of channeled-then-annealed NMWCNTs and c,d) SEM images of same sample

Porosity of channeled NMWCNTs

The majority of our work was performed on pyridine-derived NMWCNTs that were synthesized in a large batch continuous reactor. Unfortunately, only a finite supply of these specific tubes was available, and once they were consumed a new batch had to be made. The same reactor could not be used to make a new batch of pyridine-derived tubes, and therefore a smaller, non-continuous reactor was used to synthesize subsequent new batches of NMWCNTs. While the two sets of nanotubes are essentially

the same in terms of structure and morphology, some minor differences are observable. For this reason, modified tubes will only be compared to their same-batch precursors.

In order to more qualitatively study the effects of the Birch reaction on the morphological structure of NMWCNTs, it becomes necessary to find a bulk measurement technique that will assess more than a few isolated nanotubes as seen via electron microscopy. As mentioned earlier, the newly formed structures in the NMWCNTs appear to have an average pore diameter of 8-12nm, and IUPAC defines porosity as such: <2nm as micropore, 2nm-50nm as mesopore, and >50nm as macropore. The channels we observe are squarely in the mesoporous category.

The Langmuir equation[82] was initially derived to describe the surface area of carbons:

$$\frac{p}{V} = \frac{p}{V_m} + \frac{1}{bV_m} \qquad \text{Equation 2}$$

Where

V = equilibrium amount (mmol/g) of gas adsorbed per unit mass of adsorbent at relative pressure p/p^o

V_m = amount of gas required for monolayer coverage of adsorbent (mmol/g)

b = constant, dependent on temperature but independent of surface coverage

The Brunauer, Emmet, and Teller (BET) equation [83] was created to account for multilayer adsorption and improved on the Langmuir model[82,84] which only accounts for monolayer adsorption.

$$\frac{p}{V(p^o - p)} = \frac{1}{V_m c} + \left(\frac{c-1}{V_m c}\right)\left(\frac{p}{p^o}\right) \qquad \text{Equation 3}$$

Where

p^o = saturation vapor pressure
c = $\exp(\Delta H_A - \Delta H_L)/RT]$
ΔH_A = heat of adsorption
ΔH_L = heat of liquefaction

Due to the ease of performing the measurements (nitrogen adsorption at 77K) and it's wide variety of applications, the BET equation has been thoroughly used to describe the porosity of various carbons. One issue, however, is that the equation has been used indiscriminately and surface areas much higher than the calculated surface area of graphene[85-87] (~1800m^2/g) have been reported. The basic problem is that the BET model does not describe the adsorption process, but the term "effective surface area" can still be applied and can provide very useful information[84]. For the purposes of this dissertation, all surface area measurements will be referred to or assumed to be the surface area determined by treatment of the nitrogen adsorption isotherm by the BET method.

Type I isotherms are typical of microporous solids, with the majority of pore filling taking place at low relative pressure (<0.1 p^o/p) and almost all adsorption being complete by ~0.5 p^o/p. Type II isotherms are indicative of either non-porous solids, or a mixture of micro and mesoporous solids. At higher relative pressures, monolayer coverage is complete and multilayer formation begins. Type III and Type V isotherms are convex toward the x-axis, and represent weak gas-solid interactions. At lower relative pressures, the weakness of the solid-gas interactions cause the uptake to be small, but

once some gas is adsorbed, adsorbate-adsorbate forces promote the uptake of more gas a higher relative pressure. Type III isotherms come from nonporous and microporous solids, while Type V isotherms represent micro and mesoporous solids. Type IV isotherms (as well as Type V) possess a hysteresis loop. These are indicative of mesoporosity where capillary condensation can occur. Type VI isotherms are stepwise and represent complete formation of a monolayer followed by successive monolayer formation. This is indicative of an extremely homogeneous material.

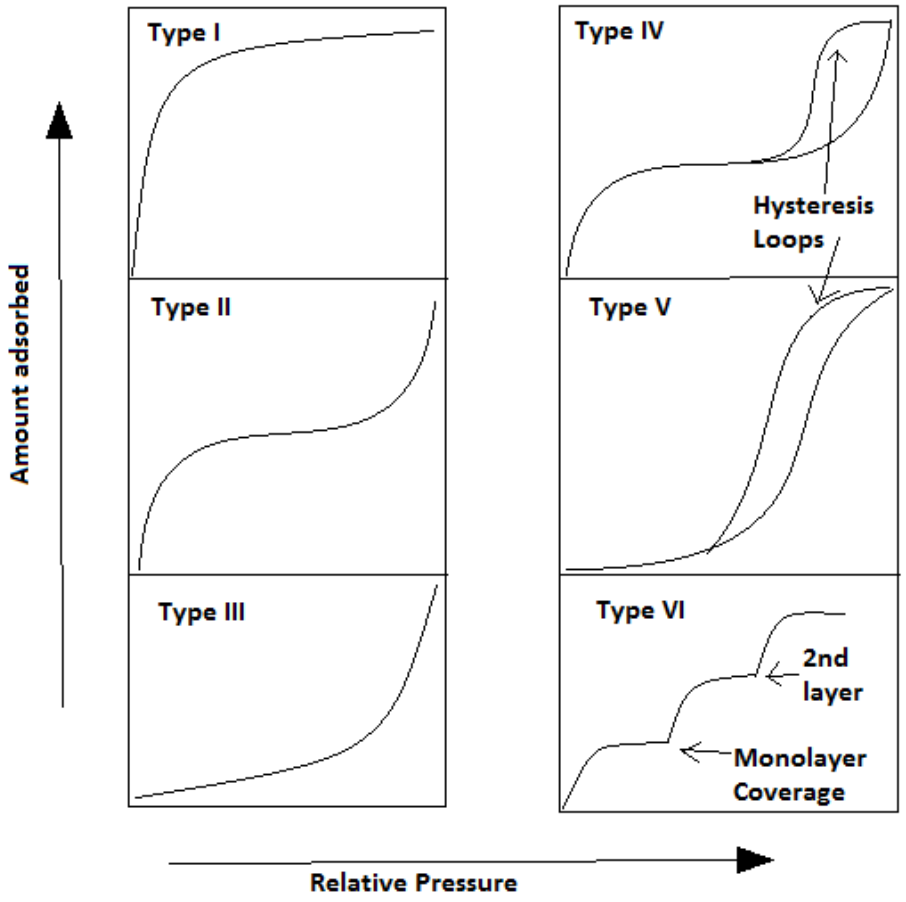

Figure 3-17: Examples of the six typical isotherms

Samples were measured using nitrogen physisorption at 77K and isotherms were calculated using the BET equation.

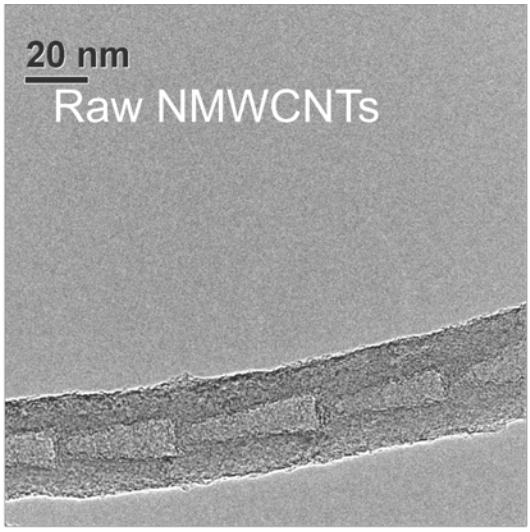

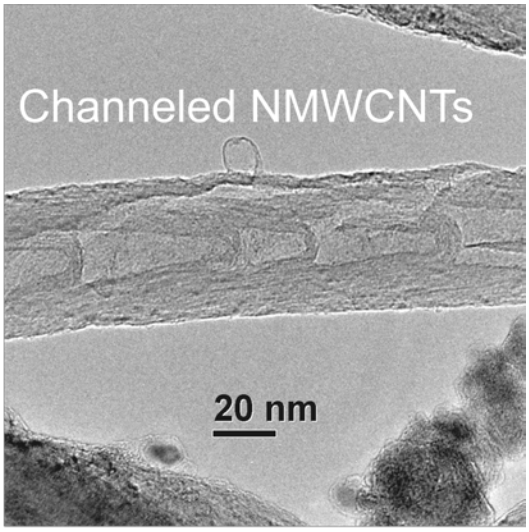

BET Surface Area (m^2/g)	45.0144	104.7392
Total Pore Volume (cm^3/g)	0.11809	0.18133
% Microporosity	2.5	4.1
% Mesoporosity	49.4	65.1
% Macroporosity	48.1	30.8

Figure 3-18 a) TEM image of as-produced NMWCNT b) TEM image of channeled NMWCNT

Table 3-1 Comparison of porosity of as-produced NMWCNTs and channeled NMWCNTs (average of 3 runs)

Upon calculating the BET isotherm of as-produced NMWCNTs, the BET surface area is found to be approximately $45m^2/g$. When looking at the same measurement on the channeled material, however, the average value increases by a factor of 2.3 to $105m^2/g$. Likewise, when one compares the calculated total pore volume of the two samples, a significant increase from $0.12cm^3/g$ to $0.18cm^3/g$ for as-produced and channeled MWCNTs, respectively, can be seen. Another interesting observation comes from

looking at the calculated porosity fractions. When going from as-produced NMWCNTs to channeled NMWCNTs, the micropore fraction remains essentially constant and too small for us to interpret. It is likely, however, that new microporosity has been created, thus helping to increase the surface area, but very little of the observed increase in pore volume can be attributed to new micropores. The mesopore fraction, however, increases significantly from 49% to 64%, and does so at the quantitative expensive of the macropore fraction, which decreases from 48% to 31%. While the values are quite low compared to more common forms of carbon,[88-91] the quantitative changes from the as-produced material to the functionalized material are quite significant. An examination of the isotherm of NMWCNTs reveals a Type II isotherm, which indicates a solid that has very little microporosity and is mostly bulk surface area (macroporosity). When the tubes are channeled, however, a Type IV isotherm can be observed, which is consistent with the increase in the calculated mesopore fraction (Table 3-1). The Type IV isotherm observed in the channeled material displayed below is indicative of all samples that can be classified as having been channeled (Figure 3-20).

When analyzing the increase in BET surface area, it becomes important to discuss what is actually being measured. In the nitrogen physisorption experiment, a precisely weighted sample of nanotubes is placed inside a sealed sample probe. The probe is then filled with a known quantity of N_2 at a constant increase of pressure until a maximum is reached, then released at the same rate of decreasing pressure until evacuated. From the data taken at the sample intervals, an isotherm can be

constructed and the BET equation can be applied to extrapolate the surface area data. Therefore, what is actually being measured is not the entire surface of the material, but *only the surface that is accessible to the applied gas.* It then becomes easier to understand the significant increase in BET surface area when comparing as-produced NMWCNTs to channeled NMWCNTs, as not only the newly creates surfaces along the channels are accessible, but more of the nanotube internal surface, which was previously inaccessible to nitrogen, can now also be observed.

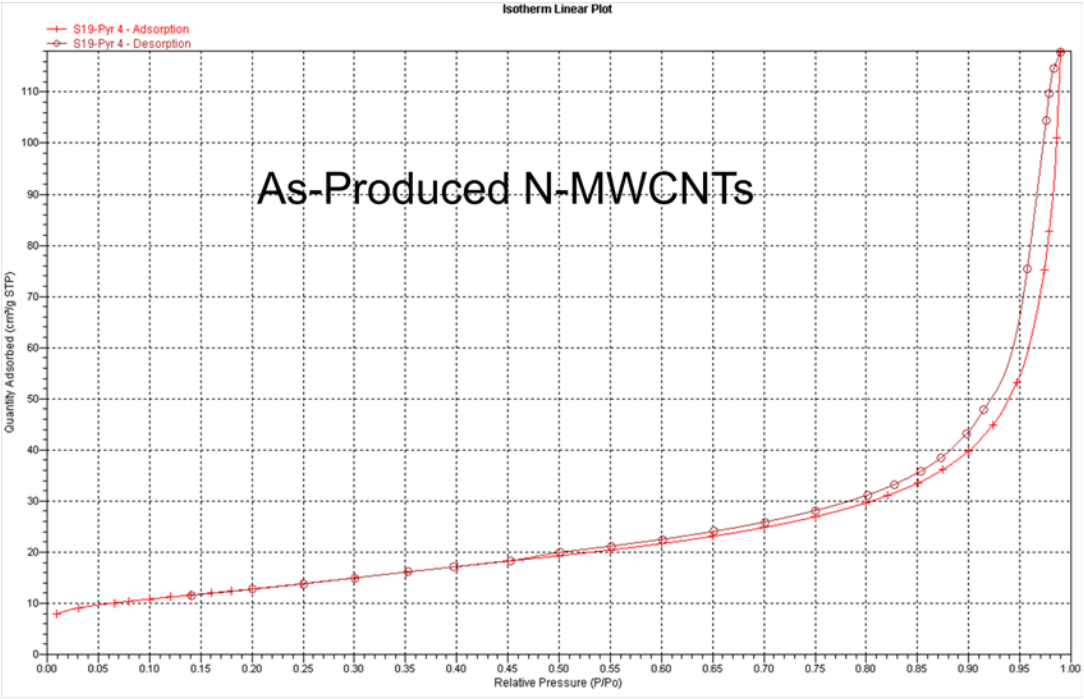

Figure 3-19: BET isotherm of as-produced NMWCNTs

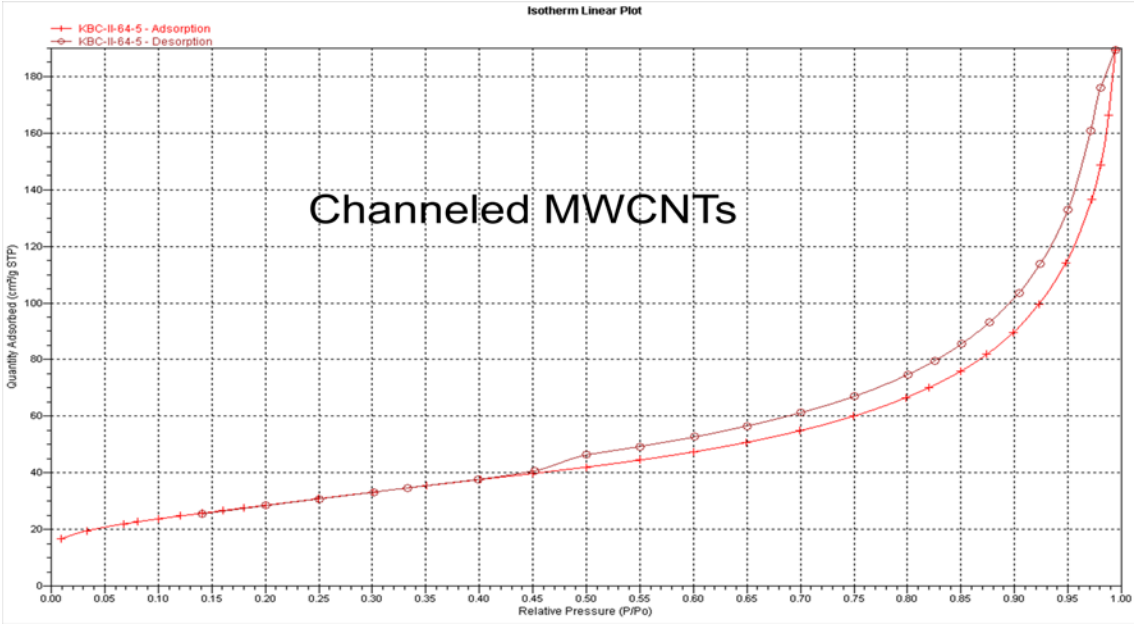

Figure 3-20: BET isotherm of channeled NMWCNTs

A mild concern in performing these measurements was that instead of measuring new changes in the nanotube morphologies, we were actually just observing the breaking up of tangles and aggregates that occurred when the NMWCNTs were converted to polyanions during the Birch reduction. To test this, samples were prepared in which nanotube pellets were made by pressing the powder samples in a hydraulic press at 100psi. This would reintroduce any agglomerations that may have broken apart during the initial reaction process. The results show that the pressing has a negligible effect on unmodified tubes, with all measurements remaining virtually unchanged. The channeled material, however, does show a slight decrease in BET surface area, total pore volume, and mesopore fraction following the pressing. This would indicate that some portion of the surface area we are observing in the channeled material was, in fact, due to disruption of tightly bound agglomerates, but a two-fold increase in BET

surface area still remained. It is possible that these changes could be classified as tube openings being filled or blocked by other tubes, and thus reducing the observable surface area and pore volume. This interpretation could be confirmed by electron microscopy, but in order to observe individual nanotubes they must be again re-dispersed and deaglomerated, which defeats the purpose of the experiment. While this experiment may provide a more accurate quantitative description of the actual surface, it does not change the qualitative observation that new surface features have been introduced into the nanotubes.

Sample	BET Surface Area m^2/g	Total Pore Volume cm^2/g	% Mesoporosity
NMWCNTs	45	0.12	49.5
Pressed NMWCNTs	43	0.14	46.5
Channeled NMWCNTs	104	0.21	65
Pressed Channeled NMWCNTs	87	0.12	57.5

Table3-2: Porosity data comparison of NMWCNTs, Pressed NMWCNTs, Channeled NMWCNTs and Pressed Channeled NMWCNTs (average of 3 runs)

Subjecting the channeled NMWCNTs to graphitization conditions affected the porosity of the sample in a very interesting way. First, the BET surface area decreased by about a factor of 2 from 104 m^2/g to 61 m^2/g. This is surprising because the TGA data, as well as several TEM images, indicate that channels are still present in the sample. When the total pore volume was calculated, however, the annealing appeared to have virtually no change on the sample. Likewise, the mesopore fraction did not change significantly.

These data are more consistent with the perception that channels still persisted following annealing. They would suggest, then, that both the pores and the inner core are still accessible to N_2. The observed decreased in BET surface area, however, is not quite as straightforward to interpret. We know that when NMWCNTs are annealed, the BET surface area drops slightly without much impact on the total pore volume or on the pore size distribution, but annealing the channeled NMWCNTs significantly decreases the BET surface area. This decrease in observed surface area could be a similar process in that the outer layers of the NMWCNTs are being "cleaned" during the annealing process. Any newly formed microporosity would be annealed out at such temperatures, thus leaving a more pristine surface with significantly less surface area, but a virtually unchanged amount of total pore volume. While as-produced NMWCNTs are thought to have more defects than their annealed counterparts, we believe the functionalized (or channeled) NMWCNTs have significantly more defect sites than their precursors. Thus, annealing would have much more overall effect on the amorphous outer surface of the channeled NMWCNTs than on as-produced NMWCNTs; accounting for the more dramatic change in BET surface area that occurs upon annealing.

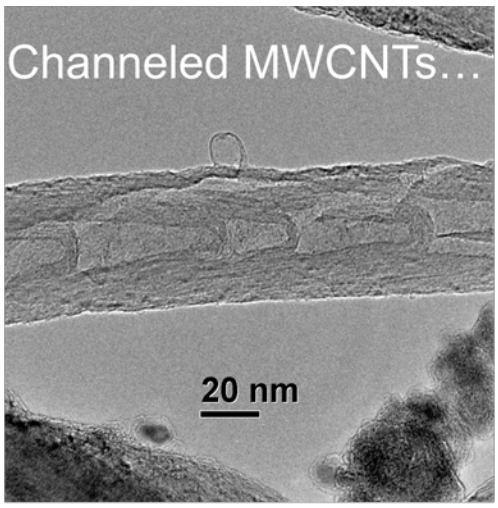

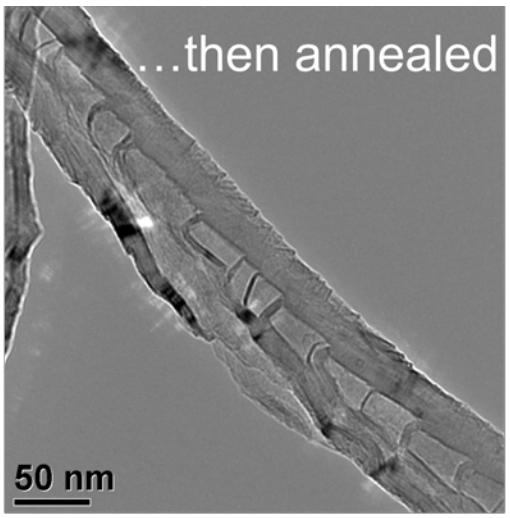

BET Surface Area (m^2/g)	104.7392	61.0666
Total Pore Volume (cm^3/g)	0.18133	0.20072
% Mesoporosity	65.1	65.0

Figure 3-21 a) TEM image of channeled NMWCNT b) TEM image of channeled NMWCNT that has been graphitized

Table 3-3: Comparison of porosity of channeled NMWCNTs and channeled-then-graphitized NMWCNTs (average of 3 runs)

It was thought that if the mechanism for channeling was dependent upon the presence of defect sites or the concentration of nitrogen, then annealing the NMWCNTs prior to exposure to the Birch conditions would prevent channeling from taking place. However, when GF-NMWCNTs were subjected to the Birch conditions, the same trend was observed. BET surface area increased by a factor of about 2.7 from $42m^2/g$ to $113m^2/g$, total pore volume more than doubled from $0.13cm^3/g$ to $0.32cm^3/g$, and about an 11% increase in the mesopore fraction could be observed.

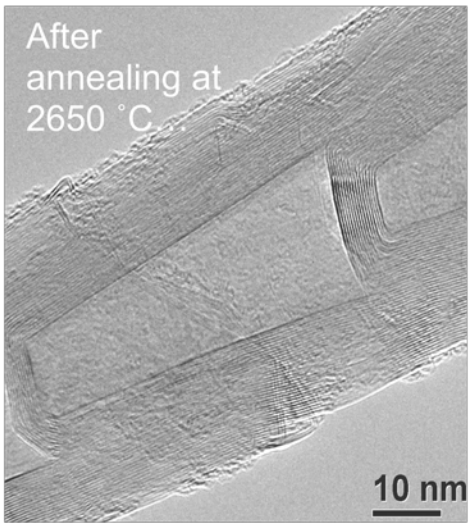

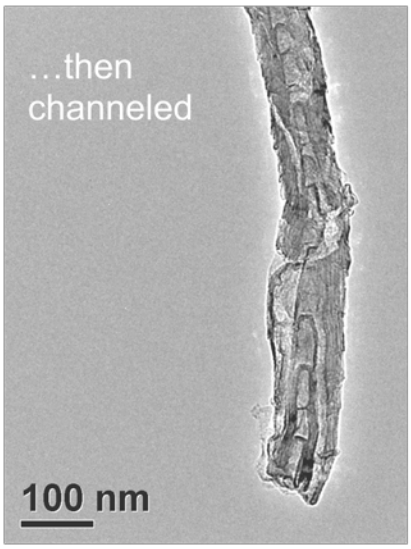

BET Surface Area (m^2/g)	42.0112	113.0663
Total Pore Volume (cm^3/g)	0.137850	0.3260
% Mesoporosity	54.6	65.5

Figure 22 a) TEM image of GF-NMWCNT b) TEM image of GF-NMWCNT that has been channeled

Table 3-4 Comparison of porosity of GF- NMWCNTs and GF- NMWCNTs that have been channeled (average of 3 runs)

Comparison of Alkylating Agents

It is clear that a great deal of energy is required in tearing through the layers of graphite in the process of opening the channels. In principle, the energy could come from the forces involved in lithium intercalation or from the strongly exothermic alkylation step. In order to explore the effect that various alkylating agents have on the channeling reaction, an array of samples were prepared using alkylating agents of increasing length and steric bulk.

Sample	BET Surface Area m^2/g	Total Pore Volume cm^3/g	% Mesoporosity
NMWCNTs	32	0.14	46.5
Ammonium Chloride	66.5	0.13	68
Iodomethane	77.5	0.13	74.5
1-bromo-pentadecane	55.5	0.26	60
t-butyl bromide	72.5	0.23	69
Trimethyl chlorosilane	72	0.22	64.8
Bromomethyl cyclehexane	84	0.21	70

Figure 3-24: structure of alkylating agents examined

Table 3-5: Porosity data of NMWCNTs reduced with lithium and quenched with varying alkylating agents (average of 3 runs)

It can be observed from the porosity data that regardless of the alkylating agent used, a significant change in BET surface area could be observed as compared to as-produced NMWCNTs. Likewise, in all cases, a spike in the mesopore fraction was also calculated. Since the change in micropore fraction was negligible, it can be assumed that any increase in the mesopore fraction comes at the expense of macroporosity or bulk

surface. In the two "non bulky" samples (NH_4Cl and CH_3I), no observable change in total pore volume could be observed. While there is no definitive trend in the surface area or porosity (and by association, with the extent of channeling) with regard to steric bulk of the alkylating agent, a few interesting observations can be made. The apparent outlier in the series is the 1-bromo pentadecane derived sample. This is not unexpected as such long chain alkyl halides are quite viscous, and more difficult to remove from the nanotube samples than any of the other lower molecular weight alkylating agents. Multiple washings were necessary to remove most of the excess starting material, and even after thorough washing, it is likely that some strongly adsorbed material remained in the sample, as indicated by the loss of 5% of the sample mass at 150^{o}C as observed in the TGA (Figure 3-35). Therefore, the slightly lower BET surface area observed in this sample may be due to adsorbed material on the carbon surface which then occupies some of the surface and pores. If 5% of the mass of the sample is adsorbed material, then a significant percentage of the surface should be covered. If the "expected" surface area should be somewhere between 65-75 m^2/g, to put the value on the same order as the other alkylating agents, then the experimental value is roughly 20-30% lower, which could correspond to the amount of the surface covered by adsorbed material. It is also of note that the two bulkiest alkylating agents, t-butyl bromide and trimethylsilyl chloride, produced nanotube samples with the most similar BET surface areas, with calculated values of approximately 72.5 and 72, respectively. Also, their TGAs are virtually identical up to the onset of oxidation, suggesting that the similar structures yield similar behavior at relatively low temperature, which is where it is

assumed any covalently bound side chains are undergoing oxidation (Figure 3-36). While no concrete trend could be established in terms of steric of bulk alkylating agents versus BET surface area, the sample that showed the greatest increase in surface was the one alkylated with bromomethyl cyclohexane ($BrCH_2Cy$) which is coincidently the bulkiest of all the alkylating agents measured due to the chair structure of the cyclohexane moiety. Likewise, the $BrCH_2Cy$ sample showed the greatest loss of mass prior to the onset of oxidation in the TGA of any sample besides the 1-bromo-pentadecane. This result is consistent with previous examples as the molecular weight of the side chains is greater than any of the other samples, save the pentadecane, and should show the greatest percentage of weight loss prior to thermal decomposition of the CNTs.

The data in Table 3-5 indicate that channeling is not dependent upon the type of alkylating agent used to quench the Birch reaction, and that changing the steric bulk of the alkylating agent has very little impact on the characteristics of the functionalized (channeled) nanotubes. While there is no trend in the surface area or in the TGA data in regards to the steric bulk of the alkylating agents used, some useful information can be extracted and can help to explain the channeling reaction, as well as to provide support of many of our previous ideas about nanotube functionalization and characterization.

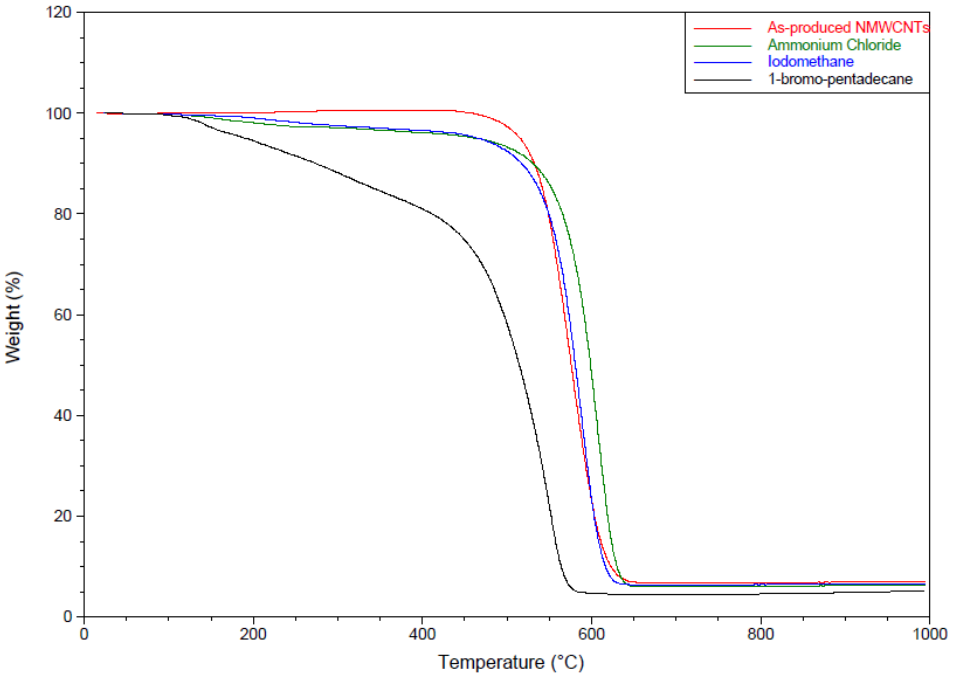

Figure 3-25: TGA of as-produced NMWCNTs, and NMWCNTs Birch-alkylated with NH_4Cl, CH_3I, and $CH_3(CH_2)_{14}Br$

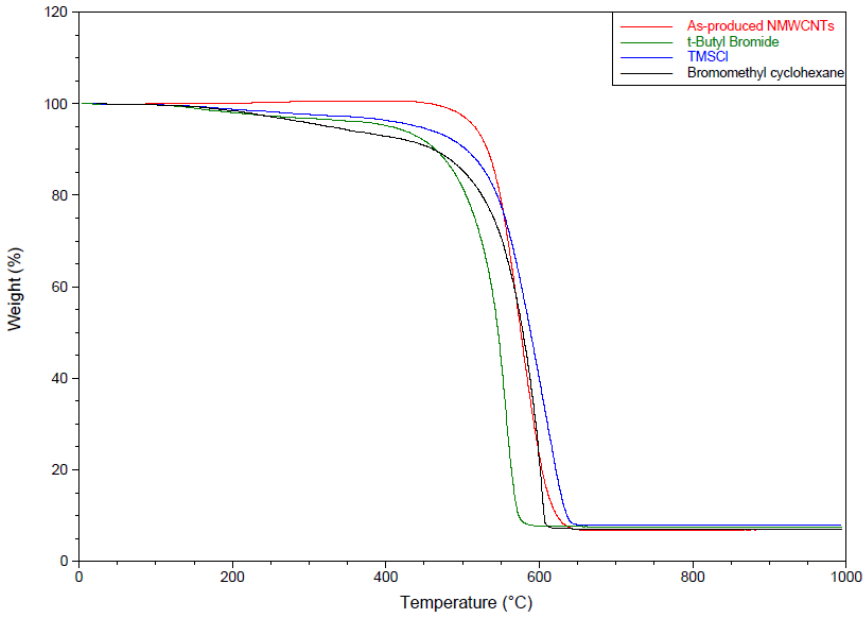

Figure 3-26: TGA of as-produced NMWCNTs, and NMWCNTs Birch-alkylated with t-Butyl Bromide, TMSCl, and Bromomethylcyclohexane

Investigation of the effect of the dissolving metal

A series of experiments was performed to investigate the effects of different reducing metals in an effort to further investigate the scope of the Birch reaction on NMWCNTs. Working under the hypothesis that metal intercalation plays a critical role in the channeling mechanism, then both the standard reduction potential of the metal[92], as well as the atomic radius[93] are potentially influential in the channeling process (Figure 3-6).

Using CH_3I as an electrophile, a series of reductive alkylations using a variety of reducing metals was performed. Of the metals studied (lithium, potassium, calcium, sodium, and magnesium), all but Mg produced more than a 2 fold increase in NMWCT surface area and a 14-18% increase in mesoporosity. This result indicated that all of these reactions successfully channeled the majority of nanotubes in the sample. If the sole factor driving the channeling reaction was the reduction potential of the metal, then lithium would be predicted to be the most effective. That lithium had virtually the same effect on the system as calcium and sodium, which have significantly lower reduction potentials, indicates that this is not necessarily the case. The only metal to have a significantly greater effect on the measured surface area was potassium. While potassium has a slightly lower reduction potential than lithium, it has a significantly larger atomic radius. Upon intercalation, the larger atom would force the graphene layers further apart, thus loading the system up with more potential energy which would make the nanotube more likely to break bonds and tear apart. This

interpretation is supported by the results with calcium and sodium which have virtually the same impact on the BET surface area of NMWCNTs as the much more reactive lithium. The least reactive metal of the series (in terms of reduction potential), magnesium, was predictably the least efficient at increasing the BET surface area of the NMWCNT samples.

Sample	Std Reduction Potential @25C of metal used [92]	Calculated Atomic Radii of metal used [93]	BET Surface Area m^2/g	Total Pore Volume cm^3/g	% Mesoporosity
NMWCNTs	N/A	N/A	45	0.12	49.5
Channeled w/ Li	-3.05 eV	167pm	104.5	0.21	65
Channeled w/ K	-2.93 eV	243pm	114	0.22	63
Channeled w/ Ca	-2.87 eV	194pm	102	0.36	63
Channeled w/ Na	-2.71 eV	190pm	100	0.17	67
Channeled w/ Mg	-2.37 eV	145pm	64	0.19	47

Table3-6: Std Reduction potentials, atomic radii, and surface area data of NMWCNTs channeled with different metals

Study of Li: C stoichiometry

In order to further investigate the effects of the Birch reaction on NMWCNTs, it is necessary to study the role of the reducing metal on the system. Previously, we looked

at the effect of different metals on the channeling reaction; and to further the study we chose the most practical metal (lithium) on which to perform a concentration study.

5 samples of Birch-alkylated NMWCNTs were prepared by standard reduction with lithium in ammonia, using iodomethane as an alkylating agent. The molar concentration of Li versus carbon (this assumes CNTs to be 100% carbon, which they clearly are not, but the ratios, qualitatively, remain constant) was increased for each sample at the following increments: 1:100, 1:50, 1:10, 1:1, and 10:1. In the low concentration samples (1:100 and 1:50), the solution barely turned a light blue and a negligible change in the nanotubes was observed by both surface area analysis (Table 3-7) and TEM microscopy (Figure 3-26). When the Li concentration was increased by an order of magnitude (as compared to the lowest concentration sample), a dark blue solution was formed, and a more significant increase in the BET surface area could be observed in the functionalized sample. The resulting material had a surface area of 58 m^2/g compared to 32 m^2/g for the as-produced material. Likewise, a 23% increase in the mesopore fraction was produced, whereas any increase in the lower concentration samples was negligible (Table 3-7). By TEM, a few of the tubes imaged contained channels, but not the majority as observed in previous samples (Figure 3-26). Upon increasing the Li concentration by another order of magnitude to a 1:1 Li:C ratio, a 300% increase in BET surface area to 100 m^2/g was calculated, which is consistent with previous reductive alkylations at similar concentrations. Likewise, the mesopore fraction increased as expected (Table 3-7), and TEM analysis showed virtually every tube had been channeled by the reaction (Figure 3-26). When the Li concentration was increased by another

order of magnitude, bronzing of the Li/NH_3 solution could be observed which is indicative of a highly reducing solution when the concentration of Li in ammonia is very high[94]. The BET surface area was slightly lower than the 1:1 concentration sample at $82m^2/g$, but the total pore volume and mesopore fraction remained essentially unchanged.

In general, an upward trend in BET surface area, total pore volume and pore size distribution could be observed within the context of the concentration study. From this, it can be asserted that at a ratio of 1 mol Li for every mol of carbon, the reaction is essentially saturated and adding any more reducing metal is not necessary for the reaction to proceed more effectively. Likewise, it can also be asserted that at least a 1:1 molar ratio of Li to carbon is necessary for the reaction to the maximum extent of channeling.

Sample	BET Surface Area m^2/g	Total Pore Volume cm^3/g	% Mesoporosity
NMWCNTs	32	0.14	46.5
1:100 Li:C	41	0.09	48.0
1:50 Li:C	30	0.12	44.0
1:10 Li:C	58	0.12	69.0
1:1 Li:C	100	0.16	72.5
10:1 Li:C	82	0.20	70

Table 3-7: Surface area data of NMWCNTs reacted with increasing lithium concentration (average of 3 runs)

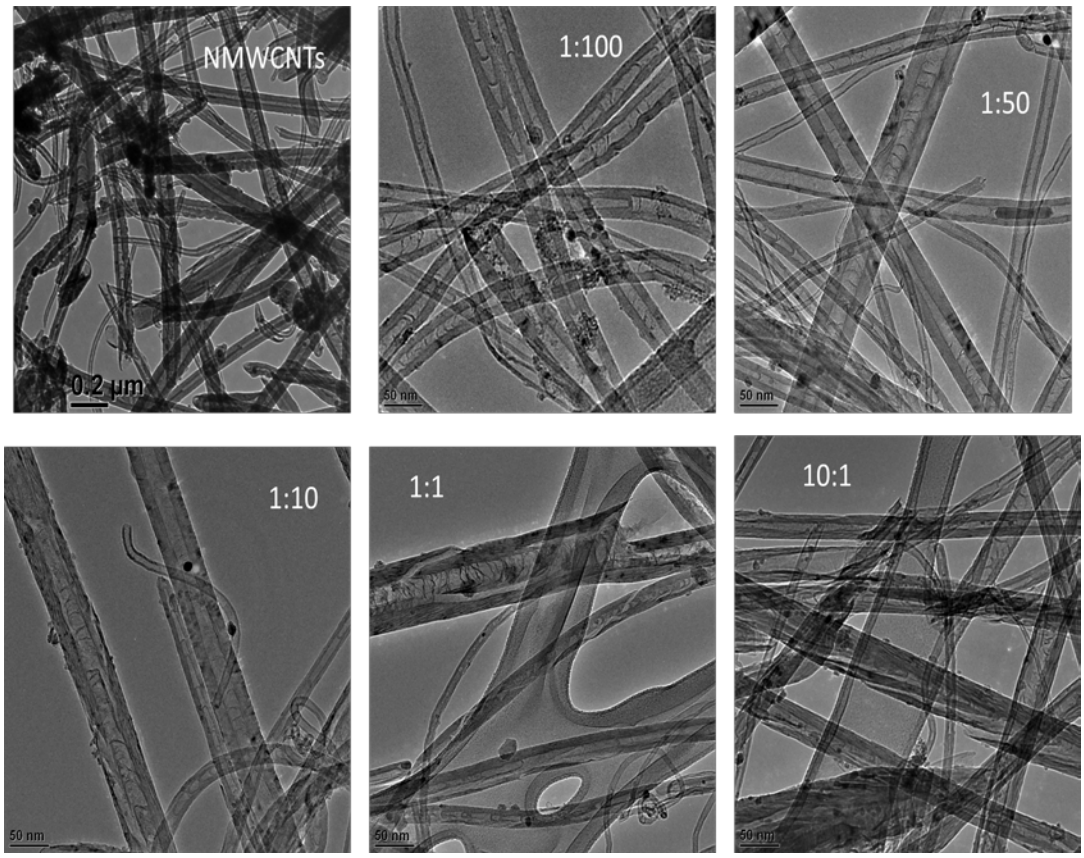

Figure 3-26: Representative TEM images of NMWCNTs reacted with increasing lithium concentration

Channeling on CH3CN-derived tubes

Thus far, the entirety of our study on the channeling reaction has been performed on NMWCNTs made from a pyridine feedstock. In order to ensure that channeling is not solely dependent on the use of pyridine-derived CNTs, it is necessary to perform the reaction on NMWCNTs that are derived from a different source of nitrogen. From CAER, we received a batch of NMWCNTs that was made from a mixture of acetonitrile and ferrocene on the smaller non-continuous reactor. From their TEM images, the acetonitrile (CH_3CN) derived NMWCNTs appear to be very similar in structure to pyridine NMWCNTs (Figure 3-27).

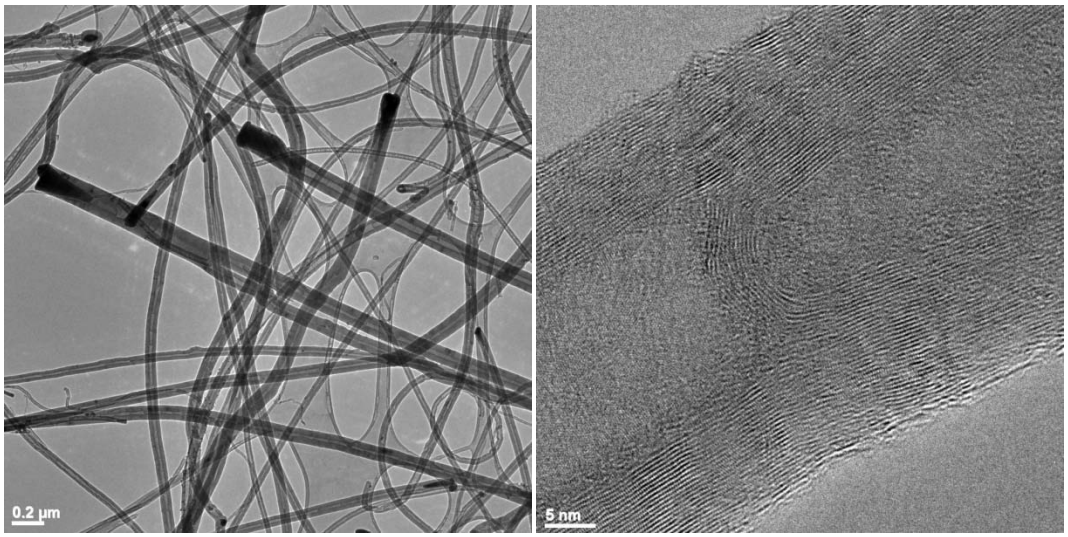

Figure 3-27: TEM images of acetonitrile derived NMWCNTs

When exposed to the Birch conditions, the CH_3CN derived NMWCNTs were essentially just as vulnerable to the channeling reaction as the previously used pyridine-derived NMWCNTs. By TEM, channels were observable in almost every CNT imaged (Figure 3-28).

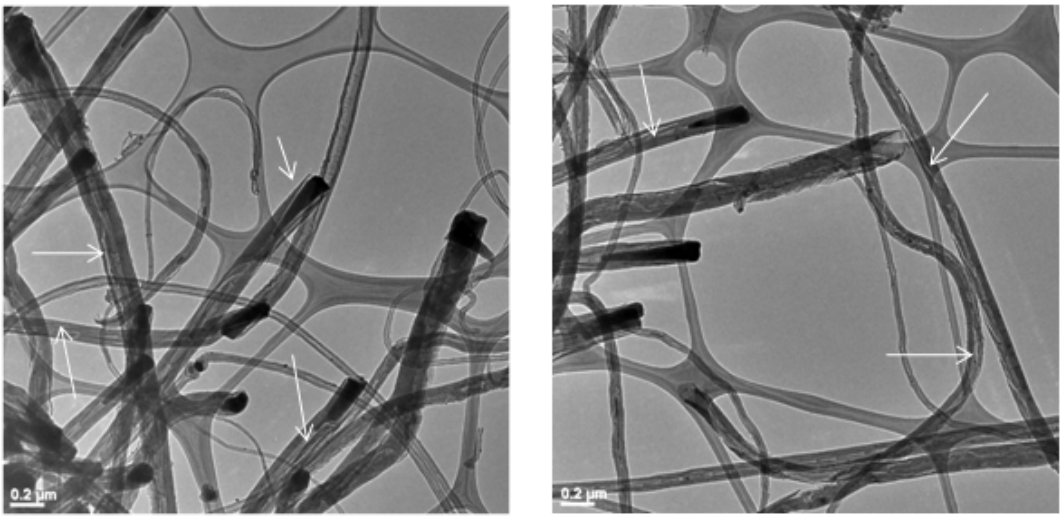

Figure 3-28: TEM images of channeled acetonitrile derived MWCNTs

Similarly, surface area analysis of the CH_3CN derived CNTs and their channeled counterparts reveal the same trend that was observed in pyridine derived CNTs. BET surface area increases by more than a factor of two, and the mesopore fraction increases by about 17%.

Sample	BET Surface Area m^2/g	Total Pore Volume cm^3/g	% Mesoporosity
CH_3CN NMWCNTs	33	0.2	51
Channeled CH_3CN NMWCNTs	77	0.12	68

Table 3- 8: Comparison of surface area data of CH3CN NMWCNTs and channeled CH3CN NMWCNTs

While a more extensive study could be done in the future exploring many different nitrogen-containing precursors, these data at least solidify the theory that the channeling reaction is not dependent on only the use of pyridine derived NMWCNTs.

Growing carbon nanotubes from a nitrogen-containing feedstock produced tubes with a stacked cup morphology. When they are treated with a reducing metal in liquid ammonia, then quenched with an electrophile, new surface features can be observed running along the tube axis and, in some cases, terminating in the nanotube's inner core. A variety of parameters have been studied to investigate the scope of the channeling reaction and probe into the mechanism of pore formation, and none of these provided a definite explaination for the formation of pores.

The results in this chapter are difficult or impossible to rationalize based a stacked cup structure. The underlying structure of the carbon within these NMWNTs appears to be more complex. Li intercalation would be expected to result in pushing cups apart along

the axis of the nanotube, possibly pushing them completely apart and produceing short tubes or individual cups. In the current materials there is no evidence for cup separation, but instead we find extensive tears in the sidewall. These features are spirals on occasion, linear in other cases. How can these features be generated in the course of a reductive alkylation?

One hypothesis is that defects in the catalyst particle could produce a similar defect in every subsequent carbon sheet formed. This might result in a weak region along the entire length of the nanotube. If true, however, this weak region is neither obvious by TEM nor is it healed by thermal annealing.

Another possibility is that the initial structure is actually better described as nesting coils of few-layer graphene sheets, and not a series of stacked cups. This would make it possible to rationalize the channels as features that have arisen from these sheets partially unwrapping. This is also difficult to believe as one would expect the sheets to completely unwrap altogether.

Another explaination could be that the individual cup layers are somehow bonded to each other, at the outer edges, along the cup bottoms, or elsewhere, thus preventing the cups from being pushed by intercalation. If this were the case, however, it would be very difficult to explain how lithium is able to intercalate all the way into the core of the nanotubes.

At this point in the project, it is very difficult to make any definitive conculsions as to either the mechanism of pore formation, or even the initial structure of the NMWCNTs themselves. However, the results in this chapter strongly suggest that the structure of these "well known" materials is not as simple or as certain as previously thought. Highly detailed structural work will need to be undertaken if a link is to be established between underlying morphology and the formation of these pores.

Chapter 4: Conclusions

Due to their unique mechanical, electrical, and thermal properties, carbon nanotubes are an exciting new class of materials that have received significant attention over the past few decades. In order to effectively utilize the physical properties of the individual nanotubes in a bulk material, it can become necessary to chemically modify the surface of the tubes to improve characteristics such as dispersability and interfacial bonding. The study of the chemistry of multiwalled carbon nanotubes is a very challenging task. Without the detailed characterization methods available to traditional organic chemists, we are compelled to turn to other methods, including thermal techniques, mechanical analysis, and microscopy. These methods probe the chemical changes made to MWCNTs, although in many cases they do indirectly, by probing how chemical modification of nanotubes affects the properties of a composite. Therefore, by nature this research area is highly cross-disciplinary, incorporating aspects of chemistry, materials science, and engineering.

We have found that by performing a dissolving-metal reduction of the MWCNTs, using a modification of the Birch reduction, it is possible to functionalize the outer shells while still maintaining the structural integrity of the MWCNTs. This reaction has proven to be reliable and reproducible in our hands, and therefore has become an extremely valuable asset in our work on nanotubes, and we have used it as our primary route to chemically modified (functionalized) nanotubes.

We have prepared functionalized nanotubes that were designed to react with polymer matrices and form covalent bonds that should facilitate load transfer from the matrix to the nanotube. We have been able to observe an exothermic crosslinking reaction in the DSC, indicating crosslinking between acid-chloride functionalized nanotubes and an epoxy matrix. By fabricating MWCNT-epoxy composites we were able to show that both acid and acid chloride functionalized MWCNTs served to consistently improve the storage modulus of the composites much greater than non-functionalized MWCNTs. Likewise, functionalized MWCNTs that we designed to crosslink with epoxy caused a decrease in the glass transition temperature in their composites, indicating a change in the chemical structure of the crosslinked matrix.

Having found that the Birch alkylation is an efficient means of MWCNT functionalization and having developed the ability to create and characterize MWCNT-polymer composites, we should be able to move forward and investigate the effects of functionalized MWCNTs on other polymer matrices. We have already begun down this path with functionalization of MWCNTs for in situ polymerization with acrylonitrile in order to form MWCNT-PAN composites that can serve as precursors to carbon fibers. Likewise, we have chemically modified MWCNTs for the sole purpose of improving dispersability in PAN, without a crosslink-capable functionality. Not only have we found that modified MWCNTs are capable of forming bonds to certain polymer matrices, but we have also discovered that by simply changing the surface chemistry of the nanotubes, composites containing these modified nanotubes are significantly easier to

process. This is due to a few factors including the breaking up of agglomerated CNTs in the reductive alkylation process, the slight shortening of tubes by mere mechanical stirring, and the changing of the surface chemisty from a mostly intert graphene-like structure, to a more sp^3 rich structure with a desired functionality For this reason, MWCNTs functionalized with both alkyl and carboxylic groups have been designed for use in PMMA composites. We believe that our ability to efficiently modify MWCNTs using the reductive alkylation method will allow us to explore the effects of functionalized nanotubes in essentially any polymer matrix desired.

It seems likely that increasing the number of functional groups on the surface of a nanotube will lead to more opportunities for crosslinking into a polymer matrix. Higher levels of crosslinking should be manifest in greater effects on the mechanical behavior of the composite. With traditional cylindrical MWCNTs, however, it was unlikely that we could create a larger number of bonds to the nanotube surface without substantially compromising the structural integrity of the nanotubes. It is for this reason that we decided to begin studying stacked cup shaped nanotubes, which have a fundamentally different structural morphology with a significantly higher density of edge sites on which to do chemistry.

Upon performing the Birch alkylation of NMWCNTs, we found that new structural features could be observed within essentially every nanotube. Using a combination of transmission- and scanning electron microscopy, these new features were determined to be cuts or channels, many of which run for microns along the entire length of the tubes. We then concentrated our efforts toward investigating the chemical and physical

nature of the channels and the of resulting nanotubes, as well was attempting to probe the possible mechanism for the formation of the channels.

When graphitized NMWCNTs were treated in the same manner, it was found that the reaction proceeded in a similar fashion. It was then concluded that neither the presence of nitrogen, nor the inclusion of defects (annealable below 2750 ^{o}C) was necessary for channeling to occur. These experiements, however, were performed on NMWCNTs that had been synthesized on the continuous batch reactor. When the tubes from the small batch reactor were annealed and subsequently Birch alkylated, some new and interesting features could be observed. It was found that, depending upon the reaction conditions, graphitized NMWCNTs not only channeled in a linear manner, but also in a spiral or helical manner. The helical features are of interest because they indicate that the structure of the nanotubes might not be exactly the stacked cup model as previously thought.

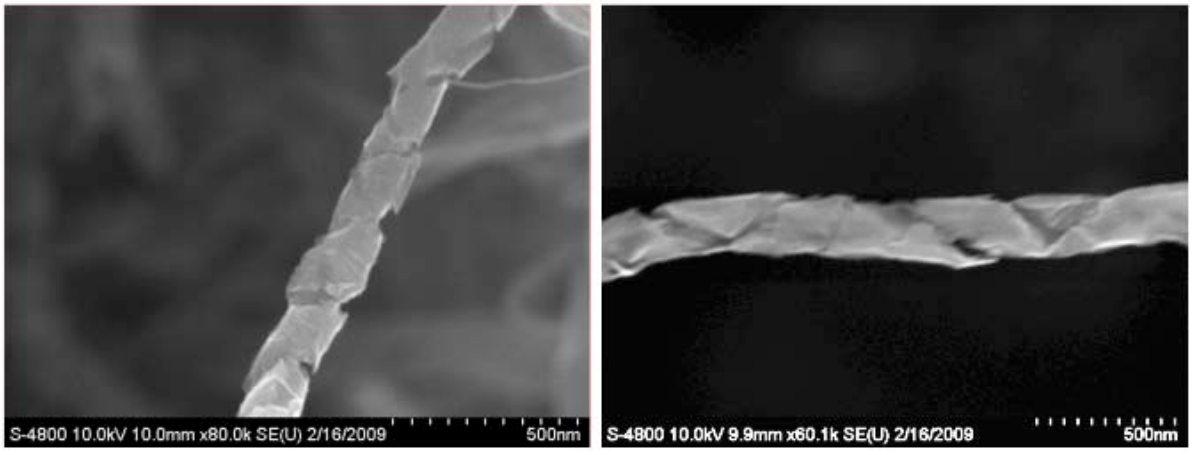

Figure 4-1: SEM images of helical cut NMWCNTs

In fact, the ribbon-like nature of the spiral cuts indicates some underlying helical structure in the starting material, but this would be very difficult to image by electron

microscopy. The structures are more easily explained if the NMWCNTs are actually composed of two morphologies; a coiled ribbon of multiple graphene layers and a stack of nesting scrolls. During the reduction, lithium could push apart the non-covalently bonded parts of the tubes to reveal the underlying structure. A more thorough study of this mechanism is currently on-going in our group.

Although carbon nanotubes have been studied extensively for the past two decades, they are still relatively novel materials. As characterization methods and techniques continue to improve, it will become easier to thoroughly study the chemistry and structure of not only CNTs, but of all carbon materials. This will serve to advance the field as a whole out of its infancy and help to unlock the great potential of these truly unique materials.

Chapter 5 Experimental Procedures

General experimental procedures:

TGA experiments were run on a TA instruments Q500 TGA and a TA instruments 2750 TGA. All samples were ground to a fine powder with sample sizes approximately 8mg and run under flowing air with a heating ramp of 10^{o}C/min from room temperature to 1000^{o}C.

All DSC experiments were run on a TA instruments Q200 DSC. Samples were prepared by thoroughly mixing appropriate amounts of nanotubes into epoxy, transferring approximately 30-50mg of uncured MWCNT/Epoxy into a DSC pan, and topping, but not sealing, with a DSC lid. Samples were run at 20^{o}C/min from 0^{o}C to 180-250^{o}C unless otherwise indicated.

All DMA experiments were run on a TA instruments Q800 DMA. A single cantilever bending experiment was performed for all samples. Samples were prepared by cutting the cured epoxy samples into approximately 30mm x 10mm x 2mm, polished to 600 grit on a wet sander, then measured precisely to 4 significant figures. Sample deflection was 5 microns at a fixed frequency of 1 Hz, carried out over a temperature range of 25 ˚C to 200 ˚C at an applied heating ramp of 2 °C/min.

All surface area measurements were performed on a Micromeritics ASAP 2020 surface analyzer. Approximately 150mg of nanotube powder was used for each run, measured precisely. All samples were degassed prior to analysis. Nitrogen physisorption at 77K was performed for all samples, using the N_2 model to calculate BET surface area data.

All SEM images were taking using a Hitachi S-4800 Scanning Electron Microscope. All TEM images were taken using a JEOL 2010F Transmission Electron Microscope.

Preparation of epoxy-MWCNT composites: An epoxy system consisting of EPON 826 (resin), nadic methyl anhydride (NMA, curing agent) and 2,4-ethyl methyl imidazole (EMI-24, catalyst), in a ratio of 100:85:1 respectively, was used in preparing epoxy-carbon nanotube (CNT) composites containing 0, 1, 2, 5 and 10 vol% nanotube filler in the following manner: The appropriate amounts of EPON 826, NMA, and CNTs were mixed in a Thinky planetary mixer for 3 minutes at 2000 rpm, and then defoamed for 2 min at 2200rpm. Defoaming is a process in which the planetary motion of the mixer is disabled, and only the centrifugal motion is used. This mixture was then placed on an EXAKT 80E 3-roll mill and mixed 5 times using the following protocol:

Pass	Gap 1 (μm)	Gap 2 (μm)	Speed (rpm)
1	50	40	200
2	25	20	200
3	10	5	200
4	5	5	250
5	5	5	250

Table 5-1: 3 Roll Milling Sequence

Volume % was calculated using the following formula:

$$v_f = (\frac{g_f}{\rho_f})/((\left(\frac{g_f}{\rho_f}\right) + \left(\frac{g_m}{\rho_m}\right))$$

Where v_f = volume of filler

g_f = grams of filler, g_m = grams of matrix

ρ_f = density of filler, ρ_m = density of matrix

Once milling was complete, EMI-24 was added and the planetary mixing procedure was repeated in order to disperse the catalyst throughout the sample. The epoxy-nanotube mixture was then poured into 80mm x 10mm x 2mm PTFE molds and placed under vacuum at 60 ^{o}C for 30 minutes. The samples were then removed from vacuum, placed in a programmable furnace, and cured with the following protocol: heated at 50 ^{o}C for 6 hours, warmed to 150 ˚C at 0.5 ^{o}C/min, and held at 150 ˚C for 3 hours.

Birch hydrogenated MWCNTs. A 3neck round bottomed flask was closed off and flushed with N_2. Approximately 50mL NH_3 was condensed into the flask using a dry ice/acetone bath. Once the ammonia was collected, 0.300 g of lithium metal was added and allowed to stir for 10min, turning the solution a dark blue. MWCNTs (0.514 g, batch S27) was then added and allowed to stir for 30min. Ammonium chloride (3.338 g) was used to quench the reaction. The solution was stirred overnight until the ammonia completely evaporated. Once the mixture was dry, approximately 50mL H_2O was added to the flask and stirred. The sample was then filtered using a Buchner funnel, and

the black solid was washed with H_2O until a neutral pH was reached, then finally washed with absolute ethanol. Sample was then dried over night under vacuum at 50 ^oC.

Birch alkylation of MWCNTs with ethyl bromoacetate (KBC-I-34). A 3-neck round bottomed flask was closed off and flushed with N_2. Approximately 200 mL NH_3 was condensed into the flask using a dry ice/acetone bath. Once the ammonia was collected, 0.896 g of lithium metal was added and stirred for 10min, turning the solution a dark blue. MWCNTs (2.066 g, batch S27) was then added and stirred for 30min. Ethyl bromoacetate (25mL) was added to quench the reaction. Solution was stirred overnight until the ammonia had completely evaporated. Once dry, approximately 50mL H_2O was added to the flask and allowed to stir. Sample was then filtered using a Buchner funnel, and washed with H_2O until a neutral pH was reached, then finally washed with absolute ethanol. Sample was then dried over night under vacuum at 50 ^oC.

TETA amidation of KBC-I-34

To a 100mL beaker was added 2.113 g of KBC-I-34 and 35mL of triethylene tetramine. Mixture was sonicated using an ultrasonic horn for 45min at 50% duty cycle and power level 2. Sample was transferred to a 150mL round bottomed flask, heated to 180 ^oC and stirred under N_2 for 48hrs. Sample was allowed to cool to room temperature, and toluene was added to dilute the mixture. Sample was then washed and filtered using

10% HCl x3, then saturated $NaHCO_3$ x 3. Final rinse was performed with absolute ethanol, and allowed to dry over night under vacuum at 50 ^{o}C.

MWCNTs Birch alkylated with ethyl bromoacetate (KBC-I-39)

A 3neck round bottomed flask was equipped with a magnetic stir bar, closed off and flushed with N_2. Approximately 500mL NH_3 was condensed into the flask using a dry ice/acetone bath. Once the ammonia was collected, 0.792 g of lithium metal was added and allowed to stir for 10min, turning the solution a dark blue. MWCNTs (2.080 g batch S27) were then added and allowed to stir for 30min. 25mL ethyl bromoacetate was used to quench the reaction. The solution was stirred overnight until the ammonia completely evaporated. Once the mixture was dry, approximately 250mL H_2O was added to the flask and stirred. The sample was then filtered using a Buchner funnel, and the black solid was washed with H_2O until a neutral pH was reached, then finally washed with absolute ethanol. Sample was then dried over night under vacuum at 50 ^{o}C.

Saponification of KBC-I-39 (KBC-I-42)

To a round bottomed was added 2.318g KBC-I-39 and 250mL 1M NaOH. Sample was heated to 80 ^{o}C and stirred for 48hrs. Sample was filtered and washed with 10% HCl, water, and finally with absolute ethanol. Sample was then dried over night under vacuum at 50^{o}C.

Peptide coupling of bromoacetic acid and TETA (KBC-I-44)

Bromoacetic acid (34.21mL) was added to 270mL CH_2Cl_2 in a 500mL round bottom flask equipped with a stir bar. The solution was placed in an ice bath and allowed to stir for 5 minutes. 29.05 g dicyclohexyl carbodiimide (DCC) was added to the solution and allowed to stir for 1 hour. Bromovacetic anhydride intermediate was generated in situ, and the solution was filtered 3 times on a Buchner funnel to collect the precipitate generated (DCU). Solvent was then removed by vacuum distillation and redisolved in hexane. 45mL TETA was diluted in 115mL THF, and added dropwise to solution and allowed to stir for 3 hours. Solvent was removed by vacuum distillation. Product was soluble in $NaHCO_3$, and extracted 3 times with CH_2Cl_2. Product was dried with $NaSO_4$ and solvent was removed by vacuum filtration.

Peptide coupling of bromovaleric acid and TETA (KBC-I-48)

Bromovaleric acid (10.107 g) was added to 270mL CH_2Cl_2 in a 500mL round bottom flask equipped with a stir bar. The solution was placed in an ice bath and allowed to stir for 5 minutes. Dicyclohexyl carbodiimide (DCC) (10.193 g) was added to the solution and allowed to stir for 1 hour. Bromovaleric anhydride intermediate was generated in situ, and the solution was filtered 3 times on a Buchner funnel to collect the precipitate generated (DCU). Solvent was then removed by vacuum distillation, and 8.123 g crude product was collected. The crude anhydride product (6.738) was added to a 3 neck round bottomed flask and diluted in 115mL THF. TETA (7mL) was diluted in 100mL THF, and added dropwise to solution and allowed to stir for 3 hours. Solvent was removed by vacuum distillation.

Birch alkylation using KBC-I-44

A 3neck round bottomed flask was equipped with a magnetic stir bar, closed off and flushed with N_2. Approximately 50mL NH_3 was condensed into the flask using a dry ice/acetone bath. Once the ammonia was collected, 0.185 g of lithium metal was added and allowed to stir for 10min, turning the solution a dark blue. MWCNTs (0.111g batch S27) were then added and allowed to stir for 30min. KBC-I-44 (25mL) was used to quench the reaction. The solution was stirred overnight until the ammonia completely evaporated. Once the mixture was dry, approximately 250mL H_2O was added to the flask and stirred. The sample was then filtered using a Buchner funnel, and the black solid was washed with H_2O until a neutral pH was reached, then finally washed with absolute ethanol. Sample was then dried over night under vacuum at 50 ^oC.

Peptide coupling of KBC-I-42 and TETA

To a round bottom flask was added 1.059g KBC-I-42 (saponifed MWCNTs), 20g DCC, and 45mL TETA. Mixture was heated to 120 ^oC and stirred under nitrogen for 24 hours. Ethanol was then added and suspension was filtered and washed with ethanol. . Sample was then washed and filtered using 10% HCl x3, then saturated $NaHCO_3$ x 3. Final rinse was performed with absolute ethanol, and allowed to dry over night under vacuum at 50 ^oC.

Birch reduction using ethyl bromobutyrate (KBC-I-50)

A 3neck round bottomed flask was equipped with a magnetic stir bar, closed off and flushed with N_2. Approximately 250mL NH_3 was condensed into the flask using a dry ice/acetone bath. Once the ammonia was collected, 0.810 g of lithium metal was added and allowed to stir for 10min, turning the solution a dark blue. MWCNTs (2.214 g batch

S27) were then added and allowed to stir for 30min. Ethyl bromobutyrate (25mL) was used to quench the reaction. The solution was stirred overnight until the ammonia completely evaporated. Once the mixture was dry, approximately 250mL H_2O was added to the flask and stirred. The sample was then filtered using a Buchner funnel, and the black solid was washed with H_2O until a neutral pH was reached, then finally washed with absolute ethanol. Sample was then dried over night under vacuum at 50 ^oC.

Saponification of KBC-I-50 (KBC-I-52)

To a round bottomed was added 1.126 g KBC-I-50 and 150mL 1M NaOH. Sample was heated to 80 ^oC and stirred for 48hrs. Sample was filtered and washed with 10% HCl, water, and finally with absolute ethanol. Sample was then dried over night under vacuum at 50 ^oC.

Peptide coupling of KBC-I-52 and TETA

To a round bottom flask was added 0.895g KBC-I-52 (saponifed MWCNTs), 20 g DCC, and 45mL TETA. Mixture was heated to 120 ^oC and stirred under nitrogen for 24 hours. Ethanol was then added and suspension was filtered and washed with ethanol. . Sample was then washed and filtered using 10% HCl x3, then saturated $NaHCO_3$ x 3. Final rinse was performed with absolute ethanol, and allowed to dry over night under vacuum at 50 ^oC.

Bromoacetic anhydride + TETA

TETA (10mL) was diluted in 150mL ether and added to a 3 neck round bottom flask equipped with a magnetic stir bar. To an addition funnel was added 10.260 g bromoacetic anhydride in 150mL ether. The anhydride solution was added dropwise to the TETA solution under nitrogen in an icebath, then stirred for 2hrs. Solvent was removed by vacuum distillation and remaining salt was diluted by saturated $NaHCO_3$. Product was extracted with CH_2Cl_2, dried with $NaSO_4$, and solvent was removed by vacuum distillation.

Birch reduction using ethyl bromobutyrate (KBC-I-69)

A 3neck round bottomed flask was equipped with a magnetic stir bar, closed off and flushed with N_2. Approximately 250mL NH_3 was condensed into the flask using a dry ice/acetone bath. Once the ammonia was collected, 0.733 g of lithium metal was added and allowed to stir for 10min, turning the solution a dark blue. MWCNTs (1.945 g batch S27) were then added and allowed to stir for 30min. Ethyl bromobutyrate (25mL) was used to quench the reaction. The solution was stirred overnight until the ammonia completely evaporated. Once the mixture was dry, approximately 250mL H_2O was added to the flask and stirred. The sample was then filtered using a Buchner funnel, and the black solid was washed with H_2O until a neutral pH was reached, then finally washed with absolute ethanol. Sample was then dried over night under vacuum at 50 ^oC.

Saponification of KBC-I-69 (KBC-I-70)

To a round bottomed was added 1.032 g KBC-I-69 and 150mL 1M NaOH. Sample was heated to 80 ^oC and stirred for 48hrs. Sample was filtered and washed with 10% HCl,

water, and finally with absolute ethanol. Sample was then dried over night under vacuum at 50 ^{o}C.

Thionyl chloride treatment of KBC-I-70

To a round bottomed flask was added 0.774 g KBC-I-70 and 100mL thionyl chloride ($SOCl_2$). Mixture was stirred under reflux for 24 hours. After the reaction time, the remaining $SOCl_2$ was distilled away, and toluene was stirred in. Sample was washed and filtered with toluene and dried under vacuum over night.

Large scale Birch alkylation using ethyl bromoacetate for use in epoxy (KBC-III-21)

A 5neck 12L round bottomed flask was equipped with a mechanical stirrer, 2 coldfinger condensers, closed off and flushed with N_2. Approximately 6L NH_3 was condensed into the flask using a dry ice/acetone bath. Once the ammonia was collected, 6 g of lithium metal was added and allowed to stir for 10min, turning the solution a dark blue. MWCNTs (20 g batch S31) were then added and allowed to stir for 30min. Ethyl bromoacetate (50mL) was used to quench the reaction. The solution was stirred overnight until the ammonia completely evaporated. Once the mixture was dry, approximately 6L H_2O was added to the flask and stirred. The sample was then filtered using a Buchner funnel, and the black solid was washed with H_2O until a neutral pH was reached, then washed with ethanol, DCM and finally washed with absolute ethanol. Sample was then dried over night under vacuum at 50 ^{o}C.

Saponification of KBC-III-21 (KBC-III-21)

To a round bottomed was added 10 g KBC-III-21 and 1.5L 1M NaOH. Sample was heated to 80 ^{o}C and stirred for 48hrs. Sample was filtered and washed with 10% HCl, water, and finally with absolute ethanol. Sample was then dried over night under vacuum at 50 ^{o}C.

Thionyl chloride treatment of KBC-III-23 (KBC-III-25)

To a round bottomed flask was added 10 g KBC-III-23 and 1500mL $SOCl_2$. Mixture was stirred under reflux for 24 hours. After the reaction time, the remaining $SOCl_2$ was distilled away, and toluene was stirred in. Sample was washed and filtered with toluene and pentane and dried under vacuum over night.

Birch methylation of NMWCNTs

A 3neck round bottomed flask was equipped with a magnetic stir bar, closed off and flushed with N_2. Approximately 75mL NH_3 was condensed into the flask using a dry ice/acetone bath. Once the ammonia was collected, 0.150 g of lithium metal was added and allowed to stir for 10min, turning the solution a dark blue. NMWCNTs (0.10 g batch S19) were then added and allowed to stir for 30min. Iodomethane (2mL) was used to quench the reaction. The solution was stirred overnight until the ammonia completely evaporated. Once the mixture was dry, approximately 250mL H_2O was added to the flask and stirred. The sample was then filtered using a Buchner funnel, and the black solid was washed with H_2O until a neutral pH was reached, then finally washed with absolute ethanol. Sample was then dried over night under vacuum at 50 ^{o}C.

Birch methylation of GF-51 NMWCNTs

A 3neck round bottomed flask was equipped with a magnetic stir bar, closed off and flushed with N_2. Approximately 50mL NH_3 was condensed into the flask using a dry ice/acetone bath. Once the ammonia was collected, 0.370 g of lithium metal was added and allowed to stir for 10min, turning the solution a dark blue. NMWCNTs (0.53 g batch GF 51) were then added and allowed to stir for 30min. Iodomethane (10mL) was used to quench the reaction. The solution was stirred overnight until the ammonia completely evaporated. Once the mixture was dry, approximately 250mL H_2O was added to the flask and stirred. The sample was then filtered using a Buchner funnel, and the black solid was washed with H_2O until a neutral pH was reached, then finally washed with absolute ethanol. Sample was then dried over night under vacuum at 50 ^{o}C.

Birch alkylation of NMWCNTs using 1-bromopentadecane

A 3neck round bottomed flask was equipped with a magnetic stir bar, closed off and flushed with N_2. Approximately 150mL NH_3 was condensed into the flask using a dry ice/acetone bath. Once the ammonia was collected, 0.418 g of lithium metal was added and allowed to stir for 10min, turning the solution a dark blue. NMWCNTs (0.42 g) were then added and allowed to stir for 30min. 1-bromopentadecane (7mL) was used to quench the reaction. The solution was stirred overnight until the ammonia completely evaporated. Once the mixture was dry, approximately 250mL H_2O was added to the flask and stirred. The sample was then filtered using a Buchner funnel, and the black solid was washed with H_2O until a neutral pH was reached, then finally washed with absolute ethanol. Sample was then dried over night under vacuum at 50 ^{o}C. After

drying, sample retained adsorbed 1-bromopentadecane, and was washed using Soxlet for 3 days. Sample was then dried over night under vacuum at 50^{o}C.

Birch alkylation of NMWCNTs using t-butyl bromide

A 3neck round bottomed flask was equipped with a magnetic stir bar, closed off and flushed with N_2. Approximately 150mL NH_3 was condensed into the flask using a dry ice/acetone bath. Once the ammonia was collected, 0.41 g of lithium metal was added and allowed to stir for 10min, turning the solution a dark blue. 0.41 g of NMWCNTs (0.41 g) were then added and allowed to stir for 30min. Tert-butyl bromide (4mL) was used to quench the reaction. The solution was stirred overnight until the ammonia completely evaporated. Once the mixture was dry, approximately 250mL H_2O was added to the flask and stirred. The sample was then filtered using a Buchner funnel, and the black solid was washed with H_2O until a neutral pH was reached, then finally washed with absolute ethanol. Sample was then dried over night under vacuum at 50 ^{o}C.

Birch alkylation of NMWCNTs using TMSCl

A 3neck round bottomed flask was equipped with a magnetic stir bar, closed off and flushed with N_2. Approximately 150mL NH_3 was condensed into the flask using a dry ice/acetone bath. Once the ammonia was collected, 0.46 g of lithium metal was added and allowed to stir for 10min, turning the solution a dark blue. NMWCNTs (0.46 g) were then added and allowed to stir for 30min. TMSCl (5mL) was used to quench the reaction. The solution was stirred overnight until the ammonia completely evaporated. Once the mixture was dry, approximately 250mL H_2O was added to the flask and stirred. The sample was then filtered using a Buchner funnel, and the black solid was washed

with H_2O until a neutral pH was reached, then finally washed with absolute ethanol. Sample was then dried over night under vacuum at 50 ^oC.

Birch alkylation of NMWCNTs using iodomethane

A 3neck round bottomed flask was equipped with a magnetic stir bar, closed off and flushed with N_2. Approximately 150mL NH_3 was condensed into the flask using a dry ice/acetone bath. Once the ammonia was collected, 0.40 g of lithium metal was added and allowed to stir for 10min, turning the solution a dark blue. NMWCNTs (0.45 g) were then added and allowed to stir for 30min. 4mL iodomethane was used to quench the reaction.The solution was stirred overnight until the ammonia completely evaporated. Once the mixture was dry, approximately 250mL H_2O was added to the flask and stirred. The sample was then filtered using a Buchner funnel, and the black solid was washed with H_2O until a neutral pH was reached, then finally washed with absolute ethanol. Sample was then dried over night under vacuum at 50 ^oC.

Birch reduction of NMWCNTs using NH_4Cl

A 3neck round bottomed flask was equipped with a magnetic stir bar, closed off and flushed with N_2. Approximately 150mL NH_3 was condensed into the flask using a dry ice/acetone bath. Once the ammonia was collected, 0.433 g of lithium metal was added and allowed to stir for 10min, turning the solution a dark blue. NMWCNTs (0.431 g) were then added and allowed to stir for 30min. Ammonium chloride (4.2 g) was used to quench the reaction. The solution was stirred overnight until the ammonia completely evaporated. Once the mixture was dry, approximately 250mL H_2O was added to the flask and stirred. The sample was then filtered using a Buchner funnel, and the black

solid was washed with H_2O until a neutral pH was reached, then finally washed with absolute ethanol. Sample was then dried over night under vacuum at 50 ^oC.

Birch methylation of NMWCNTs using potassium

A 3neck round bottomed flask was equipped with a magnetic stir bar, closed off and flushed with N_2. Approximately 150mL NH_3 was condensed into the flask using a dry ice/acetone bath. Once the ammonia was collected, 3 g of potassium metal was added and allowed to stir for 10min, turning the solution a dark blue. NMWCNTs (1.001 g) were then added and allowed to stir for 30min. Iodomethane (5mL) was used to quench the reaction. The solution was stirred overnight until the ammonia completely evaporated. Once the mixture was dry, approximately 250mL H_2O was added to the flask and stirred. The sample was then filtered using a Buchner funnel, and the black solid was washed with H_2O until a neutral pH was reached, then finally washed with absolute ethanol. Sample was then dried over night under vacuum at 50 ^oC.

Birch methylation of NMWCNTs using sodium

A 3neck round bottomed flask was equipped with a magnetic stir bar, closed off and flushed with N_2. Approximately 150mL NH_3 was condensed into the flask using a dry ice/acetone bath. Once the ammonia was collected, 1.06 g of sodium metal was added and allowed to stir for 10min, turning the solution a dark blue. NMWCNTs (0.526 g) were then added and allowed to stir for 30min. Iodomethane (2.5mL) was used to quench the reaction. The solution was stirred overnight until the ammonia completely evaporated. Once the mixture was dry, approximately 250mL H_2O was added to the

flask and stirred. The sample was then filtered using a Buchner funnel, and the black solid was washed with H_2O until a neutral pH was reached, then finally washed with absolute ethanol. Sample was then dried over night under vacuum at 50 ^{o}C.

Birch methylation of NMWCNTs using magnesium

A 3neck round bottomed flask was equipped with a magnetic stir bar, closed off and flushed with N_2. Approximately 150mL NH_3 was condensed into the flask using a dry ice/acetone bath. Once the ammonia was collected, 0.502 g of magnesium metal was added and allowed to stir for 10min. NMWCNTs (5.02 g) were then added and allowed to stir for 30min. Iodomethane (3mL) was used to quench the reaction. The solution was stirred overnight until the ammonia completely evaporated. Once the mixture was dry, approximately 250mL H_2O was added to the flask and stirred. The sample was then filtered using a Buchner funnel, and the black solid was washed with H_2O until a neutral pH was reached, then finally washed with absolute ethanol. Sample was then dried over night under vacuum at 50 ^{o}C.

Birch methylation of NMWCNTs using calcium

A 3neck round bottomed flask was equipped with a magnetic stir bar, closed off and flushed with N_2. Approximately 200mL NH_3 was condensed into the flask using a dry ice/acetone bath. Once the ammonia was collected, 1.663 g of sodium metal was added and allowed to stir for 10min, turning the solution a dark blue. NMWCNTs (0.503 g) were then added and allowed to stir for 30min. Iodomethane (3mL) was used to quench the reaction. The solution was stirred overnight until the ammonia completely evaporated. Once the mixture was dry, approximately 250mL H_2O was added to the

flask and stirred. The sample was then filtered using a Buchner funnel, and the black solid was washed with H_2O until a neutral pH was reached, then finally washed with absolute ethanol. Sample was then dried over night under vacuum at 50 ^{o}C.

Birch methylation of NMWCNTs 1:100 Li:C

A 3neck round bottomed flask was equipped with a magnetic stir bar, closed off and flushed with N_2. Approximately 150mL NH_3 was condensed into the flask using a dry ice/acetone bath. Once the ammonia was collected, 8.3 mg (0.0012mol) of lithium metal was added and allowed to stir for 10min, turning the solution a light blue. NMWCNTs (1.44 g, 0.12mol) were then added and allowed to stir for 30min. Iodomethane (10mL) was used to quench the reaction. The solution was stirred overnight until the ammonia completely evaporated. Once the mixture was dry, approximately 250mL H_2O was added to the flask and stirred. The sample was then filtered using a Buchner funnel, and the black solid was washed with H_2O until a neutral pH was reached, then finally washed with absolute ethanol. Sample was then dried over night under vacuum at 50 ^{o}C.

Birch methylation of NMWCNTs 1:50 Li:C

A 3neck round bottomed flask was equipped with a magnetic stir bar, closed off and flushed with N_2. Approximately 150mL NH_3 was condensed into the flask using a dry ice/acetone bath. Once the ammonia was collected, 0.0206 g (0.003mol) of lithium metal was added and allowed to stir for 10min, turning the solution a light blue. NMWCNTs (1.80 g, 0.15mol) were then added and allowed to stir for 30min. Iodomethane (10mL) was used to quench the reaction. The solution was stirred

overnight until the ammonia completely evaporated. Once the mixture was dry, approximately 250mL H_2O was added to the flask and stirred. The sample was then filtered using a Buchner funnel, and the black solid was washed with H_2O until a neutral pH was reached, then finally washed with absolute ethanol. Sample was then dried over night under vacuum at 50 ^oC.

Birch methylation of NMWCNTs 1:10 Li:C

A 3neck round bottomed flask was equipped with a magnetic stir bar, closed off and flushed with N_2. Approximately 200mL NH_3 was condensed into the flask using a dry ice/acetone bath. Once the ammonia was collected, 0.060 g (0.0086mol) of lithium metal was added and allowed to stir for 10min, turning the solution a dark blue. NMWCNTs (1.04 g, 0.086mol) were then added and allowed to stir for 30min. Iodomethane (10mL) was used to quench the reaction. The solution was stirred overnight until the ammonia completely evaporated. Once the mixture was dry, approximately 250mL H_2O was added to the flask and stirred. The sample was then filtered using a Buchner funnel, and the black solid was washed with H_2O until a neutral pH was reached, then finally washed with absolute ethanol. Sample was then dried over night under vacuum at 50 ^oC.

Birch methylation of NMWCNTs 1:1 Li:C

A 3neck round bottomed flask was equipped with a magnetic stir bar, closed off and flushed with N_2. Approximately 150mL NH_3 was condensed into the flask using a dry ice/acetone bath. Once the ammonia was collected, 0.440 g (0.064mol) of lithium metal

was added and allowed to stir for 10min, turning the solution a dark blue. NMWCNTs (0.768 g, 0.064mol) were then added and allowed to stir for 30min. Iodomethane (5mL) was used to quench the reaction. The solution was stirred overnight until the ammonia completely evaporated. Once the mixture was dry, approximately 250mL H_2O was added to the flask and stirred. The sample was then filtered using a Buchner funnel, and the black solid was washed with H_2O until a neutral pH was reached, then finally washed with absolute ethanol. Sample was then dried over night under vacuum at 50 ^oC.

Birch methylation of NMWCNTs 10:1 Li:C

A 3neck round bottomed flask was equipped with a magnetic stir bar, closed off and flushed with N_2. Approximately 150mL NH_3 was condensed into the flask using a dry ice/acetone bath. Once the ammonia was collected, 2.69 g (0.388mol) of lithium metal was added and allowed to stir for 10min, turning the solution a dark blue with bronzing. NMWCNTs (0.465 g, 0.038mol) were then added and allowed to stir for 30min. Iodomethane (5mL) was used to quench the reaction. The solution was stirred overnight until the ammonia completely evaporated. Once the mixture was dry, approximately 250mL H_2O was added to the flask and stirred. The sample was then filtered using a Buchner funnel, and the black solid was washed with H_2O until a neutral pH was reached, then finally washed with absolute ethanol. Sample was then dried over night under vacuum at 50 ^oC.

References

(1) Monthioux, M.; Kuznetsov, V. L. *Carbon* **2006**, *44*, 1621.

(2) Bethune, D. S.; Kiang, C. H.; Devries, M. S.; Gorman, G.; Savoy, R.; Vazquez, J.; Beyers, R. *Nature* **1993**, *363*, 605.

(3) Boehm, H. P. *Carbon* **1997**, *35*, 581.

(4) Iijima, S. *Nature* **1991**, *354*, 56.

(5) Iijima, S.; Ichihashi, T. *Nature* **1993**, *363*, 603.

(6) Oberlin, A.; Endo, M.; Koyama, T. *J Cryst Growth* **1976**, *32*, 335.

(7) Baughman, R. H.; Zakhidov, A. A.; de Heer, W. A. *Science* **2002**, *297*, 787.

(8) Fal'ko, V. I.; Geim, A. K. *Eur Phys J-Spec Top* **2007**, *148*, 1.

(9) Geim, A. K.; MacDonald, A. H. *Phys Today* **2007**, *60*, 35.

(10) Geim, A. K.; Novoselov, K. S. *Nat Mater* **2007**, *6*, 183.

(11) Meyer, J. C.; Geim, A. K.; Katsnelson, M. I.; Novoselov, K. S.; Booth, T. J.; Roth, S. *Nature* **2007**, *446*, 60.

(12) Du, F.; Ma, Y.; Lv, X.; Huang, Y.; Li, F.; Chen, Y. *Carbon* **2006**, *44*, 1327.

(13) Matthews, K. D.; Lemaitre, M. G.; Kim, T.; Chen, H.; Shim, M.; Zuo, J.-M. *Journal of Applied Physics* **2006**, *100*, 044309/1.

(14) Andrews, R.; Rantell, T.; Jacques, D.; Qian, D. *Accounts of Chemical Research* **2002**, *35*, 1008.

(15) Sinnott, S. B.; Andrews, R. *Crit Rev Solid State* **2001**, *26*, 145.

(16) Avouris, P.; Collins, P. G. *Scientific American* **2000**, 62.

(17) Marrs, B.; Andrews, R.; Pienkowski, D. *Carbon* **2007**, *45*, 2098.

(18) Wichmann, M. H. G.; Sumfleth, J.; Fiedler, B.; Gojny, F. H.; Schulte, K. *Mechanics of Composite Materials* **2006**, *42*, 395.

(19) Li, N.; Huang, Y.; Du, F.; He, X.; Lin, X.; Gao, H.; Ma, Y.; Li, F.; Chen, Y.; Eklund, P. C. *Nano Letters* **2006**, *6*, 1141.

(20) Sinha, N.; Ma, J.; Yeow John, T. W. *J Nanosci Nanotechnol* **2006**, *6*, 573.

(21) Avouris, P. *Accounts of Chemical Research* **2002**, *35*, 1026.

(22) Martel, R.; Schmidt, T.; Shea, H. R.; Hertel, T.; Avouris, P. *Applied Physics Letters* **1998**, *73*, 2447.

(23) Andrews, R.; Qian, D.; Jacques, D. *ACS National Meeting, Fall 2001* **2001**.

(24) Hirsch, A. *Synthesis* **1995**, 895.

(25) Hirsch, A. *Top Curr Chem* **1999**, *199*, 1.

(26) Kalamkarov, A. L.; Georgiades, A. V.; Rokkam, S. K.; Veedu, V. P.; Ghasemi-Nejhad, M. N. *Int J Solids Struct* **2006**, *43*, 6832.

(27) Bekyarova, E.; Thostenson, E. T.; Yu, A.; Itkis, M. E.; Fakhrutdinov, D.; Chou, T.-W.; Haddon, R. C. *Journal of Physical Chemistry*, ACS ASAP.

(28) Hemraj-Benny, T.; Wong, S. S. *Chemistry of Materials* **2006**, *18*, 4827.

(29) McKee, G. S. B.; Vecchio, K. S. *Journal of Physical Chemistry B* **2006**, *110*, 1179.

(30) Engtrakul, C.; Davis Mark, F.; Gennett, T.; Dillon Anne, C.; Jones Kim, M.; Heben Michael, J. *J Am Chem Soc* **2005**, *127*, 17548.

(31) Alemany, L. B.; Zhang, L.; Zeng, L.; Edwards, C. L.; Barron, A. R. *Chemistry of Materials* **2007**, *19*, 735.

(32) Georgakilas, V.; Kordatos, K.; Prato, M.; Guldi, D. M.; Holzinger, M.; Hirsch, A. *J. Am. Chem. Soc.* **2002**, *124*, 760.

(33) Kyotani, T.; Nakazaki, S.; Xu, W.-H.; Tomita, A. *Carbon* **2001**, *39*, 782.

(34) Liang, F.; Sadana, A. K.; Peera, A.; Chattopadhyay, J.; Gu, Z.; Hauge, R. H.; Billups, W. E. *Nano Letters* **2004**, *4*, 1257.

(35) Forrest, G. A.; Alexander, A. J. *Journal of Physical Chemistry C* **2007**, *111*, 10792.

(36) Birch, A. J. *Journal of the Chemical Society* **1944**, 430.

(37) Liang, F.; Alemany, L. B.; Beach, J. M.; Billups, W. E. *Journal of the American Chemical Society* **2005**, *127*, 13941.

(38) Baldwin, J. E. *J Chem Soc Chem Comm* **1976**, 734.

(39) Hall, H. K. *J Am Chem Soc* **1955**, *77*, 5993.

(40) Glerup, M.; Castignolles, M.; Holzinger, M.; Hug, G.; Loiseau, A.; Bernier, P. *Chem. Commun.* **2003**, 2542.

(41) He, M.; Zhou, S.; Zhang, J.; Liu, Z.; Robinson, C. *J. Phys. Chem. B* **2005**, *109*, 9275.

(42) Lee, D. H.; Lee, W. J.; Kim, S. O. *Nano Lett.* **2009**, *9*, 1427.

(43) Liu, J.; Czerw, R.; Carroll, D. L. *J. Mater. Res.* **2005**, *20*, 538.

(44) Maldonado, S.; Morin, S.; Stevenson, K. J. *Carbon* **2006**, *44*, 1429.

(45) Terrones, M.; Ajayan, P. M.; Banhart, F.; Blase, X.; Carroll, D. L.; Charlier, J. C.; Czerw, R.; Foley, B.; Grobert, N.; Kamalakaran, R.; Kohler-Redlich, P.; Ruhle, M.; Seeger, T.; Terrones, H. *Appl. Phys. A: Mater. Sci. Process.* **2002**, *74*, 355.

(46) Yang, Z.; Xia, Y.; Mokaya, R. *Chem. Mater.* **2005**, *17*, 4502.

(47) Koos, A. A.; Dowling, M.; Jurkschat, K.; Crossley, A.; Grobert, N. *Carbon* **2009**, *47*, 30.

(48) Qian, D. L.; Andrews, R.; Jacques, D.; Kichambare, P.; Lian, G.; Dickey, E. C. *J Nanosci Nanotechno* **2003**, *3*, 93.

(49) Glerup, M.; Castignolles, M.; Holzinger, M.; Hug, G.; Loiseau, A.; Bernier, P. *Chem Commun* **2003**, 2542.

(50) Cui, H.; Zhou, O.; Stoner, B. R. *J Appl Phys* **2000**, *88*, 6072.

(51) Saito, Y. *Carbon* **1995**, *33*, 979.

(52) Li, Y. F.; Qiu, J. S.; Zhao, Z. B.; Wang, T. H.; Wang, Y. P.; Li, W. *Chem Phys Lett* **2002**, *366*, 544.

(53) Lin, M.; Tan, J. P. Y.; Boothroyd, C.; Loh, K. P.; Tok, E. S.; Foo, Y. L. *Nano Lett* **2007**, *7*, 2234.

(54) Jang, J. W.; Lee, C. E.; Lyu, S. C.; Lee, T. J.; Lee, C. J. *Appl Phys Lett* **2004**, *84*, 2877.

(55) Lee, C. J.; Park, J. *Appl Phys Lett* **2000**, *77*, 3397.

(56) Chen, Y.; Conway, M. J.; Fitz Gerald, J. D. *Appl Phys a-Mater* **2003**, *76*, 633.

(57) Lu, Y.; Zhu, Z. P.; Su, D. S.; Wang, D.; Liu, Z. Y.; Schlogl, R. *Carbon* **2004**, *42*, 3199.

(58) Liu, J.; Webster, S.; Carroll, D. L. *Appl Phys Lett* **2006**, *88*.

(59) Jacques, D.; Andrews, R. In *US 7,160,531 B1*; University of Kentucky: USA, 2007.

(60) Jacques, D.; Andrews, R. In *US 7,504,078 B1*; The University of Kentucky: USA, 2009.

(61) Boehm, H. P.; Setton, R.; Stumpp, E. *Pure Appl Chem* **1994**, *66*, 1893.

(62) Dresselhaus, M. S.; Dresselhaus, G. *Adv Phys* **1981**, *30*, 139.

(63) Emery, N.; Herold, C.; Lagrange, P. *Prog Solid State Ch* **2008**, *36*, 213.

(64) Gauzzi, A.; Bendiab, N.; d'Astuto, M.; Canny, B.; Calandra, M.; Mauri, F.; Loupias, G.; Emery, N.; Herold, C.; Lagrange, P.; Hanfland, M.; Mezouar, M. *Phys Rev B* **2008**, *78*.

(65) Emery, N.; Herold, C.; Mareche, J. F.; Lagrange, P.; Bellouard, C.; Lamura, G.; Di Gennaro, E.; Andreone, A. *Solid State Sci* **2008**, *10*, 466.

(66) Emery, N.; Herold, C.; Lagrange, P. *Carbon* **2008**, *46*, 72.

(67) Nakamae, S.; Gauzzi, A.; Ladieu, F.; L'Hote, D.; Emery, N.; Herold, C.; Mareche, J. F.; Lagrange, P.; Loupias, G. *Solid State Commun* **2008**, *145*, 493.

(68) Kukovecz, Á.; Kanyó, T.; Kónya, Z.; Kiricsi, I. *Carbon* **2005**, *43*, 994.

(69) Shao, W.; Wang, Q.; Wang, F.; Chen, Y. *Carbon* **2006**, *44*, 2708.

(70) Banhart, F. *Reports on Progress in Physics* **1999**, 1181.

(71) Lu, K. L.; lago, R. M.; Chen, Y. K.; Green, M. L. H.; Harris, P. J. F.; Tsang, S. C. *Carbon* **1996**, *34*, 814.

(72) Shelimov, K. B.; Esenaliev, R. O.; Rinzler, A. G.; Huffman, C. B.; Smalley, R. E. *Chem. Phys. Lett.* **1998**, *282*, 429.

(73) Chen, X.; Burger, C.; Fang, D.; Sics, I.; Wang, X.; He, W.; Somani, R. H.; Yoon, K.; Hsiao, B. S.; Chu, B. *Macromolecules* **2006**, *39*, 5427.

(74) Chen, Y. K.; Green, M. L. H.; Griffin, J. L.; Hammer, J.; Lago, R. M.; Tsang, S. C. *Adv. Mater.* **1996**, *8*, 1012.

(75) Srivastava, D.; Brenner, D. W.; Schall, J. D.; Ausman, K. D.; Yu, M.; Ruoff, R. S. *J. Phys. Chem. B* **1999**, *103*, 4330.

(76) Allen, M. J.; Tung, V. C.; Kaner, R. B. *Chem. Rev.* **2009**, *110*, 132.

(77) Kosynkin, D. V.; Higginbotham, A. L.; Sinitskii, A.; Lomeda, J. R.; Dimiev, A.; Price, B. K.; Tour, J. M. *Nature* **2009**, *458*, 872.

(78) Zhang, Z.; Sun, Z.; Yao, J.; Kosynkin, D. V.; Tour, J. M. *J. Am. Chem. Soc.* **2009**, *131*, 3460.

(79) Jiao, L.; Zhang, L.; Wang, X.; Diankov, G.; Dai, H. *Nature* **2009**, *458*, 877.

(80) Elías, A. L.; Botello-Mendez, A. R.; Meneses-Rodrigues, D.; Jehova-Gonzalez, V.; Ramierez-Gonzalez, D.; Munoz-Sandoval, L. C. E.; Ajayan, P. M.; Terrones, H.; Terrones, M. *Nano Lett.* **2009**, *10*, 366.

(81) Cano-Marquez, A. G.; Rodriguez-Maciás, F. J.; Campos-Delgado, J.; Espinosa-Gonzaléz, C. G.; Tristán-López, F.; Ramarez-Gonzallèz, D.; Cullen, D. A.; Smith, D. J.; Terrones, M.; Vega-Cantú, Y. I. *Nano Lett.* **2009**, *9*, 1527.

(82) Langmuir, I. *J Am Chem Soc* **1916**, *38*, 2221.

(83) Brunauer, S.; Emmett, P. H.; Teller, E. *J Am Chem Soc* **1938**, *60*, 309.

(84) Gregg, S. J.; Sing, K. S. W. *Adsorption, surface area, and porosity*; 2nd ed.; Academic Press: London ; New York, 1982.

(85) Hee K. Chae, D. Y. S.-P. r., Jaheon Kim, YongBok Go,; Mohamed Eddaoudi, A. J. M., Michael O'Keeffe; Yaghi, O. M. *Nature* **2004**, *427*, 523.

(86) Hiraoka, T.; Izadi-Najafabadi, A.; Yamada, T.; Futaba, D. N.; Yasuda, S.; Tanaike, O.; Hatori, H.; Yumura, M.; Iijima, S.; Hata, K. *Adv Funct Mater* **2010**, *20*, 422.

(87) Stoller, M. D.; Park, S. J.; Zhu, Y. W.; An, J. H.; Ruoff, R. S. *Nano Lett* **2008**, *8*, 3498.

(88) Benard, P.; Chahine, R. *Scripta Mater* **2007**, *56*, 803.

(89) Jiang, Q.; Zhao, Y. *Micropor Mesopor Mat* **2004**, *76*, 215.

(90) Kaneko, K.; Ishii, C.; Ruike, M.; Kuwabara, H. *Carbon* **1992**, *30*, 1075.

(91) Bueres, R. F.; Asedegbega-Nieto, E.; Diaz, E.; Ordonez, S.; Diez, F. V. *Catal Today* **2010**, *150*, 16.

(92) Ebbing, D. D. **1990**.

(93) Clementi, E.; Raimondi, D. L.; Reinhard.Wp *J Chem Phys* **1967**, *47*, 1300.

(94) Mueller, R. H.; Gillick, J. G. *J Org Chem* **1978**, *43*, 4647.

Vita

Kelby B. Cassity was born on the 19th of May, 1981, in Versailles, KY. He obtained his high school diploma at Woodford County High School in 1999. He received a Bachelor degree in both Chemistry and Mathematics in December 2003 from Western Kentucky University and enrolled in the Chemistry Department at the University of Kentucky in August of 2005. He joined the group of Dr. Mark Meier in January of 2006.

Talks and Presentations

1. "Covalent Chemistry of Carbon Nanotubes," **Meier, M. S.**; Cassity, K. B.; Yeary, P. Invited talk at the Carbon Society Workshop on Porous Carbons ("Adsorbent Carbons for Chemical and Biological Protection"), Seattle, Washington, July 14, 2007.
2. "Functionalized Carbon Nanotubes for Composite Materials," **Meier, M. S.**; Andrews, R.; Cassity. K. B.; Weisenberger, M.; Yeary, P. Presented at the International Conference on Carbon, Seattle, Washington, July 19, 2007.
3. "Fracture Formation of Nitrogen-doped Multiwall Carbon Nanotubes", Meier, M.S.; Andrews, R; **Cassity, K.B**.; Qian, D.; Jacques, D. Presented at the Spring 2008 American Chemical Society conference in New Orleans, LA
4. "Chemistry on N-doped MWCNTs", Meier, M.S.; Andrews, R; **Cassity, K.B**.; Qian, D.; Jacques, D. Poster at the Spring 2008 American Chemical Society conference in New Orleans, LA.

5. "Functionalized MWCNTs for epoxy composites," **Cassity, K.B.**; Andrews, R.; Meier, M.S; Weisenberger, M.; Petty, K., Freibert, R. Presented at the International Conference on Carbon, Biarritz, France, June 17, 2009.
6. "Fracture Formation in N-Doped MWCNTs," **Cassity, K.B.**; Andrews, R.; Meier, M.S; Jacques, D, Qian, D. Presented at the International Conference on Carbon, Biarritz, France, June 15, 2009.

Publications

1. Rodney Andrews , Matthew C. Weisenberger, Dali Qian, Mark S. Meier, Kelby Cassity, Paul E. Yeary, *"Carbon Nanotubes, Multi-Walled", Encyclopedia of Inorganic Chemistry, 2009 John Wiley & Sons, Inc.*
2. "Tearing Open Nitrogen-Doped Carbon Nanotubes", Mark S. Meier, Rodney Andrews, David Jacques**,** Kelby B. Cassity, and Dali Qian; *Journal of Materials Chemistry,* **2008**, 18, 4143-4145
3. "Linear and spiral forms of longitudinal cuts in graphitized N-doped multiwalled carbon nanotubes (g-N-MWCNTs)," Meier, M. S.; Selegue, J. P.; Cassity, K. B.; Kaur, A. P.; Qian, D. *J. Phys. (Cond. Matter), accepted*.
4. "Synthesis and Surface Studies of Fenton Hydroxylated Multi-Wall Carbon Nanotubes", Robert H Bradley, Kelby B. Cassity, Rodney Andrews, Mark Meier, Susan Osbeck, Aurik Andreu, Colin Johnston, *Journal of Materials Chemistry, submitted*